

Stochastic Simulation Methods for Structural Reliability under Mixed Uncertainties

Von der Fakultät für Bauingenieurwesen und Geodäsie
der Gottfried Wilhelm Leibniz Universität Hannover
zur Erlangung des Grades

Doktor der Ingenieurwissenschaften

Dr.-Ing.

genehmigte Dissertation

von

Dipl.-Ing. Jingwen Song

2020

Referent: Prof. Dr.-Ing. Michael Beer

Korreferent: Prof. Dr.-Ing. Ingo Neumann

Prof. Dr.-Ing. Udo Nackenhorst

Prof. Dr. Sifeng Bi (Beijing Institute of Technology)

Tag der Promotion: 12.08.2020

Dedicated to my family

Erklärung zum Promotionsgesuch

Ich erkläre, dass ich die Bestimmungen für Doktoranden an der Fakultät für Bauingenieurwesen und Geodäsie der Gottfried Wilhelm Leibniz Universität Hannover kenne und befolgt habe und einer Prüfung gemäß den Bestimmungen der Promotionsbestimmungen zustimme. Ich habe die Dissertation unabhängig abgeschlossen, keine Textabschnitte von Dritten ohne Identifikation kopiert und alle in den Referenzen verwendeten Materialien aufgelistet. Darüber hinaus habe ich weder direkt noch indirekt Leistungen Dritter für die Vermittlung von Aktivitäten oder für den Inhalt der Dissertation erbracht und die Dissertation noch nicht als Prüfungsarbeit für eine staatliche oder andere wissenschaftliche Prüfung eingereicht. Die vorliegende Arbeit wurde auch nicht als Dissertation an einer anderen Universität eingereicht. Ich bin damit einverstanden, dass die Dissertation auch dazu verwendet wird, die Einhaltung allgemein geltender wissenschaftlicher Standards zu überprüfen, insbesondere auch unter Verwendung elektronischer Datenverarbeitungsprogramme.

Hannover, am _____

Datum _____

Unterschrift _____

Acknowledgments

This dissertation is the summary of my research at the Institute for Risk and Reliability at Leibniz University Hannover (LUH), where each step of progress has received tremendous encouragement and help from my supervisor, colleagues, families, and friends. My gain is not only limited to the research experience as a Ph.D. student but also learning the way of doing research, which will benefit me through my whole research carrier.

First and foremost, I would like to show my great thankfulness to my supervisor, Prof. Dr.-Ing. Michael Beer, who has not only led me to the academic area of uncertainty quantification and reliability analysis but also provides me suggestions of great help whenever I meet obstacles. The study in the institute for Risk and Reliability has largely broadened my research view, reformed my way of thinking scientific problems, and raises me up to the international horizon. All these achievements in my dissertation are attributed to him. Prof. Beer also leaves me sufficient freedom to think and implement the research in my own way, but always gives me advice at the right time, which has prevented me from going astray. He has also provided me plenty of opportunities to get involved in international academic conferences such as CIVIL-COMP 2019, ESREL 2019 and SAMO 2019, which have largely broadened my academic horizon, and also deeply influenced my academic growth. I am really grateful to him for all these achievements.

Then I'd like to take this opportunity to thank Marcos and Pengfei for collaboration and fruitful discussions. During Marcos's Humboldt stay at LUH, he gave me tremendous specific advice for all these developments, especially those on line sampling. I have learned not only the theoretical and historical details of many important concepts in structural reliability from Marcos, but also the importance of cultivating specialists attitude of exploring the truth, and the spirit of being rigorous in scientific research. Pengfei, as the co-author of my three journal papers, gave me a full range of guidance on all aspects of research. Without his encouragement, it is impossible for me to receive these research achievements.

Further, I also want to thank all dear colleagues at the Institute for Risk and Reliability for all their help and discussions, such as Matteo, Tim, Jasper, Marius, Marco, Natalia, et al.

Particularly, thank Julian for helping check the German part of this dissertation. Thank Prof. Kok Kwang Phoon from National University of Singapore for all the truths of research and life I have learned from him during his Humboldt stay in Hannover. Thank for all the help from the warmhearted Chinese colleagues in my institute, especially, thank for the regular English discussions with Peihua, which pushed me to express my idea in English and summarize the research work timely.

My heartfelt thanks are given to my husband, my 4-year-old son, and my parents. For their persistent support of all my decisions, and I can always receive encouragement and love from them.

Abstract

Uncertainty quantification (UQ) has been widely recognized as one of the most important, yet challenging task in both structural engineering and system engineering, and the current researches are mainly on the proper treatment of different types of uncertainties, resulting from either natural randomness or lack of information, in all related sub-problems of UQ such as uncertainty characterization, uncertainty propagation, sensitivity analysis, model updating, model validation, risk and reliability analysis, etc. It has been widely accepted that those uncertainties can be grouped as either aleatory uncertainty or epistemic uncertainty, depending on whether they are reducible or not. For dealing with the above challenge, many non-traditional uncertainty characterization models have been developed, and those models can be grouped as either imprecise probability models (e.g., probability-box model, evidence theory, second-order probability model and fuzzy probability model) or non-probabilistic models (e.g., interval/convex model and fuzzy set theory).

This thesis concerns the efficient numerical propagation of the three kinds of uncertainty characterization models, and for simplicity, the precise probability model, the distribution probability-box model, and the interval model are taken as examples. The target is to develop efficient numerical algorithms for learning the functional behavior of the probabilistic responses (e.g., response moments and failure probability) with respect to the epistemic parameters of model inputs, which is especially useful for making reliable decisions even when the available information on model inputs is imperfect.

To achieve the above target, my thesis presents three main developments for improving the Non-intrusive Imprecise Stochastic Simulation (NISS), which is a general methodology framework for propagating the imprecise probability models with only one stochastic simulation. The first development is on generalizing the NISS methods to the problems with inputs

including both imprecise probability models and non-probability models. The algorithm is established by combining Bayes rule and kernel density estimation. The sensitivity indices of the epistemic parameters are produced as by-products. The NASA Langley UQ challenge is then successfully solved by using the generalized NISS method. The second development is to inject the classical line sampling to the NISS framework so as to substantially improve the efficiency of the algorithm for rare failure event analysis, and two strategies, based on different interpretations of line sampling, are developed. The first strategy is based on the hyperplane approximations, while the second-strategy is derived based on the one-dimensional integrals. Both strategies can be regarded as post-processing of the classical line sampling, while the results show that their resultant NISS estimators have different performance. The third development aims at further substantially improving the efficiency and suitability to highly nonlinear problems of line sampling, for complex structures and systems where one deterministic simulation may take hours. For doing this, the active learning strategy based on Gaussian process regression is embedded into the line sampling procedure for accurately estimating the interaction point for each sample line, with only a small number of deterministic simulations.

The above three developments have largely improved the suitability and efficiency of the NISS methods, especially for real-world engineering applications. The efficiency and effectiveness of those developments are clearly interpreted with toy examples and sufficiently demonstrated by real-world test examples in system engineering, civil engineering, and mechanical engineering.

Keywords: Uncertainty quantification; Imprecise probabilities; Non-probabilistic; Line sampling; Active Learning; Gaussian process regression; Bayes rule

Kurzfassung

Unsicherheitsquantifizierung (UQ) ist weithin als eine der wichtigsten, aber auch herausforderndsten Aufgaben sowohl im konstruktiven Ingenieurbau als auch im System-Engineering anerkannt. In allen mit der UQ verwandten Teilbereichen wie z.B. Unsicherheitscharakterisierung, Unsicherheitsausbreitung, Sensitivitätsanalyse, Modellaktualisierung, Modellvalidierung, Risiko- und Zuverlässigkeitssanalyse usw., befasst sich die aktuelle Forschung hauptsächlich mit der richtigen Handhabung verschiedener Arten von Unsicherheiten, die sich entweder aus natürlicher Zufälligkeit oder aus Informationsmangel ergeben. Es ist allgemein anerkannt, dass diese Unsicherheiten als aleatorische bzw. epistemische Unsicherheiten gruppiert werden können, je nachdem, ob sie reduzierbar sind oder nicht. Zur Bewältigung der obigen Herausforderung wurden bereits viele nicht-traditionelle Modelle zur Charakterisierung der Unsicherheit entwickelt. Diese Modelle können entweder als unpräzise Wahrscheinlichkeitsmodelle (z.B. Wahrscheinlichkeits-Box-Modell, Evidenztheorie, Wahrscheinlichkeitsmodell zweiter Ordnung und Fuzzy-Wahrscheinlichkeitsmodell) oder als nicht-probabilistische Modelle (z.B. Intervall/konvexes Modell und Fuzzy-Mengen-Theorie) gruppiert werden.

Die vorliegende Arbeit befasst sich mit der effizienten numerischen Propagierung von drei Arten von Modellen zur Charakterisierung der Unsicherheit. Der Einfachheit halber werden das präzise Wahrscheinlichkeitsmodell, das Verteilungswahrscheinlichkeits-Box-Modell und die Intervallmodelle als Beispiele herangezogen. Ziel ist es, effiziente numerische Algorithmen zum

Lernen des funktionalen Verhaltens der probabilistischen Antworten (z.B. Antwortmomente und Ausfallwahrscheinlichkeit) in Bezug auf die epistemischen Parameter der Modelleingaben zu entwickeln, was insbesondere nützlich ist, um zuverlässige Entscheidungen zu treffen, auch wenn die verfügbaren Informationen über Modelleingaben unvollkommen sind.

Um das oben motivierte Ziel zu erreichen, stellt meine Arbeit drei Hauptentwicklungen zur Verbesserung der Non-intrusive Imprecise Stochastic Simulation (NISS) vor, bei der es sich um einen allgemeinen methodischen Ansatz handelt, um unpräzise Wahrscheinlichkeitsmodelle mit nur einer stochastischen Simulation propagieren zu können. Die erste Entwicklung besteht in der Verallgemeinerung der NISS-Methoden auf Probleme mit Inputs, die sowohl unpräzise probabilistische Modelle als auch nicht-probabilistische Modelle umfassen. Der Algorithmus wird durch die Kombination von Bayes-Regel und Kernel-Dichte-Schätzung erstellt. Die Sensitivitätsindizes der epistemischen Parameter werden dabei als Nebenprodukte erzeugt. Das NASA Langley Uncertainty Quantification Challenge wird anschließend mit der verallgemeinerten NISS-Methode erfolgreich gelöst. Die zweite Entwicklung besteht darin, die klassische Line-Sampling-Methode in das NISS-Framework einzufügen, um die Effizienz des Algorithmus für die Analyse seltener Fehlerereignisse wesentlich zu verbessern. Es werden zwei Strategien entwickelt, die auf unterschiedlichen Interpretationen der Line-Sampling-Methode basieren. Die erste Strategie basiert auf den Hyperebenen-Approximationen, während die zweite Strategie aus eindimensionalen Integralen abgeleitet wird. Beide Strategien können als Postprocessing des klassischen Line Samplings betrachtet werden, die Ergebnisse zeigen allerdings, dass ihre resultierenden NISS-Schätzer eine unterschiedliche Performanz aufweisen. Die dritte Entwicklung zielt darauf ab, die Effizienz und Eignung der Line-Sampling-Technik für

hochgradig nichtlineare Probleme bei komplexen Strukturen und Systemen, bei denen selbst eine einzige deterministische Simulation Stunden dauern kann, weiter wesentlich zu verbessern. Zu diesem Zweck wird das aktive Lernen auf der Grundlage der Gaußschen Prozessregression in das Line-Sampling-Verfahren, zur genauen Schätzung des Interaktionspunktes für jede Linie mit nur wenigen deterministischen Simulationen, eingebettet.

Die oben genannten drei Entwicklungen haben die Anwendbarkeit und Effizienz der NISS-Methoden, insbesondere für reale technische Anwendungen, maßgeblich verbessert. Die Effizienz und Effektivität dieser Entwicklungen sind eindeutig anhand von Musterbeispielen dargestellt und durch reale Testbeispiele in den Bereichen Systemtechnik, Bauingenieurwesen und Maschinenbau hinreichend belegt.

Schlüsselwörter: Unsicherheitsquantifizierung; Unpräzise Wahrscheinlichkeiten; Nicht-probabilistisch; Line sampling; Aktives Lernen; Gaußsche Prozessregression; Bayes-Regel

Contents

Abstract	I
Kurzfassung.....	III
Introduction	1
1. Research Background	1
1.1. Categorization and Sources of uncertainties	3
1.2. Uncertainty characterization models.....	6
1.3. Uncertainty propagation and structural reliability	14
2. Aims and Objectives	21
3. Original Contributions	21
4. Structure of the Thesis.....	23
Research article 1: Generalization of non-intrusive imprecise stochastic simulation for mixed uncertain variables.....	25
1. Introduction.....	28
2. Brief review of NISS	31
3. Generalization of NISS	35
3.1 Discussions on non-probabilistic models	35
3.2 The developed method	36
3.3 Conditional density estimations	43
4. Test examples and applications.....	44
4.1 A toy test example	44
4.2 The NASA Langley multidisciplinary UQ challenge.....	48
5. Conclusions and discussions	55
Acknowledgments.....	56
Reference.....	57
Research article 2: Non-intrusive imprecise stochastic simulation by line sampling	61
1. Introduction.....	64
2. Background of imprecise stochastic simulation and line sampling.....	67
2.1 Problem statement	67
2.2 Imprecise stochastic simulation	67
2.3 Line sampling	70
3. Imprecise line sampling method.....	73
3.1 Hyperplane-approximation based imprecise line sampling.....	73
3.2 Weighted-integral based imprecise line sampling	80

4.	Case studies	83
4.1	Analytical example	83
4.2	A shallow foundation model	87
4.3	Confined seepage model.....	91
4.4	Transmission tower	95
5.	Conclusions	99
	Acknowledgment	100
	Appendix A : Derivation of failure probability function for Eq.(35)	100
	Appendix B: Derivation of analytical failure probability function of Eq.(41)	102
	References	103
	Research article 3: Active Learning Line Sampling for Rare Event Analysis.....	107
1	Introduction.....	110
2	Review of Line Sampling.....	113
3	The proposed method.....	116
3.1	Brief introduction of the GPR model	116
3.2	Learning function	117
3.3	The AGPR-LS algorithm	119
4	Case studies	123
4.1	A two-dimensional numerical example.....	123
4.2	Dynamic response of a nonlinear oscillator.....	129
4.3	Confined seepage model	132
4.4	A two-dimensional wing flutter model.....	135
4.5	Transmission tower.....	138
4.6	Final remarks	140
5	Conclusions and discussions	141
	Acknowledgment	142
	References	143
	Conclusions and Prospects.....	147
1.	Conclusions	147
2.	Open problems and Prospects.....	150
	Bibliography.....	153
	Curriculum Vitae.....	157

Introduction

1. Research Background

In structural and system reliability engineering, the proper treatment of different sources of uncertainties has proven to be extremely important nowadays. However, due to the complexities of structures and systems, analytically deriving the system behavior is intractable, and numerical techniques such as computer simulators, have to be developed for filling this gap, which makes the treatment of uncertainty tremendously difficult. The uncertainty quantification (UQ) aims at properly characterizing and analyzing all kinds of uncertainties during the modeling process, with the target to properly quantifying the uncertainty of model responses which simulating the behavior of structural systems subjected to environmental excitations. This treatment also provides necessary information for assessing the reliability of the structural systems under consideration.

The tasks in UQ and reliability analysis are summarized in Figure 1, with also the focus on the logical flow of implementing these tasks. Given a structural system under consideration, the physics laws (e.g., the principle of minimum potential energy) are commonly developed for *model abstraction*, so as to create a mathematical model (e.g., partial differential equations (PDEs)) for representing the response of structural systems to specific environment excitations. Then, *numerical solution* (e.g., the finite difference method) is implemented for solving the mathematical model so as to develop a numerical computer simulator (e.g., finite element model (FEM)) that can be easily implemented with computer codes. In this step, the *model verification* commonly needs to be implemented to identify whether the mathematical model is correctly solved, and code verification is required to test whether the numerical solution is correctly implemented by the computer codes without bugs in any cases. The above procedure produces

deterministic computer simulators for simulating the behavior of structural systems. By saying “deterministic” it mean that, given deterministic structural parameters, boundary/initial conditions, and environment excitations, the computer simulator produces deterministic model responses.

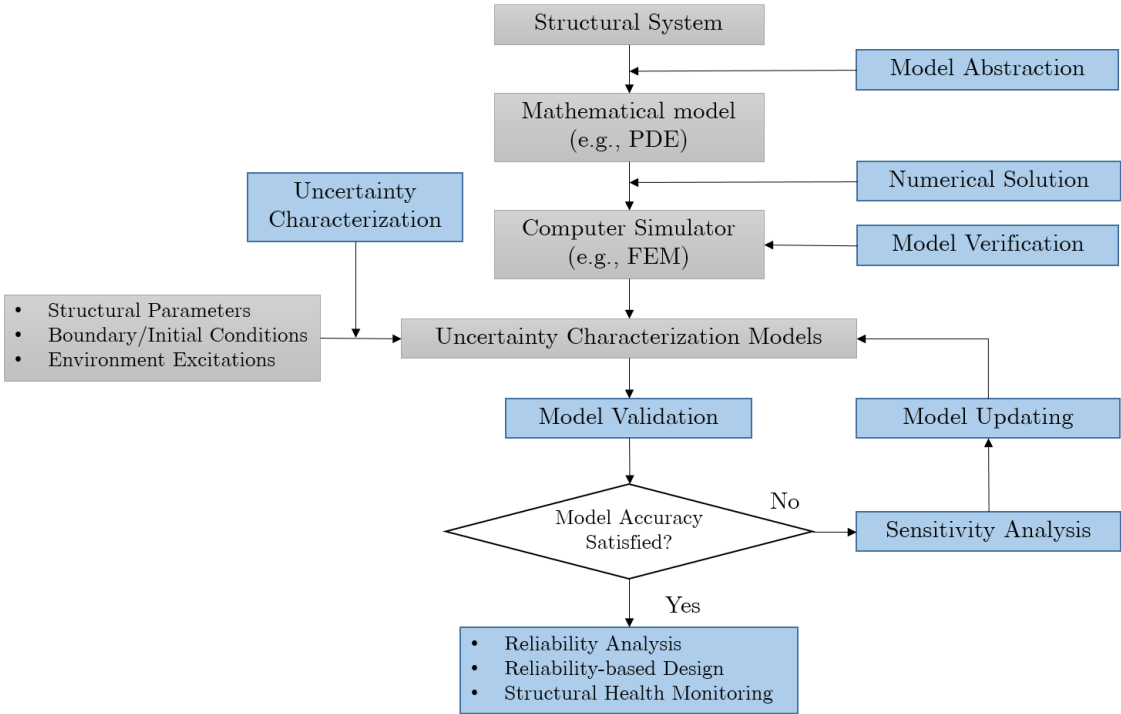


Figure 1 Structural UQ and reliability analysis framework

However, in practical engineering applications, the structural parameters are not deterministic, suffering from different sources of uncertainties. Thus, another key task, named as *uncertainty characterization*, needs to be implemented so as to characterize these uncertainties with proper mathematical models. Given the uncertainty characterization models as the inputs of the computer simulators, one more key task, named as *model validation*, is required for validating the consistency between the responses of the simulator and those of the structural systems under consideration. A very famous quote related to this task is given by the British mathematician George E. P. Box as “All models are wrong, but some are useful” (Box et al., 2005). This quote is not only true for statistic inference models, but also definitely true for computer simulators, and it means that there is no model that can simulate the behavior of a

real-world system precisely. As long as a simulator can predict the responses of the system subjected to any environmental excitations correctly within pre-specified error bounds, it is useful. If not, then another key procedure, termed as *model updating*, should be implemented, based on experimental measurements of system responses, so as to update the input uncertainty characterization models, and also to quantify the bias of the simulator. During this procedure, the *sensitivity analysis* may serve as a useful tool for identifying the important input parameters to be calibrated in the model updating. If the simulator prediction accuracy is acceptable, then the input uncertainty characterization models and the simulator can be utilized for engineering application tasks such as reliability analysis, reliability-based design optimization (known as RBO), and structural health monitoring (SHM).

In the above framework, different sources and different categories of uncertainties need to be carefully treated in each procedure, and next, I provide a brief view of the uncertainties affecting the simulator prediction and also the related analysis results in applications.

1.1. Categorization and Sources of uncertainties

Nowadays, the research community has already reached an agreement on the categorization of uncertainties, and the most widely accepted one is to group the presented uncertainty as either aleatory uncertainty or epistemic uncertainty (see, e.g. Der Kiureghian and Ditlevsen, 2009). The aleatory uncertainty, also called objective uncertainty and type I uncertainty, is caused by the random nature of things, and cannot be reduced by collecting more information; whereas, the epistemic uncertainty, also named as subjective uncertainty and type II uncertainty, is due to the lack of knowledge or the poor quality of information, thus can be further reduced by, e.g., collecting more information or improving the quality of available information. The coin flipping is a good example to explain the above concepts. The result we concern is the side which is showing. Before throwing the coin, the only prediction we can make, depending on our experience, is that the probability of seeing each side is 50%, but it is impossible to predict which side will be definitely showing, and this kind of uncertainty is aleatory uncertainty since it cannot be reduced. However, if someone has already thrown the coin, and ask you which side is

showing. You are not sure about the result, but you can always learn it, by, e.g., observation. This kind of being unknown can be reduced by collecting more information, thus it should be grouped into epistemic uncertainty. In the framework shown in Figure 1, these two kinds of uncertainties are ubiquitous but may come from different sources in each task.

Any mathematical model for simulating a system should be developed based on proper assumption, which is one of the core steps in model abstraction. Those assumptions are helpful for developing practical models, and also result in model bias, which is a kind of uncertainty represented by the difference between the mathematical model predictions and the real-world system responses. This kind of uncertainty should be classified into epistemic uncertainty.

The uncertainty to be coupled within the numerical solution and the model verification is mostly numerical errors due to, e.g., discretization of the fields, and should be treated as epistemic uncertainty. The code verification mainly deals with the incorrectness and bug in the computer implementation of the numerical algorithms, which should be regarded as epistemic uncertainty, and should be avoided or at least limited to a certain degree.

The uncertainties presented in uncertainty characterization can be quite universal and diverse. The uncertainty characterization models are commonly generated by statistical inference based on available information, which may come from measurements, expert opinions, observations, etc. The available information may turn out to be random, scarce, incomplete (e.g., due to sensor failure), imprecise (e.g., due to measurement error), abstract (e.g., with only sample mean), vague (e.g., linguistic description), etc. All the above sources of uncertainties in the available information can be categorized either as aleatory uncertainty or epistemic uncertainty, depending on whether it is reducible. For example, for an existing structure, the dimension sizes and material properties should be deterministic, and the available information may only involve epistemic uncertainty due to, e.g., measurement error, which can be reduced by using better measurement devices; for the future structure, both the dimension sizes and material properties also involve aleatory uncertainty due to their intrinsic randomness caused by, e.g., manufacturing errors. The uncertainty due to scarcity, incompleteness, imprecision, vagueness, and abstraction can be reduced by collecting more information or improving the

quality of information, thus is reducible, and should be grouped into epistemic uncertainty. Besides, for developing the uncertainty characterization models from those data, some assumptions, such as distribution type, need to be made in advance, which may also introduce another source of epistemic uncertainty, that is, the model bias.

During the task of model updating, the sensitivity analysis is commonly implemented as a pre-analysis to cope with the epistemic uncertainty, so as to reduce the number of parameters to be calibrated based on the relative contribution of their epistemic uncertainty to the model response. The model updating deals with the epistemic uncertainty involved in simulator parameters and the bias of the simulator, and nowadays, the Bayesian updating has been widely investigated and accepted as the most potential technique for this task.

Even in the case that the computer simulator and the input uncertainty characterization have been validated to be accurate enough for the application, both aleatory and epistemic uncertainties may be involved in both objects, and need to be carefully treated in the model applications such as reliability analysis, RBO, and SHM.

Nowadays, researchers have almost reached an agreement that the aleatory uncertainty and epistemic uncertainty should be properly distinguished and separated, not only in philosophy, but also in the uncertainty characterization models and the whole analysis, design, and decision-making processes, because these two kinds of uncertainties come from definitely different sources and also have definitely different effects on our analysis. Take the structural reliability analysis as an example, where the probability of failure of the structural system is of great importance, and the presence of aleatory uncertainty results in the random failure, which is an intrinsic property of the structure system. The epistemic uncertainty, however, does not affect the true value of probability of failure, but only prevents us from correctly learning this value. With the reduction of the epistemic uncertainty, our knowledge of the failure probability can be improved. Based on the above fact, the two kinds of uncertainties should undoubtedly be distinguished properly and separated from the very beginning of the analysis.

In this thesis, I only consider the aleatory and epistemic uncertainties presented in input uncertainty characterization models, but not the epistemic uncertainty caused by model bias. In

the next subsection, the uncertainty characterization models established for characterizing the aleatory and epistemic uncertainty will be briefly reviewed.

1.2. Uncertainty characterization models

The available uncertainty characterization models can generally be grouped into three groups, based on the probabilistic and/or non-probabilistic information delivered. They are precise probability models, non-probabilistic models and imprecise probability models, as shown in Figure 2.

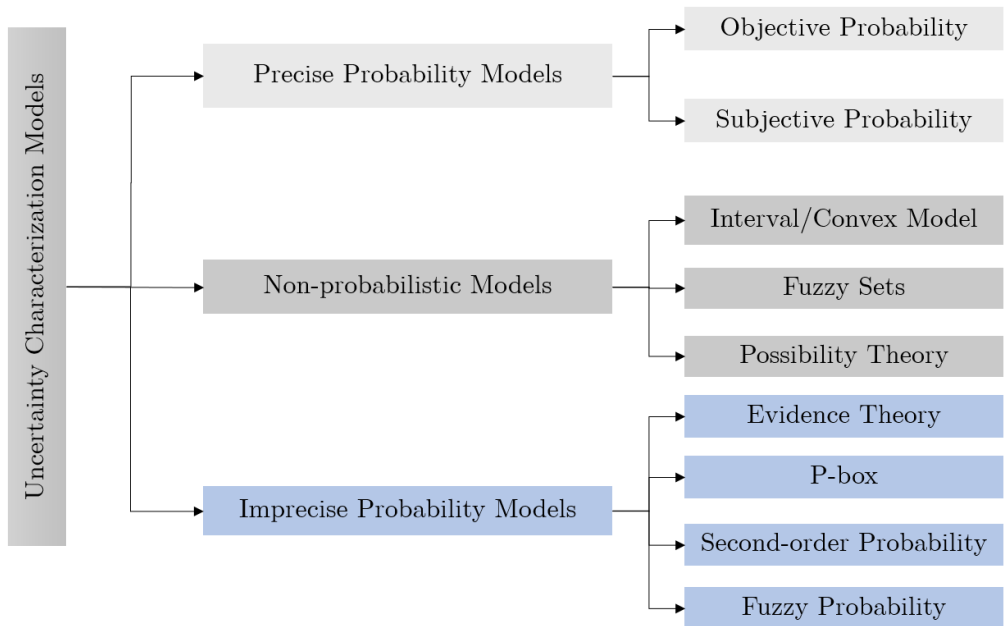


Figure 2 Categorization of uncertainty characterization models

Probability models, compared with imprecise probability models, termed as precise probability models, have been regarded as the most appealing models for characterizing uncertainty due to the simplicity and perfectness of probability theory. A probability model is uniquely characterized by a probability space $(\Omega, \mathcal{F}, \mathcal{P})$, where Ω is termed as sample space, which is a set of all possible outcomes, the σ -algebra \mathcal{F} is a collection of events with each component being a set of containing zero or more outcomes and \mathcal{P} is a deterministic function from events to probabilities reflecting the probability assigned to each event included in \mathcal{F} . The probability model can be utilized for characterizing either the aleatory uncertainty or epistemic

uncertainty, but not both of them in a separable scheme. When it is utilized for characterizing the aleatory uncertainty, it can be termed as *objective probability*, and the probability measure \mathcal{P} reflects the objective probability that each event in \mathcal{F} happens. Otherwise, if it is used for characterizing the epistemic uncertainty, it is commonly named as *subjective probability*, the probability measure \mathcal{P} reflects someone's personal belief (measured by probability) on this event, but not the actual probability that this event happens. For example, in the classical Bayesian model updating scheme (Kennedy and O'Hagan, 2001), the prior information on the parameters to be calibrated is always assumed to be a probability model, and by multiplying with the likelihood function derived from experiment data, a posterior probability distribution with, e.g., smaller support, can be obtained. In the above procedure, it is implicitly assumed that the prior probability model (partly) characterizes the epistemic uncertainty since it can be reduced by Bayesian inference with more data. The above difference between objective probability and subjective probability also reflects the different philosophies between frequentists and Bayesians. We don't go further on these topics as it involves an endless debate in which no one wins and no one loses.

The non-probabilistic models (Faes and Moens, 2019) can be especially useful for characterizing the uncertainty due to imprecision, vagueness, scarcity, etc. Commonly used non-probabilistic models include the convex model, fuzzy set model, and the induced possibility theory, etc. (Helton et al., 2014). Those models do not include any probability information. A simple two-dimensional convex model is schematically illustrated in Figure 3, where three different cases of dependency between the two variables are shown. In Figure 3 (a), the two variables are assumed to be independent, thus the marginal models of both variables are simple intervals $[\underline{x}_i, \bar{x}_i]$, and their joint model is a rectangle or hyper-rectangle (for higher dimensions). In Figure 3 (b), the two variables are linearly dependent or correlated, the marginal characterization models are still intervals, but the joint model is characterized by a convex model with the bounds of support modeling by an ellipse or a hyper-ellipsoid (for higher dimensions). However, as the two variables are nonlinearly dependent, the bounds of their joint

characterization model may be any arbitrary convex set, as shown in Figure 3 (c). The convex model has also been extended for time-variant/spatial variables, where the induced models are commonly named as interval process or interval field (Verhaeghe et al., 2013; Jiang et al., 2016). One important issue in these models is to characterize the spatial dependencies at different locations.

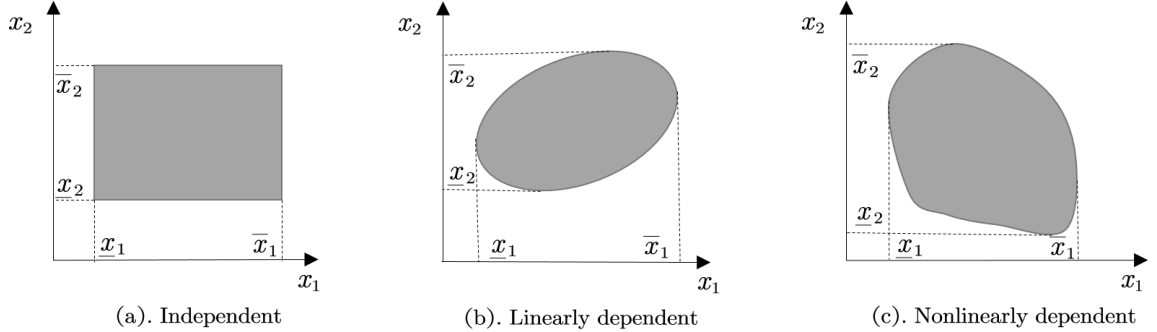


Figure 3 Illustration of convex models.

The fuzzy set model can be regarded as a convex model with soft bounds (Helton et al., 2014). Two very important elements of a univariate fuzzy set model are the support $\mathcal{X} = [\underline{x}, \bar{x}]$ and the membership function $\mu(x)$, as illustrated in Figure 4. Given a membership level α , an α -cut set can be derived from the membership function as $A_\alpha = [\underline{x}_\alpha, \bar{x}_\alpha]$, and it commonly holds that $A_0 = \mathcal{X}$. The membership level reflects the analyst's risk that he would like to take for determining the hard support of the variable. Larger membership value implies higher risk, meanwhile indicates that narrower α -cut set will be induced. Take the measurement as an example, when a device is utilized for measuring a deterministic quantity, he may give the measured result as $[x^* + x_\alpha/2, x^* + x_\alpha/2]$, where x_α reflects the measurement error. In many cases, x_α is not precisely known, and then a varying x_α with respect to the membership level α can be attributed, where α reflects the risk he would like to take. In this way, the membership function is derived. If he doesn't want to take any risk, then a large bound \mathcal{X} with high confidence is derived; otherwise, while he is willing to take a certain degree of risk, narrower bounds with less confidence can be derived. The above feature makes the fuzzy set theory, although more complex than the convex model, more informative for decision-making.

The possibility theory is derived from fuzzy set model, and the two very important concepts are the possibility measure and the necessity measure. Given a subset $\mathcal{U} \subseteq \mathcal{X}$, the possibility measure, denoted as $\text{Pos}(\mathcal{U})$, and the necessity measure, denoted by $\text{Nec}(\mathcal{U})$ are defined by (Helton, et al., 2010):

$$\text{Pos}(\mathcal{U}) = \sup_{x \in \mathcal{U}} \mu(x) \quad (1)$$

and

$$\text{Nec}(\mathcal{U}) = 1 - \text{Pos}(\bar{\mathcal{U}}) = 1 - \sup_{x \in \bar{\mathcal{U}}} \mu(x) \quad (2)$$

where $\bar{\mathcal{U}}$ indicates the complementary set of \mathcal{U} . The possibility measure $\text{Pos}(\mathcal{U})$ quantifies the possibility of the event that the subset \mathcal{U} contains the true value of x , while the necessity measure $\text{Nec}(\mathcal{U})$ quantifies the non-possibility of the event that the subset \mathcal{U} does contain the true value of x . These two measures satisfy $\text{Nec}(\mathcal{U}) \leq \text{Pos}(\mathcal{U})$. Generally, the possibility measure overestimates the probability that the appropriate value of x is included in \mathcal{U} , while the necessity measure underestimates this probability.

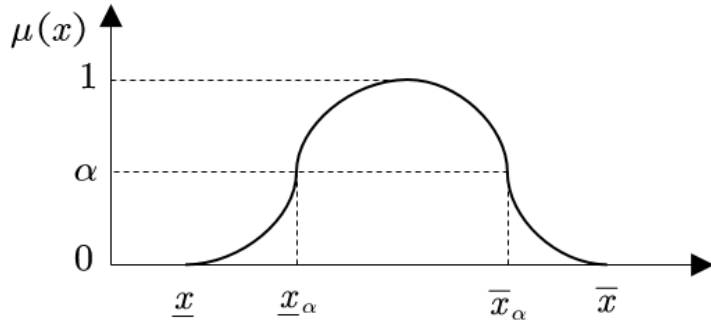


Figure 4 Illustration of a univariate fuzzy set model

The above-mentioned non-probabilistic models are mostly utilized for characterizing only the epistemic uncertainty, but there are also researchers who suggest using the non-probabilistic models as long as the available information is bad, without separating the aleatory and epistemic uncertainty (Jiang et al., 2013). In this thesis, I follow the philosophy that those two kinds of uncertainties must be separated from the very beginning when one models these uncertainties from data. Therefore, throughout this thesis, it is assumed that non-probabilistic models are

only used for characterizing the epistemic uncertainty.

The imprecise probability models are a set of hierarchical mathematical models combining the precise probability model and the non-probabilistic models, and are especially useful for characterizing the variables with both aleatory and epistemic uncertainties (or called polymorphic uncertainty) in a separable framework (Beer et al., 2013). The well-established imprecise probability models include evidence theory (Sentz and Ferson, 2002), probability-box (*p*-box) model (Ferson et al., 2015), second-order probability models (Sankararaman and Mahadevan, 2011), fuzzy probability model (Stein et al., 2013), etc.

The evidence theory, also named as Dempster-Shafer (D-S) theory (Sentz and Ferson, 2002), is rooted in the classical probability theory. For a univariate variable x , the uncertainties are characterized by a triplet (Ω, \mathcal{F}, m) , where Ω is called sample space, and it indicates the support of x which consists of all possible values of x ; one subset \mathcal{U} of Ω is named as a focal element, and \mathcal{F} is the countable collection of all focal elements of Ω ; $m(\mathcal{U})$ is called the Basic Probability Assignment (BPA) of the focal element \mathcal{U} , which satisfies: (i) $0 \leq m(\mathcal{U}) \leq 1$; (ii) $\sum_{\mathcal{U} \in \mathcal{F}} m(\mathcal{U}) = 1$; (iii) if $\mathcal{U} \in \mathcal{F}$, then $m(\mathcal{U}) > 0$, else $m(\mathcal{U}) = 0$. Compared with the probability space $(\Omega, \mathcal{F}, \mathcal{P})$, the definition of sample space Ω is the same, but the definitions for \mathcal{F} and \mathcal{P} are different. For probability theory, \mathcal{F} is required to be a σ -algebra, while for evidence theory, there is no such a requirement. For probability theory, $\mathcal{P}(\mathcal{U})$ measures the probability that one sample of x is contained in \mathcal{U} , while for evidence theory, such kind of probability is measured by two new concepts named as Belief Function $\text{Bel}(\mathcal{U})$ and Plausibility Function $\text{Pl}(\mathcal{U})$, which are defined as (Helton et al., 2010):

$$\text{Bel}(\mathcal{U}) = \sum_{\mathcal{V} \subseteq \mathcal{U}} m(\mathcal{V}) \quad (3)$$

and

$$\text{Pl}(\mathcal{U}) = \sum_{\mathcal{V} \cap \mathcal{U} \neq \emptyset} m(\mathcal{V}) \quad (4)$$

Thus, it holds that $\text{Bel}(\mathcal{U}) \leq P(\mathcal{U}) \leq \text{Pl}(\mathcal{U})$, indicating that the real value of the probability $P(\mathcal{U})$ is bounded by $\text{Bel}(\mathcal{U})$ and $\text{Pl}(\mathcal{U})$, and the gap length of this bounds

reflects the magnitude of the epistemic uncertainty on the probability $P(\mathcal{U})$. The statistical inference of an evidence theory model from a given set of evidence can be found in Sentz and Ferson (2002), and we don't give more details for simplicity.

The p -box model can be regarded as a combination of the precise probability model and the convex model. The aleatory uncertainty is characterized by the inner-loop probability model, while the epistemic uncertainty is characterized by the outer-loop convex model. The p -box model is an extension of the precise probability model. Given a probability space $(\Omega, \mathcal{F}, \mathcal{P})$, for precise probability model, the probability measure $\mathcal{P}(\mathcal{U})$ of any given event $\mathcal{U} \in \mathcal{F}$ is a precise value, and it represents the aleatory uncertainty of the variable; while for p -box model, this probability measure is no longer deterministic, but a non-deterministic value characterized by an interval/convex model, which represents the epistemic uncertainty related to this variable. The p -box models can be divided into distributional and distribution-free models, depending on whether the distribution type is assumed. For the distributional p -box model, the distribution type is exactly known, but the exact values of the distribution parameters are non-deterministic and characterized by interval-convex model, due to lack of information. An example of the distributional p -box is shown in Figure 5 (a), where the distribution type is exactly known as normal, but the mean parameter and standard deviation parameter are bounded by $[3, 7]$ and $[1, 2]$ respectively. The possible cumulative distribution function (CDF) can only be realized as a normal CDF with distribution parameters determined in the above two intervals. Figure 5 (a) shows one hundred of those possible CDFs. For the distribution-free p -box model, the distribution type is unknown, and the probability distribution function is bounded. Figure 5 (b) shows such an example, where the p -box model is bounded by the CDFs of the two probability distribution $N(3, 2^2)$ and $N(7, 1^2)$, and the CDF can be any possible CDF between these two CDFs as long as it satisfies the property of a CDF. Based on the above interpretation, one can easily find the difference between the distributional and distribution-free p -box models. In this thesis, only the distributional p -box model will be considered. In practical applications, the distributional p -box model can be inferred from data by, e.g., confidence interval estimation.

The second-order probability model can also be grouped as distributional model or distribution-free model, depending on whether the distribution type is known or not (Sankararaman and Mahadevan, 2013). Taking the distributional model as an example: The

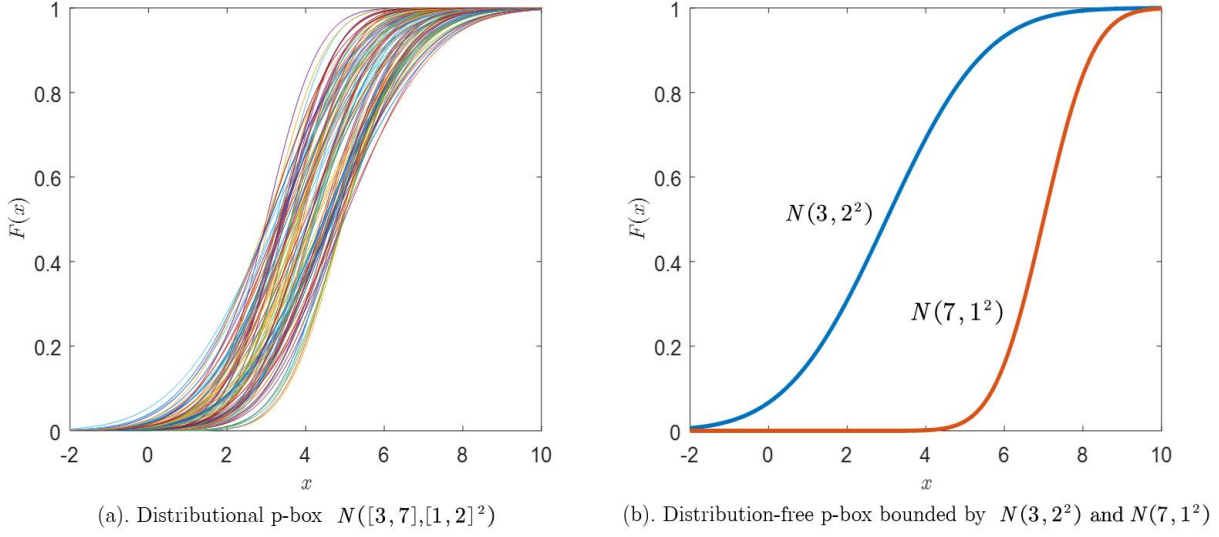


Figure 5 Illustration of distributional and distribution-free *p*-box models

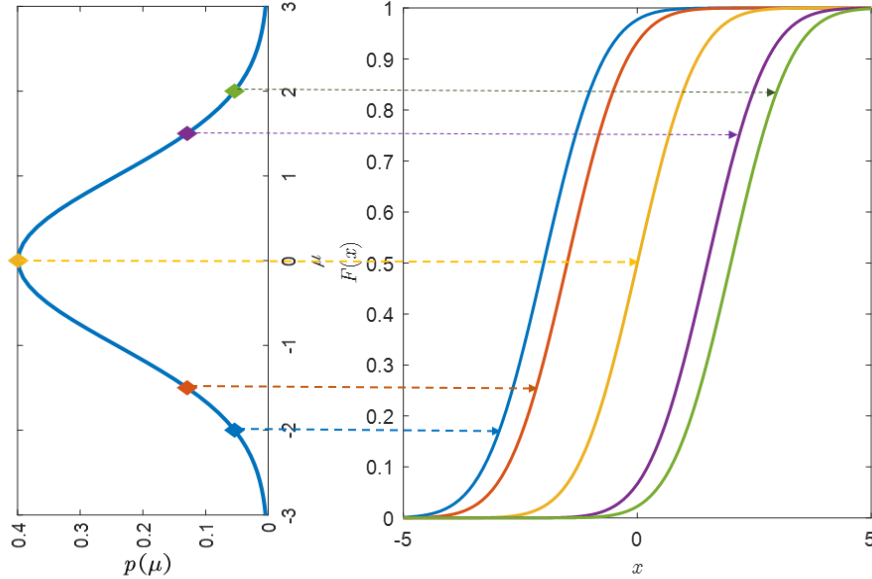


Figure 6 Illustration of the distributional second-order probability model

distribution type is exactly known, but the distribution parameters are not known, and their uncertainty is characterized by the (subjective) probability model. This subjective probability model of the distribution parameters characterizes the epistemic uncertainty related to this

variable. As an example, the distributional second-order probability model $N(\mu, 1^2)$ with $\mu \sim N(0, 1^2)$ is shown in Figure 6. The left plot shows the density $p(\mu)$ of the mean parameter μ , and its five realizations. The right plot shows the CDFs $F(x)$ of x corresponding to these five realizations of μ . Given sparse data and specified distribution type, the probability distribution of the distribution parameters can be inferred from Bayesian inference, and one can refer to Sankararaman and Mahadevan (2013) for more details.

The fuzzy probability model provides a different way of modeling the epistemic uncertainty. For distributional model, the epistemic uncertainty is characterized by the fuzzy set model of the distribution parameters, instead of the subjective probability model as used in the second-order probability model. The membership functions of these distribution parameters can also be inferred by, e.g., Bayesian inference (see, e.g., Stein et al., 2013).

The above three groups of uncertainty characterization models are widely used in many research areas, although slightly different interpretations can be given for each kind of model. In this thesis, we only consider the precise probability model, the interval model, and the distributional p -box model, but all the developments can also be extended for the other models. We assume that the precise probability model is only used for characterizing the aleatory uncertainty, the interval model is only utilized for modeling the epistemic uncertainty, and the p -box model is presented for modeling the mixed uncertainties with the epistemic uncertainty being characterized by the interval models of the distribution parameters. The above setting and assumption are consistent with most research and engineering practices, e.g., the NASA Langley UQ challenge (Patelli et al., 2014). In this challenging problem, a total number of twenty-one input variables are concerned, where four of them are characterized by precise probability models, another four are characterized by interval model, and the remaining thirteen variables are characterized by distributional p -box models. We will go into the details of this challenging problem in the next chapter. Given the above three kinds of uncertainty characterization models, the next task is how to propagate them through the computer simulators so as to quantify the mixed uncertainty of the model responses and to assess the (imprecise) reliability of the structures.

1.3. Uncertainty propagation and structural reliability

Uncertainty propagation aims at propagating the uncertainty from the input variables \mathbf{x} to the output variable y , through the computer simulator $y = g(\mathbf{x})$, so as to properly quantifying the uncertainty of output variables y . One should note that the output variable is not always univariate and time-invariant. However, in this thesis, we take such an assumption for ease of description. The reliability analysis concerns the estimation of the probability that an undesired failure event happens, where the failure event is commonly characterized by $g(\mathbf{x}) < 0$. For example, given the stress function $s(\mathbf{x})$ and strength function $r(\mathbf{x})$, the failure happens when $g(\mathbf{x}) = r(\mathbf{x}) - s(\mathbf{x}) < 0$. The sensitivity analysis aims at quantifying the contributions of the uncertainties in each input variable to those of output variables. The sensitivity indices can be used for ranking the importance of input variables, identifying the most important sources of epistemic uncertainty, and also learning the behavior of model response function $g(\mathbf{x})$. The scope of this paper is mainly on the reliability and sensitivity analysis of structures when the input variables are characterized by precise probability models, interval models, and imprecise probability models.

For reliability analysis with inputs characterized by only precise probability models, many numerical methods have been developed, and those methods can generally be grouped into four categories, i.e., (i) approximate analytical methods, (ii) stochastic simulation methods, (iii) probability conservation methods, and (iv) surrogate model methods. The approximate analytical methods (see e.g., Zhao and Ono, 1999), such as first-order reliability method (FORM) and second-order reliability method (SORM), aim at analytical deriving the failure probability based on the statistical moments of model responses, which are analytically computed based on, e.g., the Taylor series expansion of the model response function around the most probable point (MPP). The MPP is defined as the failure point of input variables with the largest probability density value, thus the areas around this point commonly account for the most probability mass for the failure probability. Those methods are extremely efficient as only derivatives need to be computed at the MPP, however, those methods are only accurate when the model response

function shows low nonlinearity around the MPP.

The stochastic simulation methods are a set of numerical integration methods based on random sampling, and the convergence of the estimators is promised by the Law of Large Number and the Central Limit Theorem. The simplest stochastic simulation technique is the Monte Carlo simulation (MCS), which involves first creating a set of random samples following the probability distribution of input variables, and then estimate the failure probability by the rate of samples contained in the failure domain. This procedure is simple and of wide applicability, but it is less efficient especially when the failure probability is low (e.g., less than 10^{-3}) and the structure simulator is expensive to estimate. For improving efficiency, plenty of advanced MCS techniques, such as the importance sampling (IS), subset simulation (SS), line sampling (LS) and directional sampling (DS), have been developed. The IS technique improves the convergence by generating random samples with man-made quasi-optimal density functions, and then estimating the failure probability by a weighting scheme (Au and Beck, 1999). The SS technique aims at introducing a set of intermediate failure surface so as to efficiently approach the real failure surface, and then estimating the failure probability based conditional probability formula (Au and Beck, 2001). The LS technique aims at searching the failure surface with a set of lines, which are all parallel to the important direction, and then estimating the probability of failure along each line by numerical interpolation, and further generating the final estimate of the failure probability by averaging the estimates across all lines (Pradlwarter et al., 2007). The performance of this method is highly dependent on the pre-specified important direction. In this thesis, the LS technique will be improved so as to substantially reduce the computational cost, especially for highly nonlinear problems, and also be extended to the situations of imprecise probabilities. The DS is also a line searching technique that aims at searching the failure domain along each line uniformly distributed in the polar coordinate system (Bjerager, 1988). There are also many works aiming at improving the above stochastic simulation techniques, but we don't review them for simplicity.

The probability conservation methods, such as the probability density evolution method (Li and Chen, 2004) and the direct probability integral method (Chen and Yang, 2019), aims at

propagating the probability distributions of the inputs to the outputs based on the law of probability conservation. The numerical implementations of those methods require the proper design of experiments in the input space such that the probability can be propagated numerically through a set of cells.

The surrogate model methods, especially those coupled with active learning and stochastic simulation, have received the most attention among the past decade. The most well-known method in this group is the so-called AK-MCS method (Echard et al., 2011), which combines the Active learning Kriging surrogate model and the MCS. The most appealing character of this procedure is that the optimal training points can be adaptively identified by the trained Kriging surrogate model so as to improve the accuracy rare of predicting the failure/functioning state for each MCS sample in the most efficient way. Many works have been published on improving the performance of AK-MCS for rare event analysis, e.g., by combining with advanced MCS procedures such as those based on IS or adaptive IS (see e.g., Dubourg et al, 2013; Balesdent et al., 2013) and SS (Wei et al., 2019c). In this thesis, the LS will be combined with AK-MCS so as to substantially improve the efficiency of rare failure event analysis.

For non-probabilistic models such as the convex model, the model responses are also characterized by the same type of non-probabilistic models, and commonly interval analysis based on, e.g., numerical optimization, is required for propagating the uncertainty models. Besides, some of the reliability analysis methods for precise probability models, such as FORM and SORM (Jiang et al., 2013) as well as AK-MCS (Yang et al., 2015), have been extended for propagating the non-probabilistic models, and numerically estimating the reliability of structures.

The uncertainty propagation and reliability analysis based on imprecise probability models have also received extensive attention among the past decade. The most straightforward way to solve this problem is to develop double-loop strategies based on those classical stochastic simulation techniques for precise probability models.

Two double-loop strategies can be developed. Take the distributional (or parameterized) *p*-box models as an example, the first strategy involves doing optimization in the outer loop by

setting the input distribution parameters as design variables, and then for each iteration, doing stochastic simulation in the inner loop so as to estimate the failure probability corresponding to the deterministic distribution parameters. There are many methods have been developed based on this strategy. For example, de Angelis et al. (2015) have developed an adaptive LS algorithm for improving the performance of the classical LS, then extended this development to the propagation of *p*-box models, by reusing the samples of input variables for specifying the important direction and estimation in each inner-loop iteration. This strategy has been applied to the NASA Langley UQ challenge (see e.g., Pedroni and Zio, 2015).

The second strategy is based on doing sampling in the outer loop so as to draw a set of interval samples for the input variables, and then in the inner loop, for each interval sample, estimating the bounds of the model response function by, e.g., intrusive finite element analysis or optimization, with which the bounds of failure probability can be estimated. There are a lot of methods that have been developed based on this strategy. For example, Zhang et al. (2013) developed the interval MCS (IMCS) method, which is based on MCS sampling in the outer loop; Alvarez et al. (2018) introduces the SS to deal with the sampling problem in this strategy so to propagate a plenty kinds of imprecise probability models; Crespo et al. (2013) studied the reliability analysis problem for polynomial systems based on the interval propagation in the inner loop. This strategy has also been applied to the NASA Langley UQ challenge (see, e.g., Patelli et al., 2015). Besides, the multi-level surrogate model methods have also been developed by using a double-loop strategy (Schöbi and Sudret, 2017).

Besides the above double-loop strategies, single-loop strategies by reusing the stochastic simulation samples with a weighting scheme have also been developed. This strategy, termed as “Extended Monte Carlo Simulation (EMCS)” has been developed in 2014 by the author and other co-authors (Wei et al., 2014) and then been also reported by Zhang and Shields (2018) with the focus of deriving the optimal density for sampling. This strategy is extremely efficient for propagating the distributional imprecise probability models since only one stochastic simulation is required, however, for the high-dimensional problem with many non-deterministic distribution parameters of inputs, the algorithm can be less effective due to the large variation of

the weight functions. To fill this gap, and largely improve the potential advantages, the author and the other co-authors have developed the *Non-intrusive Imprecise Stochastic Simulation* (NISS) methodology framework (Wei et al, 2019(a), 2019(b)), which lays the foundation of this thesis. Thus, for the readers to get easier to follow the main contents of this thesis, we briefly review the details of this methodology by taking the model response expectation E_Y as an example.

Assume that the input variables $\mathbf{x} = (x_1, x_2, \dots, x_n)$ are independent, and are characterized by *p*-box models, with density $f_{\mathbf{x}}(\mathbf{x}|\boldsymbol{\theta}) = \prod_{i=1}^n f_{X_i}(x_i|\boldsymbol{\theta}_i)$, where $f_{X_i}(x_i|\boldsymbol{\theta}_i)$ is the marginal density of x_i with nondeterministic distribution parameters $\boldsymbol{\theta}_i$. Let $\boldsymbol{\theta} = (\boldsymbol{\theta}_1, \boldsymbol{\theta}_2, \dots, \boldsymbol{\theta}_n) = (\theta_1, \theta_2, \dots, \theta_m)$ indicates the vector of all non-deterministic distribution parameters of the input variables with assumed auxiliary density $f_{\boldsymbol{\Theta}}(\boldsymbol{\theta}) = \prod_{j=1}^m f_{\Theta_j}(\theta_j)$. Then, the model response expectation E_Y is no longer constant value, but a function with respect to $\boldsymbol{\theta}$.

With high-dimensional model representation (HDMR) decomposition, the response expectation function can be decomposed as:

$$E_y(\boldsymbol{\theta}) = E_{y,0} + \sum_{i=1}^m E_{y,i}(\theta_i) + \sum_{j=i+1}^m \sum_{i=1}^{m-1} E_{y,ij}(\boldsymbol{\theta}_{ij}) + \dots + E_{y,1:m}(\boldsymbol{\theta}) \quad (5)$$

where $\boldsymbol{\theta}_{ij} = (\theta_i, \theta_j)$. There are two kinds of HDMR decomposition, i.e., the cut-HDMR and RS (Random Sampling)- HDMR. If the cut-HDMR decomposition is utilized, the induced NISS method is called local NISS, while the RS-HDMR if used, it is called global NISS. With cut-HDMR decomposition, the functional components on the right side of Eq. (5) are formulated as:

$$\begin{aligned} E_{y,\text{cut},0} &= E_y(\boldsymbol{\theta}^*) \\ E_{y,\text{cut},i}(\theta_i) &= E_y(\boldsymbol{\theta}_{-i}^*, \theta_i) - E_{y,\text{cut},0} \\ E_{y,\text{cut},ij}(\boldsymbol{\theta}_{ij}) &= E_y(\boldsymbol{\theta}_{-ij}^*, \boldsymbol{\theta}_{ij}) - E_{y,\text{cut},i} - E_{y,\text{cut},j} - E_{y,\text{cut},0} \end{aligned} \quad (6)$$

where $\boldsymbol{\theta}^*$ denotes any fixed point of $\boldsymbol{\theta}$ in its support, $\boldsymbol{\theta}_{-i}$ refers to the vector of all components of $\boldsymbol{\theta}$ except θ_i , and $\boldsymbol{\theta}_{-ij}$ indicates the vector of all elements of $\boldsymbol{\theta}$ except $\boldsymbol{\theta}_{ij}$.

If the RS-HDMR decomposition is applied in Eq. (5), the functional components are

formulated by:

$$\begin{aligned} E_{y, \text{RS}, 0} &= \mathbb{E}[E_y(\boldsymbol{\theta})] \\ E_{y, \text{RS}, i}(\theta_i) &= \mathbb{E}[E_y(\boldsymbol{\theta})|\theta_i] - E_{y, \text{RS}, 0} \\ E_{y, \text{RS}, ij}(\boldsymbol{\theta}_{ij}) &= \mathbb{E}[E_y(\boldsymbol{\theta})|\boldsymbol{\theta}_{ij}] - E_{y, \text{RS}, i} - E_{y, \text{RS}, 0} \end{aligned} \quad (7)$$

where $\mathbb{E}[\cdot|\theta_i]$ and $\mathbb{E}[E_y(\boldsymbol{\theta})|\boldsymbol{\theta}_{ij}]$ indicate the conditional expectation operator.

The basic idea of the NISS method is to first conduct a stochastic simulation for estimating the constant component $E_{y, \text{cut}, 0}$ (or $E_{y, \text{RS}, 0}$), and then with the same set of samples, to estimate the higher-order component functions $E_{y, \text{cut}, i}(\theta_i)$, $E_{y, \text{cut}, ij}(\boldsymbol{\theta}_{ij})$ (or $E_{y, \text{RS}, i}(\theta_i)$, $E_{y, \text{RS}, ij}(\boldsymbol{\theta}_{ij})$), et al. In most cases, the first two order component functions are accurate enough for approximating the response expectation function. Basically, any kind of stochastic simulation techniques can be used for the above framework. For example, in Wei et al. (2019(b)), the SS procedure is utilized for reliability analysis in both local and global NISS methods. Besides, the sensitivity indices have also been introduced for the above framework. For example, for global NISS, the sensitivity indices for the first-order and second-order component functions are defined as (Wei et al, 2019(a)):

$$S_i = \frac{\mathbb{V}[E_{y, \text{RS}, i}(\theta_i)]}{\mathbb{V}[E_y(\boldsymbol{\theta})]} \quad (8)$$

and

$$S_{ij} = \frac{\mathbb{V}[E_{y, \text{RS}, ij}(\boldsymbol{\theta}_{ij})]}{\mathbb{V}[E_y(\boldsymbol{\theta})]} \quad (9)$$

The above sensitivity indices are nothing but the classical Sobol' sensitivity indices (see, e.g., Wei et al., 2015), and can be served for three purposes. First, the sensitivity indices measure the relative contribution of each epistemic distribution parameter to the epistemic uncertainty (measured by variance) of the probabilistic responses (e.g., model response expectation), thus can be especially useful for directing the future data collection. Second, the sensitivity indices can be used for identifying the non-influential component functions which can be neglected when they are utilized for synthesizing the estimation of the probabilistic response function (e.g.,

$E_y(\boldsymbol{\theta})$). Third, the sensitivity indices can serve as a measure of truncation error when, e.g., one takes a second-order HDMR truncation for approximating the probabilistic response function. For more details on sensitivity analysis, the reader can read our review paper (Wei et al., 2015).

Given the above theoretical framework, the left key component of NISS is the numerical implementation. We take the MCS as an example to illustrate the numerical implementation of both local and global NISS. For local NISS, given a set of samples $\mathbf{x}^{(k)} (k = 1, 2, \dots, N)$ can be drawn from the precise density $f_{\mathbf{x}}(\mathbf{x}|\boldsymbol{\theta}^*)$ ^①, and by calling the black-box simulator $y = g(\mathbf{x})$, a set of response samples $y^{(k)}$ can be generated, and then the estimators for the constant, first-order and second-order cut-HDMR component functions are formulated as:

$$\begin{aligned}\hat{E}_{y,\text{cut},0} &= \frac{1}{N} \sum_{k=1}^N y^{(k)} \\ \hat{E}_{y,\text{cut},i}(\theta_i) &= \frac{1}{N} \sum_{k=1}^N y^{(k)} \frac{f_{\mathbf{x}}(\mathbf{x}^{(k)}|\boldsymbol{\theta}_{-i}^*, \theta_i)}{f_{\mathbf{x}}(\mathbf{x}^{(k)}|\boldsymbol{\theta}^*)} - \hat{E}_{y,\text{cut},0} \\ \hat{E}_{y,\text{cut},ij}(\boldsymbol{\theta}_{ij}) &= \frac{1}{N} \sum_{k=1}^N y^{(k)} \frac{f_{\mathbf{x}}(\mathbf{x}^{(k)}|\boldsymbol{\theta}_{-ij}^*, \boldsymbol{\theta}_{ij})}{f_{\mathbf{x}}(\mathbf{x}^{(k)}|\boldsymbol{\theta}^*)} - \hat{E}_{y,\text{cut},i}(\theta_i) - \hat{E}_{y,\text{cut},j}(\theta_j) - \hat{E}_{y,\text{cut},0}\end{aligned}\quad (10)$$

The above estimators are all unbiased, and their variances can be easily derived. One can refer to Wei et al. (2019(a)) for details.

For the global NISS method, a set of joint samples $(\mathbf{x}^{(k)}, \boldsymbol{\theta}^{(k)})_{k=1}^N$ can be drawn by the joint density $f_{\mathbf{x}}(\mathbf{x}|\boldsymbol{\theta})f_{\boldsymbol{\Theta}}(\boldsymbol{\theta})$ ^②, and the response samples can be computed by $y^{(k)} = g(\mathbf{x}^{(k)})$. Then, the RS-HDMR component functions in Eq. (7) can be estimated by:

$$\begin{aligned}\hat{E}_{y,\text{RS},0} &= \frac{1}{N} \sum_{k=1}^N y^{(k)} \\ \hat{E}_{y,\text{RS},i}(\theta_i) &= \frac{1}{N} \sum_{k=1}^N y^{(k)} \frac{f_{\mathbf{x}}(\mathbf{x}^{(k)}|\boldsymbol{\theta}_{-i}^{(k)}, \theta_i)}{f_{\mathbf{x}}(\mathbf{x}^{(k)}|\boldsymbol{\theta}^{(k)})} - \hat{E}_{y,\text{RS},0} \\ \hat{E}_{y,\text{RS},ij}(\boldsymbol{\theta}_{ij}) &= \frac{1}{N} \sum_{k=1}^N y^{(k)} \frac{f_{\mathbf{x}}(\mathbf{x}^{(k)}|\boldsymbol{\theta}_{-ij}^{(k)}, \boldsymbol{\theta}_{ij})}{f_{\mathbf{x}}(\mathbf{x}^{(k)}|\boldsymbol{\theta}^{(k)})} - \hat{E}_{y,\text{RS},i}(\theta_i) - \hat{E}_{y,\text{RS},j}(\theta_j) - \hat{E}_{y,\text{RS},0}\end{aligned}\quad (11)$$

The above NISS methodology provides a general framework for propagating the precise and

^① For the determination of the fixed value $\boldsymbol{\theta}^*$, one can refer to Wei et al. (2014) and Wei et al. (2019a).

^② For the auxiliary distribution $f_{\boldsymbol{\Theta}}(\boldsymbol{\theta})$, one can refer to Wei et al. (2019a) for details.

imprecise probability models, and theoretically, any stochastic simulation methods developed for precise probability models can be injected into this framework to meet specific requirements. However, it is not applicable when all the three groups of uncertainty characterization models are presented in the inputs, just as that in the NASA Langley UQ challenge. Besides, the performance of NISS for rare event analysis still needs to be improved.

2. Aims and Objectives

The aim of this thesis is on the efficient propagation of the three groups of uncertainty characterization models and the related reliability analysis problems, and the focus will be on precise probability model (Category I), interval model (Category II), and distributional *p*-box model (Category III). I assume that the precise probability model is only utilized for modeling the aleatory uncertainty, the interval model is only used for characterizing the epistemic uncertainty, and the *p*-box model is applied for modeling the mixed uncertainty, with the inner-loop probability distribution modeling and the aleatory uncertainty and the outer-loop interval models of distribution parameters characterizing the epistemic uncertainty.

The objective of this thesis is to further improve the NISS methodology so as to extend the scope of application, and to improve the performance when utilized for rare event analysis. There are three specific objectives.

- i. Generalize the NISS framework to deal with uncertainty propagation when all three categories of uncertainty characterization models are presented;
- ii. Inject the LS into the NISS framework improve its performance for rare event analysis;
- iii. Improve the LS method with active learning so as to make it efficient enough for real-world engineering applications especially when the time-consuming simulators are involved.

3. Original Contributions

The contributions of this thesis are mainly on the development of efficient numerical algorithms for reliability analysis when the input variables are characterized by the three

categories of models, i.e., the precise probability model, the interval model, and the distributional *p*-box models. The three main contributions are described as follows.

First, the global NISS method is generalized for propagating the three categories of uncertainty characterization models, by combining with the Bayes rule. All the advantages of the classical NISS method are reserved in this generalization, and both the statistical errors and truncation errors are properly addressed. The sensitivity indices are computed as by-products of the NISS method, which are shown to be especially useful for learning the relative contribution of the input epistemic uncertainty to that of failure probability or other probabilistic responses. By utilizing this development, the reliability analysis sub-problem in the NASA Langley challenge, which involves twenty-one input variables of three categories and eight failure modes, is successfully solved.

Then two strategies are developed for injecting the LS method to the local NISS framework so as to deal with the rare event analysis with input variables characterized by distribution *p*-box models. The first strategy is derived from the set of hyperplanes introduced in the classical LS method, while the second strategy is based on the one-dimensional integral along each line. Both strategies can be regarded as post-processing of the classical LS method, thus the computational cost is the same as the classical LS method. The developed methods are both shown to be suitable for problems with moderate nonlinear limit state function and small failure probability. Three engineering problems with input dimensions up to 160 are used for demonstrating the effectiveness of the two developed methods.

At last, an active learning algorithm, which combines the Gaussian Process regression (GPR) and LS, is developed for rare failure event analysis. The algorithm can automatically find the optimal training points by adding which the accuracy of LS estimation can be improved the most. Both toy and engineering examples are introduced for demonstrating the advantages of this algorithm. It is shown that the algorithm makes the best use of the high efficiency of one-dimensional search of the LS method, and the spatial correlation information revealed by the GPR model, thus it is extremely efficient for rare event analysis with even highly nonlinear limit state function.

The above three original contributions have largely improved the efficiency and engineering applicability of the classical NISS and LS methods for mixed uncertainty propagation and reliability analysis, thus are of significance for uncertainty quantification as well as risk and reliability analysis when the available information is imperfect.

4. Structure of the Thesis

This dissertation is composed of three journal articles. Each article deals with a different aspect of the uncertainty propagation and reliability analysis, and is tightly related to each other.

The first research article develops the generalized NISS method for dealing with the propagation of the three categories of uncertainty characterization models (i.e., the precise probability model, the interval model and the distributional *p*-box model) simultaneously in a unified framework, and for solving the related reliability analysis problem. The NASA Langley UQ challenge is also solved by the developed method in this article.

In the second article, two strategies are developed to improve the suitability of the NISS methodology for rare vent analysis. Two different interpretations are firstly introduced for the classical LS algorithm, then based on these two interpretations, two strategies are developed for injecting the LS method into the NISS framework. The effectiveness of these two algorithms for solving engineering problems is also demonstrated in this article.

To further improve the efficiency of LS method for rare event analysis involving computationally expensive computer simulators, the third article presents an active learning algorithm combining the advantages of both GPR model and LS method. This algorithm allows estimating the extremely small failure probability at a very low cost.

Research article 1: Generalization of non-intrusive imprecise stochastic simulation for mixed uncertain variables

This is the first phase of this thesis, which aims at generalizing the Non-intrusive Imprecise Stochastic Simulation (NISS) for the general uncertainty propagation problems with all three categories of uncertainty characterization models, i.e., the precise probability model (category I), the non-probabilistic interval model (category II) and the imprecise probability models (category III). As has been mentioned in the Introduction part of this thesis, the NISS framework is originally developed for propagating the category I and category III, where both are used for modeling the random input variables, except that the category III models also incorporates the epistemic uncertainty. In practical engineering applications, the computer simulators may also include deterministic-but-unknown inputs, and it is natural to use the non-probabilistic models such as convex/interval models and fuzzy set model. Thus, to improve the wide applicability of the NISS methods, it is necessary to extend it to the cases with all the three categories of input uncertainty characterization models. A direct example of this engineering scenario is the NASA Langley uncertainty quantification (UQ) challenge to be solved in this chapter. In this challenge, a total number of twenty-one input variables are involved, where four inputs are characterized by category I model, four other inputs are characterized by category II model, and the remaining thirteen inputs are characterized by category III models. The computer simulator of this system consists of five fixed disciplinary black-box simulators and eight cross-disciplinary black-box simulators, thus the involved uncertainty propagation problem can be quite computationally challenging. We take this challenge as a motivation to develop the generalized NISS method. In accordance with this challenge, we only consider the

interval model as an example of the category II models, and the distributional *p*-box model as an example of the category III models.

With the above setting, the epistemic uncertainty is characterized by the interval models of category II inputs, and the interval models of the distribution parameters of the category III inputs. We then take the failure probability estimation as an example to illustrate the developed NISS method. This method involves three ingredients. First, for the epistemic parameters (category II inputs and the distribution parameters of category III inputs), auxiliary probability distribution needs to be assumed in advance, and with the toy example, we illustrate the influence by assuming different types of auxiliary distribution. Second, Bayes rule is introduced to formulate the failure probability function with respect to the category II as the ratio of the conditional and unconditional density function. Third, the kernel density function is utilized for estimating the conditional density function. Similar to the original NISS, the truncation error due to HDMR truncation is measured by the sensitivity indices, and the statistical errors are quantified by the coefficient of variation of the NISS estimators. At last, a toy example and the NASA challenge are used for demonstrating the proposed method.

Although we only consider the estimation of the failure probability, it can be easily extended for estimating the other quantities of interest, such as the bounds of the cumulative distribution function of the model response. With the above development, the NISS framework is largely enriched, thus can be more applicable to real-world engineering problems.

Generalization of non-intrusive imprecise stochastic simulation for mixed uncertain variables

Jingwen Song^{a,d}, Pengfei Wei^{b, d,*}, Marcos Valdebenito^c, Sifeng Bi^d, Matteo Broggi^d, Michael Beer^{d,e,f}, Zuxiang Lei^g

^a School of Aeronautics, Northwestern Polytechnical University, Xi'an 710072, China

^b School of Mechanics, Civil Engineering and Architecture, Northwestern Polytechnical University, Xi'an 710072, China

^c Departamento de Obras Civiles, Universidad Tecnica Federico Santa Maria, Av. Espana 1680, Valparaiso, Chile

^d Institute for Risk and Reliability, Leibniz Universität Hannover, Callinstr. 34, Hannover, Germany

^e Institute for Risk and Uncertainty, University of Liverpool, Peach Street, L69 7ZF Liverpool, United Kingdom

^f International Joint Research Center for Engineering Reliability and Stochastic Mechanics, Tongji University, Shanghai 200092, China

^g Institute of Geotechnical Engineering, School of Civil Engineering and Architecture, East China Jiaotong University, Nanchang 330013, China

Published in Mechanical Systems and Signal Processing in December 2019

Abstract: Non-intrusive Imprecise Stochastic Simulation (NISS) is a recently developed general methodological framework for efficiently propagating the imprecise probability models and for estimating the resultant failure probability functions and bounds. Due to the simplicity, high efficiency, stability and good convergence, it has been proved to be one of the most appealing forward uncertainty quantification methods. However, the current version of NISS is only applicable for model with input variables characterized by precise and imprecise probability models. In real-world applications, the uncertainties of model inputs may also be characterized by non-probabilistic models such as interval model due to the extreme scarcity or imprecise

information. In this paper, the NISS method is generalized for models with three kinds of mixed inputs characterized by precise probability model, non-probabilistic models and imprecise probability models respectively, and specifically, the interval model and distributional *p*-box model are exemplified. This generalization is realized by combining Bayes rule and the global NISS method, and is shown to conserve all the advantages of the classical NISS method. With this generalization, the three kinds of inputs can be propagated with only one set of function evaluations in a pure simulation manner, and two kinds of potential estimation errors are properly addressed by sensitivity indices and bootstrap. A numerical test example and the NASA uncertainty quantification challenging problem are solved to demonstrate the effectiveness of the generalized NISS procedure.

Keywords: Non-intrusive imprecise stochastic simulation; Uncertainty quantification; Non-probabilistic; Imprecise probability; Sensitivity; Bayes rule; Interval model; Bootstrap

1. Introduction

Uncertainty quantification (UQ) has been widely accepted as an important task in a variety of research and engineering fields. For example, in the analysis and design of large civil engineering systems, the uncertainties presented in system excitations (e.g., caused by natural disasters such as earthquake and flood), material properties, degradation process modeling, etc., are quite substantial and have to be carefully treated. Commonly, there are two kinds of uncertainties, i.e., aleatory uncertainty and epistemic uncertainty [1], while the former one is due to the intrinsic random property of parameters or events, thus cannot be reduced by collecting more information, and the later one is caused by the incompleteness of knowledge, and can be reduced by further collecting information. The above two kinds of uncertainties may appear alone, but in most real-world applications, may occur simultaneously. Characterization of the above two kinds of uncertainties with mathematical models is the first key problem of UQ.

Generally, three groups of uncertainty characterization models have been developed, i.e., the precise probability model, the non-probabilistic models [2][3], and the imprecise probability models [4]. The precise probability model (Category I) is the most classical uncertainty model,

and is commonly used for characterizing the aleatory uncertainty, which usually requires a large number of data of good quality. The non-probabilistic models (Category II), including interval/convex model, fuzzy set theory, etc., can be especially useful for characterizing the imprecision of constant-but-unknown variables or for situations that the available data for random variables is extremely scarce/incomplete/imprecise [3]. As the level of knowledge increases, the interval model will degrade into its true value. The imprecise probability models (Category III), such as probability-box (p -box), evidence theory and fuzzy probability model, can be regarded as the combination of the former two kinds of models, and can be especially useful for separately characterizing the two kinds of uncertainty in a unified model framework [4]. As the volume of available information increases, the category III model will shrink to the true cumulative distribution function (CDF). The roles of three categories of characterization models are shown in Figure 1.

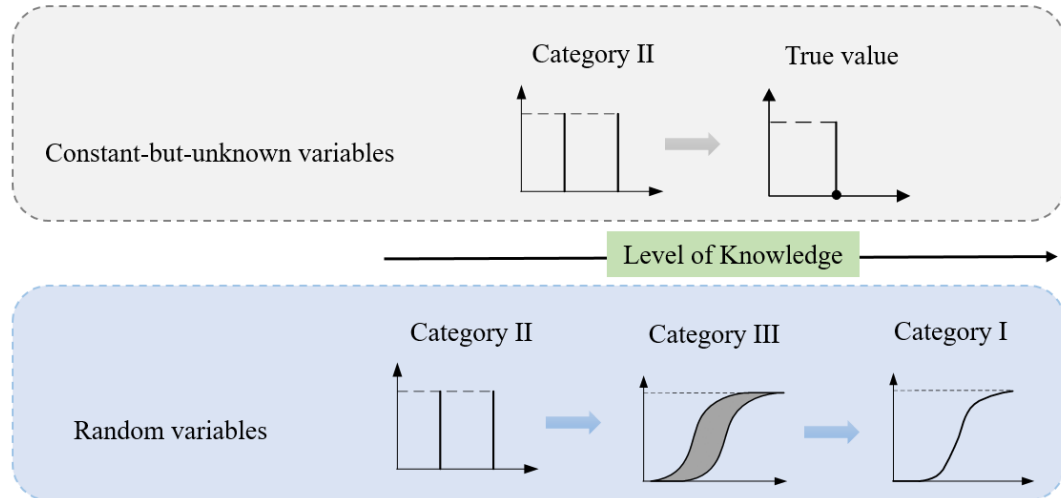


Figure 1 The roles of the three categories of characterization models in UQ.

The second key problem is the propagation of the characterization models through the computational models so as to quantify the uncertainties of the model responses, and to assess the reliability of the systems. This has been a quite big challenge especially when all the three categories of characterization models are present as model inputs. For example, in the NASA multidisciplinary Langley UQ challenge [5], the subproblem of uncertainty propagations involves

21 inputs variables characterized by the three categories of models. Propagation of the category I model has been widely studied, and a plenty of methods, such as probability density evaluation [6], importance sampling [7], subset simulation [8], line sampling [9] and active learning based surrogate model methods [10], have been developed, and shown to be effective for real-world applications. The propagation of Category II models has also been studied, and the current methods are mainly driven by optimization algorithms [2][3], which are commonly computationally expensive especially for problems with non-convex response functions and high-dimensional inputs.

The propagation of category III models is generally a double-loop process, and several strategies have been developed. The simplest procedure is to perform optimization for distribution parameters in the outer loop and then propagate the degraded category I model in the inner loop with, e.g., precise stochastic simulation method [11]. This strategy has been applied to the NASA Langley challenge with the utilization of genetic algorithm for outer loop optimization and Monte Carlo simulation for the inner loop analysis [12]. The second strategy is based on sampling in the outer loop so as to generate a set of interval samples for input variables, and then propagate each interval sample in the inner loop by, e.g., interval finite element analysis or optimization algorithms [13]-[15]. This strategy has been recently extended to problems with spatial/time-variant inputs [16]-[18]. The third strategy involves generating a set of samples for input variables, and then estimating the performance values (e.g., failure probability) w.r.t. different values of the distribution parameters of category III models based on a weighting scheme. This strategy, termed as “Extended Monte Carlo simulation”, was originally developed in Ref. [19], and was strengthened in Ref. [20]. Although being efficient, it does not perform well for problems with high-dimensional inputs. To overcome the above shortcoming, a new methodology framework, termed as “Non-intrusive Imprecise Stochastic Simulation (NISS)”, has been developed in a set of companion paper [21][22], and two groups of methods, i.e., the local NISS methods and the global NISS methods, have been presented. The NISS framework owns many advantages. It is applicable for high-dimensional problems with numerical estimation errors being properly addressed, and meanwhile, provides good balance for local and

global performances. Any precise stochastic simulation such as subset simulation and line sampling can be injected into this framework so as to properly address different types of problems, and the sensitivity information of the epistemic uncertainty is generated as a byproduct. Besides, the NISS framework avoids performing optimization on the model response functions, thus can properly address problems with even non-convex response functions. However, the current version of NISS is only applicable for problems with inputs characterized by category I and category III models.

The aim of this paper is to generalize NISS to the situation where all the three categories of characterization models are involved, and specifically, the interval model in category II and the distributional p -box model in category III are concerned. The generalization is realized based on Bayes rule and the global NISS method, and is shown to own all the advantages of the original NISS method. The truncation errors as well as the influential component functions are identified by the Sobol' sensitivity indices, and the statistical errors are quantified by bootstrap scheme. The proposed method is demonstrated by a toy test example, and is then applied to solve the reliability analysis subproblem of the NASA Langley UQ challenge.

The rest of this paper is organized as follows. Section 2 gives briefly reviews the NISS method, followed by the generalization of NISS in section 3. In section 4, the toy test example and the NASA Langley UQ challenge are introduced to demonstrate the proposed method. Section 5 gives conclusions and useful discussions.

2. Brief review of NISS

In this section, we briefly review the classical NISS method for propagating imprecise probability models, and specifically, for distributional p -box model. Let $\mathbf{x} = (x_1, x_2, \dots, x_n)^T$ denote the n -dimensional vector of random input variables with joint probability density function (PDF) $f_{\mathbf{x}}(\mathbf{x}|\boldsymbol{\theta})$, where $\boldsymbol{\theta} = (\theta_1, \theta_2, \dots, \theta_d)^T$ refers to the d -dimensional vector of non-deterministic distribution parameters, each θ_i of which is assumed to be an interval parameter with support $[\underline{\theta}_i, \bar{\theta}_i]$. Let $\underline{\boldsymbol{\theta}} = (\underline{\theta}_1, \underline{\theta}_2, \dots, \underline{\theta}_d)^T$ and $\bar{\boldsymbol{\theta}} = (\bar{\theta}_1, \bar{\theta}_2, \dots, \bar{\theta}_d)^T$. With this p -box model, the aleatory uncertainty of \mathbf{x} is characterized by its joint PDF, while the

epistemic uncertainty subjected to incomplete knowledge is represented by the hyper-rectangle support of $\boldsymbol{\theta}$. In real-world applications, the support of $\boldsymbol{\theta}$ can be estimated by confidence interval estimation procedure, and as the data volume of \mathbf{x} increases, the support of $\boldsymbol{\theta}$ will shrink, indicating the reduction of epistemic uncertainty. With enough data, the support of $\boldsymbol{\theta}$ shrinks into a fixed point, and then the p -box model degrades into a precise probability model characterizing only aleatory uncertainty. Without loss of generality, we assume that the input variables are independent, and their joint PDF can be expressed as $f_{\mathbf{X}}(\mathbf{x}|\boldsymbol{\theta}) = \prod_{i=1}^n f_{X_i}(x_i|\boldsymbol{\theta}_i)$, where $f_{X_i}(x_i|\boldsymbol{\theta}_i)$ implies the marginal PDF of x_i , and $\boldsymbol{\theta}_i = (\theta_{i1}, \theta_{i2}, \dots, \theta_{id_i})^T$ indicates the d_i -dimensional vector of the distribution parameters of x_i . For performing the global NISS procedure, an auxiliary PDF $f_{\Theta}(\boldsymbol{\theta})$ should be introduced. In this paper, we assume that each θ_i follows independent uniform distribution within its respective support $[\underline{\theta}_i, \bar{\theta}_i]$, and the marginal PDF is denoted as $f_{\Theta_i}(\theta_i)$.

Let $g(\mathbf{x})$ indicate the model response function (also called limit state function for reliability analysis, or simply g -function) of the computational model. In this paper, only one-dimensional response is exemplified for illustrating the proposed method. We define a sub-domain of input space as $Z(z) = \{\mathbf{x}: g(\mathbf{x}) < z\}$, and then the indicator function corresponding to this sub-domain can be defined as $I_Z(\mathbf{x}) = 1$ if $\mathbf{x} \in Z(z)$; else $I_Z(\mathbf{x}) = 0$. For reliability analysis, we assume that the failure happens when the model response is less than zero. Then the failure domain can be defined as $F = Z(0)$, and the corresponding indicator function of F is defined as $I_F(\mathbf{x}) = 1$ if $\mathbf{x} \in F$; else $I_F(\mathbf{x}) = 0$. Based on the above definition, the CDF of the model response w.r.t $\boldsymbol{\theta}$ can be formulated as:

$$D_Z(z|\boldsymbol{\theta}) = \mathbb{E}_{\mathbf{X}}[I_Z(\mathbf{x})] = \int_{\mathbf{R}^n} I_Z(\mathbf{x}) f_{\mathbf{X}}(\mathbf{x}|\boldsymbol{\theta}) d\mathbf{x} \quad (1)$$

, where $\mathbb{E}_{\mathbf{X}}(\cdot)$ indicates the expectation operator w.r.t. \mathbf{x} . The failure probability function can then be derived as $P_f(\boldsymbol{\theta}) = D_Z(0|\boldsymbol{\theta})$.

The NISS methods are developed based on high-dimensional model representation (HDMR) decomposition of $D_Z(z|\boldsymbol{\theta})$ w.r.t. $\boldsymbol{\theta}$, where the local NISS methods are based on cut-HDMR

decomposition and the global ones are devised from random sampling (RS)-HDMR decomposition [23]. Here only the simplest global NISS method is reviewed since only this method will be generalized. The RS-HDMR decomposition of $D_Z(z|\boldsymbol{\theta})$ reads:

$$D_Z(z|\boldsymbol{\theta}) = D_{Z,0}(z) + \sum_{1 \leq i \leq d} D_{Z,\Theta_i}(z|\theta_i) + \sum_{1 \leq i < j \leq d} D_{Z,\Theta_{ij}}(z|\boldsymbol{\theta}_{ij}) + \dots + D_{Z,\Theta}(z|\boldsymbol{\theta}) \quad (2)$$

, where $\boldsymbol{\theta}_{ij} = (\theta_i, \theta_j)^T$, and the constant component as well as the first two order component functions are formulated as:

$$\begin{aligned} D_{Z,0}(z) &= E_{\boldsymbol{\theta}}[D_Z(z|\boldsymbol{\theta})] \\ D_{Z,\Theta_i}(z|\theta_i) &= E_{\Theta_{-i}}[D_Z(z|\boldsymbol{\theta})] - D_{Z,0} \\ D_{Z,\Theta_{ij}}(z|\boldsymbol{\theta}_{ij}) &= E_{\Theta_{-ij}}[D_Z(z|\boldsymbol{\theta})] - D_{Z,\Theta_i} - D_{Z,\Theta_j} - D_{Z,0} \end{aligned} \quad (3)$$

In Eq. (3), $E_{\boldsymbol{\theta}}[\cdot]$ indicates the expectation operator w.r.t. $\boldsymbol{\theta}$, $E_{\Theta_{-i}}[\cdot]$ is the expectation operator w.r.t. the $(d-1)$ -dimensional vector $\boldsymbol{\theta}_{-i}$ consisting of all the elements of $\boldsymbol{\theta}$ but θ_i , and $E_{\Theta_{-ij}}[\cdot]$ refers to the expectation operator w.r.t. $\boldsymbol{\theta}_{-ij}$, which consists of all the components of $\boldsymbol{\theta}$ but $\boldsymbol{\theta}_{ij}$. The expectation of each component other than $D_{Z,0}$ equals to zero, and are mutually orthogonal.

Given a set of joint samples $\{\mathbf{x}^{(k)}, \boldsymbol{\theta}^{(k)}\}_{k=1,2,\dots,N}$ following $f_{\mathbf{x}}(\mathbf{x}|\boldsymbol{\theta})f_{\boldsymbol{\theta}}(\boldsymbol{\theta})$, the NISS estimators of the RS-HDMR components are given as:

$$\begin{aligned} \hat{D}_{Z,0}(z) &= \frac{1}{N} \sum_{k=1}^N I_Z(\mathbf{x}^{(k)}) \\ \hat{D}_{Z,\Theta_i}(z|\theta_i) &= \frac{1}{N} \sum_{k=1}^N I_Z(\mathbf{x}^{(k)}) r_{\Theta_i}(\theta_i|\mathbf{x}^{(k)}, \boldsymbol{\theta}^{(k)}) \\ \hat{D}_{Z,\Theta_{ij}}(z|\boldsymbol{\theta}_{ij}) &= \frac{1}{N} \sum_{k=1}^N I_Z(\mathbf{x}^{(k)}) r_{\Theta_{ij}}(\boldsymbol{\theta}_{ij}|\mathbf{x}^{(k)}, \boldsymbol{\theta}^{(k)}) \end{aligned} \quad (4)$$

, where

$$\begin{aligned} r_{\Theta_i}(\theta_i|\mathbf{x}^{(k)}, \boldsymbol{\theta}^{(k)}) &= \frac{f_{\mathbf{x}}(\mathbf{x}^{(k)}|\theta_i, \boldsymbol{\theta}_{-i}^{(k)})}{f_{\mathbf{x}}(\mathbf{x}^{(k)}|\boldsymbol{\theta}^{(k)})} - 1 \\ r_{\Theta_{ij}}(\boldsymbol{\theta}_{ij}|\mathbf{x}^{(k)}, \boldsymbol{\theta}^{(k)}) &= \frac{f_{\mathbf{x}}(\mathbf{x}^{(k)}|\boldsymbol{\theta}_{ij}, \boldsymbol{\theta}_{-ij}^{(k)})}{f_{\mathbf{x}}(\mathbf{x}^{(k)}|\boldsymbol{\theta}^{(k)})} - \frac{f_{\mathbf{x}}(\mathbf{x}^{(k)}|\theta_j, \boldsymbol{\theta}_{-j}^{(k)})}{f_{\mathbf{x}}(\mathbf{x}^{(k)}|\boldsymbol{\theta}^{(k)})} - \frac{f_{\mathbf{x}}(\mathbf{x}^{(k)}|\theta_j, \boldsymbol{\theta}_{-j}^{(k)})}{f_{\mathbf{x}}(\mathbf{x}^{(k)}|\boldsymbol{\theta}^{(k)})} + 1 \end{aligned} \quad (5)$$

The above estimators are all unbiased, and their variances can be easily derived, as shown in Ref. [21]. One should note that the ratio function in Eq. (5) are derived based on the

assumption that the auxiliary distributions of $\boldsymbol{\theta}$ are all uniform. If non-uniform distribution is assumed, the ratio functions are still made of density functions, but the formulations will be different.

The accuracy of NISS may also be affected by the RS-HDMR truncation, and as indicated in Refs. [21] and [24], the truncation errors can be subtly assessed by the Sobol' sensitivity indices. Due to the orthogonality of the RS-HDMR component functions, taking variance to both side of Eq. (2) yields [24][25]:

$$\text{var}[D_z(z|\boldsymbol{\theta})] = \sum_{1 \leq i \leq d} \text{var}[D_{z,\Theta_i}(z|\theta_i)] + \sum_{1 \leq i < j \leq d} \text{var}[D_{z,\Theta_{ij}}(z|\boldsymbol{\theta}_{ij})] + \dots + \text{var}[D_{z,\Theta}(z|\boldsymbol{\theta})] \quad (6)$$

Based on the above variance decomposition, the Sobol' sensitivity index can be defined for each component function. For the first- and second-order component functions, the Sobol' indices are defined as [25][26]:

$$S_{\Theta_i} = \frac{\text{var}[D_{z,\Theta_i}(z|\boldsymbol{\theta}_i)]}{\text{var}[D_z(z|\boldsymbol{\theta})]} \quad (7)$$

and

$$S_{\Theta_{ij}} = \frac{\text{var}[D_{z,\Theta_{ij}}(z|\boldsymbol{\theta}_{ij})]}{\text{var}[D_z(z|\boldsymbol{\theta})]} \quad (8)$$

The Sobol' indices for higher order component functions can be similarly defined. These sensitivity indices can be easily computed by numerically integrating the NISS estimators in Eq. (4). In the classical global NISS procedure, the Sobol' indices are served for three purposes. As the Sobol' indices measure the relative importance of each RS-HDMR component function, the component functions with very small values of Sobol' indices can be neglected while synthesizing the estimate of failure probability function. Based on the interpretation of Sobol' indices, the first-order index S_i measures the contribution of the epistemic uncertainty of θ_i to the epistemic uncertainty of response CDF, and the second-order index $S_{\Theta_{ij}}$ measures the second-order interaction contribution between θ_i and θ_j . Thereof, the Sobol' indices can also be used for identifying the main sources of epistemic uncertainty present in model response CDF,

thus can be especially useful for further collecting information and for specifying the important parameters to be calibrated in inverse uncertainty quantification. Besides, $1 - \sum_{1 \leq i \leq d} S_{\Theta_i} - \sum_{1 \leq i < j \leq d} S_{\Theta_{ij}}$ measures the truncation error of the second-order RS-HDMR decomposition. If this value is less than a pre-specified threshold (say 0.03), it is asserted that the truncation error is small.

For reliability and rare event analysis, the subset simulation as well as active learning procedure have both been injected into the NISS framework, and shown to be effective and of wide applicability [22]. The main drawback of the above NISS method is the inapplicability to category II models. In the next section, we discuss the necessity of the generalization of NISS for mixed uncertain variables, and then develop a simple but effective strategy for realizing the generalization.

3. Generalization of NISS

3.1 Discussions on non-probabilistic models

Aside for the precise and imprecise probability models, several non-probabilistic models, such as interval/convex models [2][3], fuzzy set theory [2][27], and possibility theory derived from fuzzy sets [27], have also been developed for characterizing uncertainty. In this paper, we take the independent interval model of category II as an example. The non-probabilistic models are important complements to the precise and imprecise probability models in the following two situations.

- **Situation 1: constant-but-unknown variable.** In this situation, we know that the variable under consideration is a constant, but due to measurement error, ambiguity, subjective of expert opinion, etc., we don't know the exact value of this constant. The available information is a collection of intervals. Based on this assumption, the variable has only epistemic uncertainty, which should be characterized by the intersection of this collection of intervals under the assumption that each interval includes the true value of the variable. A typical example of this situation is the reliability analysis of existing structures. The dimension and material property parameters of an existing structure are

unquestionably deterministic, but due to measurement errors, these parameters should be modeled as interval variables.

- **Situation 2: random variable subjected to extreme lack of information.** In this situation, the variable under consideration is a random variable, but due to the extreme lack of information, we cannot generate a proper imprecise probability model with confidence. In this situation, both aleatory and epistemic uncertainties are present, but as the epistemic uncertainty is dominant, it is better to model the variable with non-probabilistic models such as interval model. This situation often occurs in the design of future structures when new materials are utilized, and we have only small number of inaccurate experimental data (modeled by intervals) on the material property parameters. We can simply model the uncertainty of the parameter by the union of the collected intervals.

Otherwise, if the amount and quality of the available data for a random variable allow us to model its aleatory and epistemic uncertainties with imprecise probability models, we'd better use the imprecise probability models since they are more informative. The above two situations are schematically illustrated in Figure 1.

In practical applications, the three categories of input variables, i.e., the non-probabilistic variables, the imprecise random variables and the precise random variables, may exist simultaneously in the same analysis task, and it is necessary to extend the NISS method to such situation. In the next subsection, we present the generalization.

3.2 The developed method

Let the m -dimensional independent interval variables denote by $\mathbf{y} = (y_1, y_2, \dots, y_m)^T$ with hyper-rectangular support $[\underline{\mathbf{y}}, \bar{\mathbf{y}}] = \times_{i=1}^m [\underline{y}_i, \bar{y}_i]$, where \times indicates the Cartesian product, $[\underline{y}_i, \bar{y}_i]$ is the support of y_i with $\bar{y}_i > y_i$, $\underline{\mathbf{y}} = (\underline{y}_1, \underline{y}_2, \dots, \underline{y}_m)^T$ is the vector of the lower bounds, and $\bar{\mathbf{y}} = (\bar{y}_1, \bar{y}_2, \dots, \bar{y}_m)^T$ is the vector of upper bounds. Then, the model response function is written as $g(\mathbf{x}, \mathbf{y})$, and the indicator function $I_Z(\mathbf{x}, \mathbf{y})$ and $I_F(\mathbf{x}, \mathbf{y})$ can be similarly defined. In this section, we take the failure probability function $P_f(\boldsymbol{\theta}, \mathbf{y})$ as an

example to discuss the generalization of NISS. By definition, the failure probability function is formulated as:

$$P_f(\boldsymbol{\theta}, \mathbf{y}) = E_{\mathbf{x}}[I_F(\mathbf{x}, \mathbf{y})] = \int_{\mathbf{R}^n} I_F(\mathbf{x}, \mathbf{y}) f_{\mathbf{x}}(\mathbf{x}|\boldsymbol{\theta}) d\mathbf{x} \quad (9)$$

With the above setting, the epistemic uncertainties of model inputs are characterized by the hyper-rectangles $\boldsymbol{\theta} \in [\underline{\boldsymbol{\theta}}, \bar{\boldsymbol{\theta}}]$ and $\mathbf{y} \in [\underline{\mathbf{y}}, \bar{\mathbf{y}}]$. Similarly, for implementing the global NISS method, we need to attribute an auxiliary distribution for each y_i . Without loss of generality, we assume that each y_i follows independent uniform distribution, and denote the corresponding marginal PDF as $f_{Y_i}(y_i)$, and the joint PDF as $f_{\mathbf{Y}}(\mathbf{y}) = \prod_{i=1}^m f_{Y_i}(y_i)$. The effects of the auxiliary distribution will be discussed later.

With RS-HDMR, the failure probability function $P_f(\boldsymbol{\theta}, \mathbf{y})$ can be decomposed as:

$$\begin{aligned} P_f(\boldsymbol{\theta}, \mathbf{y}) &= P_{f,0} + \sum_{1 \leq i \leq d} P_{f,\Theta_i}(\theta_i) + \sum_{1 \leq i < j \leq d} P_{f,\Theta_{ij}}(\boldsymbol{\theta}_{ij}) + \sum_{1 \leq i \leq m} P_{f,Y_i}(y_i) \\ &\quad + \sum_{1 \leq i < j \leq m} P_{f,\mathbf{Y}_{ij}}(\mathbf{y}_{ij}) + \sum_{1 \leq i \leq d, 1 \leq j \leq m} P_{f,\Theta_i, Y_j}(\theta_i, y_j) + \dots + P_{f,\Theta, \mathbf{Y}}(\boldsymbol{\theta}, \mathbf{y}) \end{aligned} \quad (10)$$

where

$$\begin{aligned} P_{f,0} &= E_{\boldsymbol{\Theta}, \mathbf{Y}}[P_f(\boldsymbol{\theta}, \mathbf{y})] \\ P_{f,\Theta_i}(\theta_i) &= E_{\boldsymbol{\Theta}_{-i}, \mathbf{Y}}[P_f(\boldsymbol{\theta}, \mathbf{y})] - P_{f,0} \\ P_{f,\Theta_{ij}}(\boldsymbol{\theta}_{ij}) &= E_{\boldsymbol{\Theta}_{-ij}, \mathbf{Y}}[P_f(\boldsymbol{\theta}, \mathbf{y})] - P_{f,\Theta_i} - P_{f,\Theta_j} - P_{f,0} \\ P_{f,Y_i}(y_i) &= E_{\boldsymbol{\Theta}, \mathbf{Y}_{-i}}[P_f(\boldsymbol{\theta}, \mathbf{y})] - P_{f,0} \\ P_{f,\mathbf{Y}_{ij}}(\mathbf{y}_{ij}) &= E_{\boldsymbol{\Theta}, \mathbf{Y}_{-ij}}[P_f(\boldsymbol{\theta}, \mathbf{y})] - P_{f,Y_i} - P_{f,Y_j} - P_{f,0} \\ P_{f,\Theta_i, Y_j}(\theta_i, y_j) &= E_{\boldsymbol{\Theta}_{-i}, \mathbf{Y}_{-j}}[P_f(\boldsymbol{\theta}, \mathbf{y})] - P_{f,\Theta_i} - P_{f,Y_j} - P_{f,0} \end{aligned} \quad (11)$$

, and $E_{\boldsymbol{\Theta}, \mathbf{Y}}[\cdot]$ indicates the expectation operator w.r.t. both $\boldsymbol{\theta}$ and \mathbf{y} , $E_{\boldsymbol{\Theta}_{-i}, \mathbf{Y}}[\cdot]$ refers to the expectation taken w.r.t. $\boldsymbol{\theta}_{-i}$ and \mathbf{y} , etc.

For estimating the RS-HDMR component functions in Eq. (11), we need first to generate a joint sample set $S = \{(\mathbf{x}^{(k)}, \boldsymbol{\theta}^{(k)}, \mathbf{y}^{(k)})\}_{k=1,2,\dots,N}$ following joint PDF $f_{\mathbf{x}}(\mathbf{x}|\boldsymbol{\theta})f_{\boldsymbol{\Theta}}(\boldsymbol{\theta})f_{\mathbf{Y}}(\mathbf{y})$. As $(\mathbf{x}, \boldsymbol{\theta})$ is independent of \mathbf{y} , their samples can be generated independently, and the procedure is given as follows.

- **Generation of joint samples for $(\mathbf{x}, \boldsymbol{\theta})$** . Generate a sample matrix

$\mathbf{U} = (u_{ki})_{k=1, \dots, N, i=1, \dots, (n+d)}$ with N rows and $(n+d)$ columns by, e.g., Latin hypercube sampling, each column of which follows independent uniform distribution between 0 and 1; Then, generate the sample $\theta_i^{(k)}$ for each θ_i by $\theta_i^{(k)} = D_{\Theta_i}^{-1}(u_{k(n+i)})$, where $D_{\Theta_i}^{-1}(\cdot)$ indicates the inverse CDF of θ_i ; At last, create the sample $x_i^{(k)} = D_{X_i}^{-1}(u_{ki}|\theta_i^{(k)})$, where $D_{X_i}^{-1}(\cdot|\theta_i^{(k)})$ is the inverse CDF of x_i with its distribution parameters fixed at $\theta_i^{(k)}$.

- **Generation of samples for \mathbf{y} .** Generate a sample matrix $\mathbf{V} = (v_{ki})_{k=1, \dots, N, i=1, \dots, m}$, each column of which is independently and uniformly distributed between 0 and 1; Then, compute the sample $y_i^{(k)}$ for each y_i by $y_i^{(k)} = D_{Y_i}^{-1}(v_{ki})$, where $D_{Y_i}^{-1}(\cdot)$ is the inverse CDF of y_i .

The NISS estimators of the component functions $P_{f,0}$, $P_{f,\Theta_i}(\theta_i)$ and $P_{f,\Theta_{ij}}(\theta_{ij})$ in Eq. (11) are similar to those in Eq. (4), and are formulated as:

$$\begin{aligned}\hat{P}_{f,0} &= \frac{1}{N} \sum_{k=1}^N I_F(\mathbf{x}^{(k)}, \mathbf{y}^{(k)}) \\ \hat{P}_{f,\Theta_i}(\theta_i) &= \frac{1}{N} \sum_{k=1}^N I_F(\mathbf{x}^{(k)}, \mathbf{y}^{(k)}) r_{\Theta_i}(\theta_i | \mathbf{x}^{(k)}, \boldsymbol{\theta}^{(k)}) \\ \hat{P}_{f,\Theta_{ij}}(\theta_{ij}) &= \frac{1}{N} \sum_{k=1}^N I_F(\mathbf{x}^{(k)}, \mathbf{y}^{(k)}) r_{\Theta_{ij}}(\theta_{ij} | \mathbf{x}^{(k)}, \boldsymbol{\theta}^{(k)})\end{aligned}\quad (12)$$

The NISS estimators of $P_{f,Y_i}(y_i)$, $P_{f,\mathbf{Y}_i}(y_{ij})$ and $P_{f,\Theta_i,Y_j}(\theta_i, y_j)$ cannot be established in the similarly way since each y_i is an interval input variable other than the distribution parameter of a potential category III model.

By definition, $E_{\Theta, \mathbf{Y}_i}[P_f(\boldsymbol{\theta}, \mathbf{y})]$ can be regarded as a conditional failure probability with the condition that y_i is fixed, and $P_{f,0}$ is the corresponding unconditional probability. Thus, based on Bayes' rule, the component function $P_{f,Y_i}(y_i)$ can be derived as:

$$P_{f,Y_i}(y_i) = E_{\Theta, \mathbf{Y}_i}[P_f(\boldsymbol{\theta}, \mathbf{y})] - P_{f,0} = P_{f,0} \frac{f_{Y_i}(y_i|F)}{f_{Y_i}(y_i)} - P_{f,0} = P_{f,0} r_{Y_i}(y_i|F) \quad (13)$$

, where $r_{Y_i}(y_i|F) = f_{Y_i}(y_i|F)/f_{Y_i}(y_i) - 1$, and $f_{Y_i}(y_i|F)$ indicates PDF of y_i conditional on the failure domain $F = \{(\mathbf{x}, \mathbf{y}): g(\mathbf{x}, \mathbf{y}) < 0\}$. The conditional probability density function $f_{Y_i}(y_i|F)$ is, in general, not known analytically. Hence, it can be estimated by any density estimation

method, e.g., kernel density estimation, based on the failure samples of y_i . In other words, this conditional probability density is approximated as $f_{Y_i}(y_i|F) \approx \hat{f}_{Y_i}(y_i|F, S)$, where $\hat{f}_{Y_i}(\cdot)$ denotes the estimated density, which is deduced based on the sample set S . Then, the NISS estimator for $P_{f,Y_i}(y_i)$ can be derived as:

$$\hat{P}_{f,Y_i}(y_i) = \hat{P}_{f,0} \hat{r}_{Y_i}(y_i|F, S) \quad (14)$$

where $\hat{r}_{Y_i}(y_i|F, S) = \hat{f}_{Y_i}(y_i|F, S)/f_{Y_i}(y_i) - 1$. Similarly, the NISS estimator of $P_{f,\mathbf{Y}_{ij}}(\mathbf{y}_{ij})$ can be derived as:

$$\hat{P}_{f,\mathbf{Y}_{ij}}(\mathbf{y}_{ij}) = \hat{P}_{f,0} \hat{r}_{\mathbf{Y}_{ij}}(\mathbf{y}_{ij}|F, S) \quad (15)$$

where $\hat{r}_{\mathbf{Y}_{ij}}(\mathbf{y}_{ij}|F, S) = \hat{f}_{\mathbf{Y}_{ij}}(\mathbf{y}_{ij}|F, S)/f_{\mathbf{Y}_{ij}}(\mathbf{y}_{ij}) - \hat{f}_{Y_i}(y_i|F, S)/f_{Y_i}(y_i) - \hat{f}_{Y_j}(y_j|F, S)/f_{Y_j}(y_j) + 1$, and $\hat{f}_{\mathbf{Y}_{ij}}(\mathbf{y}_{ij}|F, S)$ is the conditional joint PDF of \mathbf{y}_{ij} estimated from the sample set S , which will be discussed in the next subsection.

Next we derive the NISS estimators for the second-order component function $P_{f,\Theta_i,Y_j}(\theta_i, y_j)$. By definition, $E_{\Theta_i, Y_j}[P_f(\boldsymbol{\theta}, \mathbf{y})]$ can also be regarded as the conditional failure probability with the condition that y_j is fixed, and based on the Bayes rule, it can be further derived as:

$$E_{\Theta_i, Y_j}[P_f(\boldsymbol{\theta}, \mathbf{y})] = E_{\Theta_i, Y_j}[P_f(\boldsymbol{\theta}, \mathbf{y})] \frac{f_{Y_i}(y_i|F)}{f_{Y_i}(y_i)} = [P_{f,\Theta_i}(\theta_i) + P_{f,0}] \frac{f_{Y_i}(y_i|F)}{f_{Y_i}(y_i)} \quad (16)$$

$$r_{Y_i}(y_i|F) = \frac{f_{Y_i}(y_i|F)}{f_{Y_i}(y_i)}$$

Thus, $P_{f,\Theta_i,Y_j}(\theta_i, y_j)$ is derived as:

$$P_{f,\Theta_i,Y_j}(\theta_i, y_j) = [P_{f,\Theta_i}(\theta_i) + P_{f,0}] r_{Y_i}(y_i|F) - P_{f,Y_j}(y_j) \quad (17)$$

, and its NISS estimator can be derived as:

$$\hat{P}_{f,\Theta_i,Y_j}(\theta_i, y_j) = [\hat{P}_{f,\Theta_i}(\theta_i) + \hat{P}_{f,0}] \hat{r}_{Y_i}(y_i|F, S) - \hat{P}_{f,Y_j}(y_j) \quad (18)$$

Till now, we have got the NISS estimators for all the first- and second-order component functions based on only one set of joint samples as well as their response values. Thus, the total number of required g -function calls is N . Naturally, the above generalized NISS procedure owns all the advantages of the classical global NISS procedure. The utilization of Bayes rule for the

above generalization is partly inspired by Ref. [28], in which the Bayes rule was utilized for estimating the global reliability sensitivity indices developed by the first author in Ref. [29]. Similarly, the idea of applying Bayes rule for deducing the dependence of the failure probability with respect to a parameter has been explored in Refs. [30] and [31].

The truncation errors as well as the relative importance of each component can be assessed by the Sobol' indices computed from the NISS estimators of the respective component functions, and we don't repeat it for simplicity. It is important to note that the Sobol' indices associated with the uncertain parameters of category II actually stem from the auxiliary probability distributions and hence, are interpreted as representative of the overall impact of those uncertain parameters on the response of interest. Such clarification is important from a theoretical point of view, as Sobol' indices are defined for random variables (and not uncertain parameters of category II). The statistical error of each NISS estimator can be assessed by deriving their respective variance, and the details can be found in Refs. [21] and [22]. In this paper, we implement the NISS method with bootstrap scheme so that the variance of each estimator can be computed in a different way. The procedure of performing the Bootstrap for NISS is given as follows.

Step 1: Generate a joint sample set $S = \{(\mathbf{x}^{(k)}, \boldsymbol{\theta}^{(k)}, \mathbf{y}^{(k)})\}$ of size N , and compute the corresponding response values $g^{(k)}$.

Step 2: Randomly generate a new sample set of size N from $\{(\mathbf{x}^{(k)}, \boldsymbol{\theta}^{(k)}, \mathbf{y}^{(k)}, \mathbf{g}^{(k)})\}_{k=1, 2, \dots, N}$ with replacement, and estimate all the component functions as well as their respective Sobol' indices based on this new sample set.

Step 3: Repeat Step 2 for n_b (e.g., 50) times so that we can obtain n_b estimates for each component function and each Sobol' index, and then compute the mean values and variances for each component function and the corresponding Sobol' index based on their n_b estimates.

With the mean value and variance of each component function, we can easily compute the standard deviation (STD) and confidence interval of each component function and sensitivity

index, based on the fact that each estimator following Gaussian distribution.

With the above procedure, we can synthesize the failure probability function by adding all the influential component functions, and also estimate the confidence bounds of $P_f(\boldsymbol{\theta}, \mathbf{y})$ based on the STDs. Third and higher order component functions as well as their corresponding sensitivity indices can be similarly estimated without calling the g -function any more. Based on the synthesized failure probability function $\hat{P}_f(\boldsymbol{\theta}, \mathbf{y})$ or the confidence interval of $P_f(\boldsymbol{\theta}, \mathbf{y})$, one can estimate the bounds of the failure probability. While the mean estimate $\hat{P}_f(\boldsymbol{\theta}, \mathbf{y})$ is used, the bounds may be either underestimated or overestimated due to the statistical error of $\hat{P}_f(\boldsymbol{\theta}, \mathbf{y})$. However, the effects of the statistical errors on the bounds can be easily assessed since the statistical error of \hat{P}_f at any fixed location of $(\boldsymbol{\theta}, \mathbf{y})$ can be computed. Besides, we can also estimate the lower bound of P_f based on the lower bound of the confidence interval of $P_f(\boldsymbol{\theta}, \mathbf{y})$, and use the upper bound of the confidence interval to estimate the upper bound of P_f . With this strategy, the generated bounds include the real bounds with specific level of confidence. For both strategies, the bounds are estimated by numerical optimization procedure. If $P_f(\boldsymbol{\theta}, \mathbf{y})$ is proven by the Sobol' indices to be additive, then only one-dimensional optimization problems need to be solved; while $P_f(\boldsymbol{\theta}, \mathbf{y})$ is also governed by low order interaction terms, then commonly only low-dimensional optimization problems need to be solved. This feature can largely improve the global convergence for estimating bounds.

The auxiliary distribution is one of the key setting for implementing NISS. Theoretically, we can use any types of probability distribution, and this will not affect the formulation of the failure probability function as well as the failure probability bounds, but they do affect the RS-HDMR decomposition in Eq. (10) as well as the distribution of Monte Carlo samples. For reliability analysis, it also affects the number of samples included in the failure domain. We will discuss carefully in the first test example the influence of the different types of auxiliary distribution.

The detailed procedure of NISS is then summarized in Figure 2. In this diagram, the statistical error for the estimate of each component function is assessed by STD in the

“Estimation” step, and the truncation error of the synthesized estimation of $P_f(\boldsymbol{\theta}, \mathbf{y})$ is measured by sensitivity indices in the “Products” step.

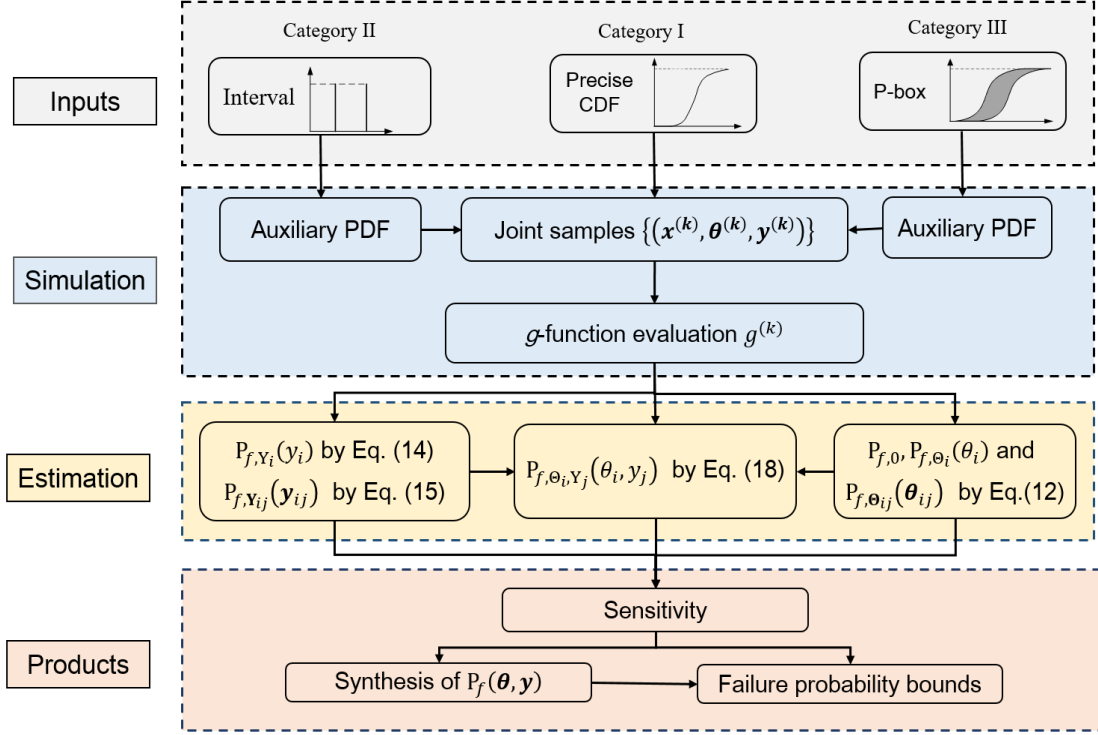


Figure 2 Diagram of the generalized NISS procedure

Although the above NISS procedure needs only one set of g -function calls, it is still computational expensive for rare event analysis. However, the computational burden can be largely relieved by injecting subset simulation and/or active learning procedure into the NISS framework, and by implementing it in a parallel scheme. One can refer to Ref. [22] for the details of injection of subset simulation into the NISS framework for estimating the component functions of $\boldsymbol{\theta}$. This strategy can also be extended for estimating the component functions of \mathbf{y} , as well as their interaction component functions with $\boldsymbol{\theta}$. This extension involves performing subset simulation, in the joint space of $(\mathbf{x}, \boldsymbol{\theta}, \mathbf{y})$, for estimating $P_{f,0}$, and then estimate the conditional density $f_{Y_i}(y_i|F)$ based on the failure samples generated with Markov Chain Monte Carlo (MCMC), so as to estimate the component function $P_{f,Y_i}(y_i)$ by Eq. (13). Further, the active learning procedure can be injected into the above Monte Carlo simulation or subset simulation based NISS framework, and with this improvement, the computational cost can be

largely reduced (see Ref. [22] for details).

One should also note that NISS in its current form is not applicable for interval analysis. In traditional interval analysis, only category II inputs are involved, and the target is to estimate the bounds of model response. However, for implementing NISS, it is required at least one category I or category III input is involved, that is, the model inputs must deliver probability distribution information, and the target is to estimate the bounds of probabilistic responses (e.g., failure probability and response distribution function), instead of the bounds of model response.

3.3 Conditional density estimations

As can be seen from Eq. (14) and Eq. (15), for interval variables, the performance of the estimators of the corresponding component functions depends on the estimation of the conditional PDFs $f_{Y_i}(y_i|F)$ and $f_{Y_j}(y_j|F)$. Thus, in this subsection, we give some useful discussion on the estimations of these two conditional PDF. As has been interpreted in subsection 3.2, both conditional PDFs are estimated based on the failure sample of the interval variables. For univariate PDF $f_{Y_i}(y_i|F)$, many non-parametric density estimation procedures have been developed, and in this paper, we suggest using the kernel density estimation (KDE) in Ref. [32] or the function ‘ksdensity’ in Matlab.

For bivariate joint PDF $f_{Y_{ij}}(y_{ij}|F)$, we can still use the 2-dimensional KDE developed in Ref. [32] to implement the method. Besides, in many situation of practical applications, the conditional samples of two interval variables may be independent with each other, thus before estimating $f_{Y_{ij}}(y_{ij}|F)$, we can also perform a hypothesis test on the dependence based on the failure samples of y_i and y_j . In section 7 of our review paper [25], several hypothesis test techniques on variable dependencies have been introduced, and one can refer to this review for more details. If y_i and y_j are independent, then $f_{Y_{ij}}(y_{ij}|F) = f_{Y_i}(y_i|F)f_{Y_j}(y_j|F)$, and the ratio function in Eq. (15) can be further derived as $r_{Y_{ij}}(y_{ij}|F) = r_{Y_i}(y_i|F)r_{Y_j}(y_j|F)$, indicating that the second-order component function of y_i and y_j can be derived based on their respective first-order component functions. If the samples of y_i and y_j are not independent, one can also use the Copula transformation which reads [33]:

$$f_{Y_{ij}}(\mathbf{y}_{ij}|F) = c_{ij}(u_i, u_j) f_{Y_i}(y_i|F) f_{Y_j}(y_j|F) \quad (19)$$

to estimate the joint PDF $f_{Y_{ij}}(\mathbf{y}_{ij}|F)$, where $c_{ij}(u_i, u_j)$ is the Copula density function of y_i and y_j , which can be estimated by parametric Copula (e.g., Clayton, Frank, or Gumbel) combined with any distribution parameter estimation procedures, based on the failure samples of y_i and y_j .

4. Test examples and applications

4.1 A toy test example

Consider a toy example with the following limit state function:

$$g(x, y) = y^3/3 + x_1^2/2 + x_2 + 1 \quad (20)$$

where y is an interval variable with support $[0, 1]$; x_1 is a Gaussian random variable characterized by a p -box model, of which the support of the mean parameter μ_1 is $[-1, 1]$, and the support of STD σ_1 is $[0.8, 1.2]$; x_2 is a standard Gaussian random variable with zero mean and unit STD. With the above assumption, the epistemic uncertainties of input variables are characterized by the intervals $y \in [0, 1]$, $\mu_1 \in [-1, 1]$ and $\sigma_1 \in [0.8, 1.2]$, while the aleatory uncertainties are characterized by the probability distributions of x_1 and x_2 . The purpose of analysis is to estimate the failure probability function w.r.t. the three epistemic parameters y , μ_1 and σ_1 .

For implementing NISS, we need first to specify the auxiliary probability distribution. Theoretically, the type of auxiliary distribution will not affect the failure probability function $P_f(y, \mu_1, \sigma_1)$ and the bounds of failure probability, however, it may affect the formulation of each component function. As illustrated in subsection 3.2, we can simply assume that y follows uniform distribution between 0 and 1. However, it is found that, with this assumption, the end regions are not sufficiently well represented, especially the left one of the first-order component function $P_{f,y}$. This is due to the lack of samples in the left end region. Here three kinds of auxiliary distribution are introduced for y , each of which has support $[-0.2, 1.2]$. The first one is uniform distribution, and it is abbreviated as “Unif”. The second one is truncated normal distribution with mean 0.5 and STD 0.35, and is denoted by “Trun-Norm”. The third one is

U-quadratic distribution with density function:

$$f_Y(y) = \frac{450}{343} (y - 0.5)^2 + 0.5$$

The density functions of three auxiliary distributions are shown in Figure 3. The auxiliary distribution of μ_1 and σ_1 are both set to be uniform. Then we set $N = 1\text{e}5$ and $n_b = 20$, and generate the joint sample set using Latin hypercube sampling.

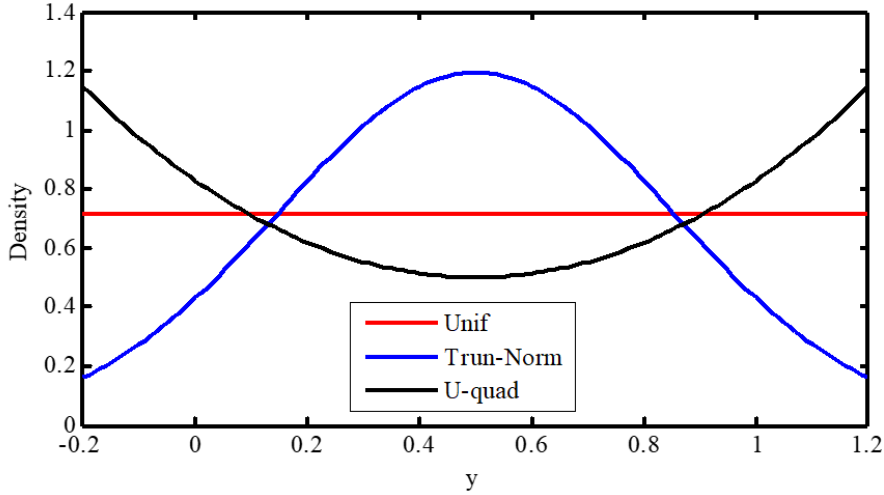


Figure 3 Density functions of the three auxiliary distributions of y

The NISS procedure is implemented with Bootstrap scheme, and the results of the constant HDMR component as well as the first- and second- order Sobol' indices corresponding to each of the three auxiliary distribution are displayed in Table 1, together with the STDs for indicating the convergence of the estimates. As can be seen, for each of the three auxiliary distributions, the relative contribution of each component function is quite similar, and the interaction effects of the three epistemic parameters are quite small. This indicates that the first-order HDMR decomposition provides good approximation for the failure probability function. It can also be seen that, among the three epistemic parameters, y is the most important one, and then μ_1 and σ_1 , indicating that reducing the epistemic uncertainty of y leads to the most reduction of the epistemic uncertainty of failure probability. This information is quite important for further collecting information on input variables.

The first-order component functions for each kind of auxiliary distribution are estimated by the NISS estimators and the Bootstrap procedure, and the estimations as well as the 95.45%

confidence intervals are shown in Figure 4, together with the reference solutions computed by double-loop crude MCS procedure with 10^5 samples in each iteration. For the three auxiliary distributions, the resulted first-order component of y shows very small difference. It is also seen that the estimates of all the three component functions computed by the NISS procedure match well with their reference solutions, and all the three confidence intervals are tight enough. Thus, all the three first-order component functions are effectively estimated by NISS. It is also shown in the first line of Figure 4 that, comparably, around the point $y=0$, the estimation error of $P_{f,y}$ is a little bit larger for each kind of auxiliary distribution. This can be improved by setting the lower bound of the auxiliary distribution of y a smaller value, say -0.5. Such results are not shown here for the sake of brevity.

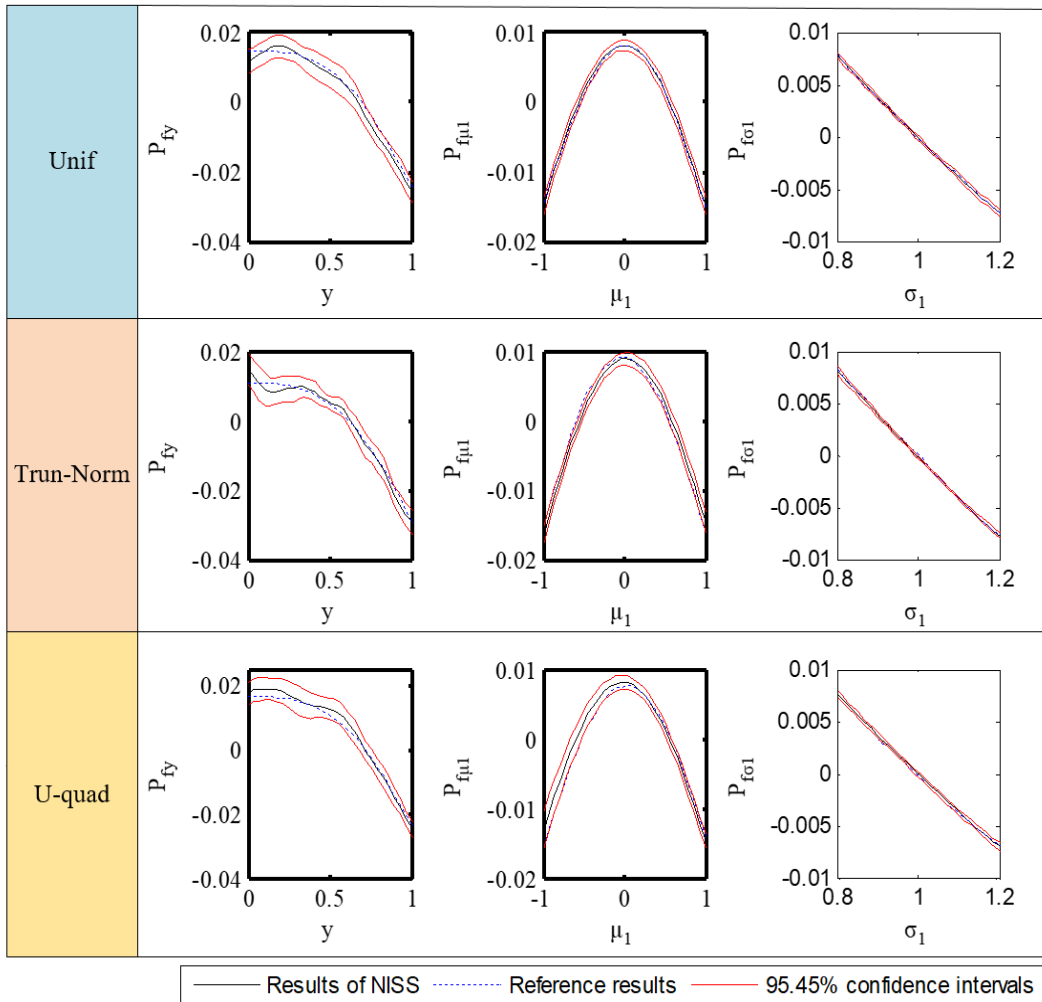


Figure 4 First-order component functions generated based on the three kinds of auxiliary distributions.

Table 1 NISS results of the toy example, where the superscripts indicates the STDs of estimates.

Distribution type	$P_{f,0}$	S_y	S_{μ_1}	S_{σ_1}	$S_{y\mu_1}$	$S_{y\sigma_1}$	$S_{\mu_1\sigma_1}$	Bounds of P_f
Unif	.071 ^(8.8e-4)	.695 ^(1.9e-2)	.2072 ^(1.4e-2)	.0793 ^(5.1e-3)	.0068 ^(2e-4)	.0026 ^(1e-4)	.0091 ^(7e-4)	[.039, .113]
Trun-Norm	.075 ^(8.7e-4)	.689 ^(1.6e-2)	.1983 ^(1.1e-2)	.0746 ^(5.2e-3)	.0351 ^(1e-3)	.0002 ^(1e-6)	.0033 ^(2e-4)	[.036, .109]
U-quad	.070 ^(7.0e-4)	.711 ^(2.0e-2)	.179 ^(1.2e-2)	.0655 ^(4.9e-3)	.0109 ^(8e-4)	.0072 ^(3e-4)	.0014 ^(1e-4)	[.037, .102]

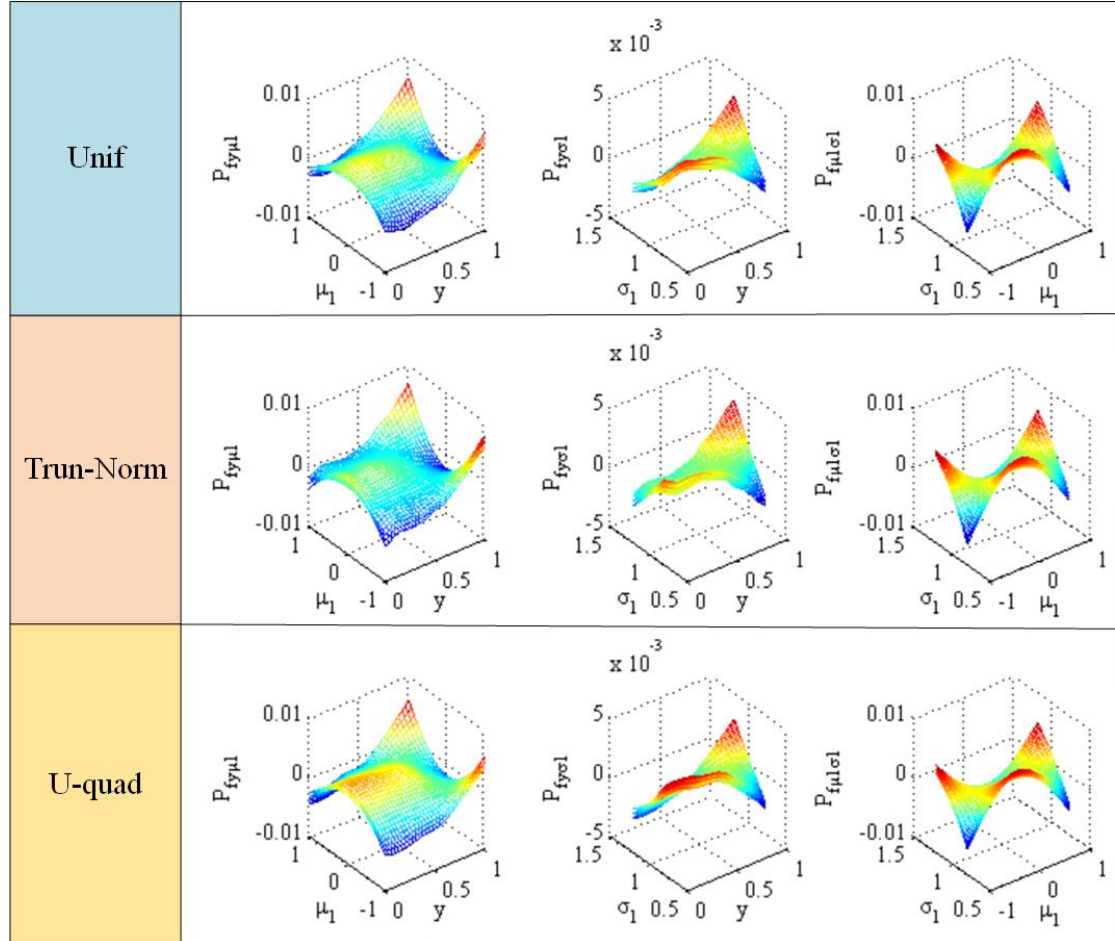


Figure 5 Second-order component functions of the toy example, where the in-between the surfaces indicate the mean estimates, and the other two surfaces indicate the 95.45% confidence intervals.

Although the second-order component functions are not very influential, we still display their estimates as well as the 95.45% confidence intervals in Figure 5. As can be seen, all the three component functions are accurately estimated, and for each kind of auxiliary distribution, the second-order component functions are quite similar. One can also find that the ranges of the variations of the three second-order component functions are smaller than those of the first-order

component functions. Based on the synthesized mean estimate of $P_f(y, \mu_1, \sigma_1)$, the bounds of failure probability is computed by genetic algorithm for each auxiliary distribution, and the results are listed in the last column of Table 1. As can be seen, the bounds generated by the three auxiliary distributions match well.

4.2 The NASA Langley multidisciplinary UQ challenge

The NASA Langley UQ challenge, released in 2014, describes a real-world aeronautics application. The simulation model aims at simulating the dynamics of remotely operated twin-jet aircraft called Generic Transport Model. One can refer to Ref. [5] for more details on the description of the simulation model. This challenge has been dealt with by many researchers (e.g., see Ref. [12][34][35] for details). The challenge consists of five subproblems, where the uncertainty propagation and reliability analysis are both important parts. The problem statement of the multidisciplinary reliability analysis is described in Figure 6. The problem is divided into three parts. The first part comprises five fixed discipline analysis, where each of the former four discipline analysis is characterized by a simulation model $h_i(\cdot)$ with five input variables, and for the fifth discipline analysis, the response equals the univariate input variable. The response of each discipline analysis is independent with that of the other discipline analysis. The second part is the cross-discipline analysis. This analysis involves eight failure modes, each of which is characterized by a limit state function $g_i(\cdot)$ with the five response variables of the fixed discipline analysis as inputs. Thus, the responses of the eight limit state functions are not independent. The third part is the reliability analysis. The eight failure modes are in series, which means that the failure of any mode results in the failure of the whole system. Thus, a composite limit state function $\omega(\mathbf{p}, \mathbf{d})$ is defined as the maximum of the eight limit state functions. In Figure 6, the vector d indicates the design variable in the fifth challenge (robust design), and in the reliability analysis setting, it is fixed at a pre-specified point $d_{baseline}$. Thus, the failure probability is defined as the probability of ω being larger than zero.

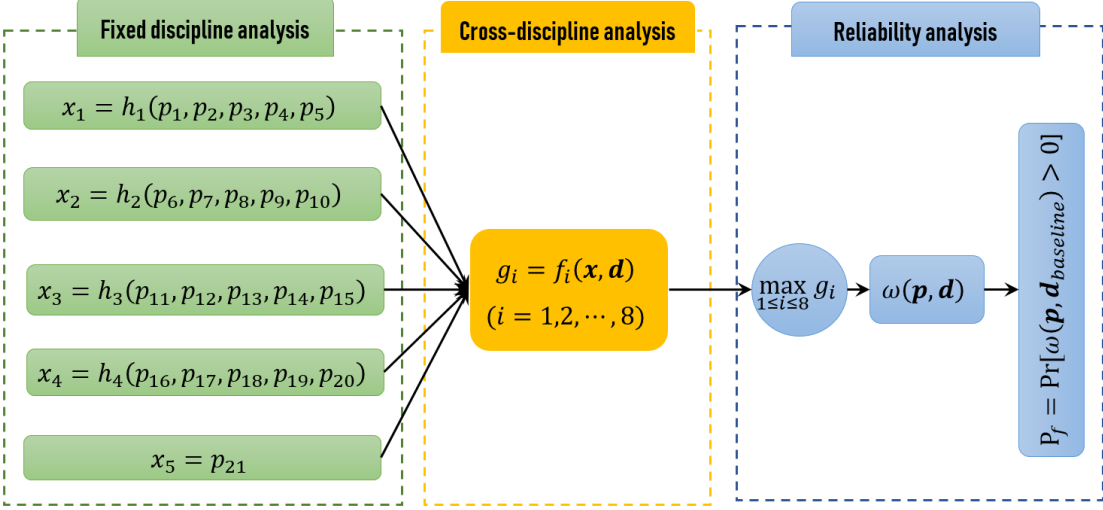


Figure 6 Description of the NASA multidisciplinary UQ challenge and the related reliability analysis sub-problem

Based on the above description, the inputs variables are in fact the 21 input variables $p_1 \sim p_{21}$ of the fixed discipline analysis, and their settings are listed in Table 2. In the first released version of the problem, these 21 inputs variables are grouped into three categories depending on their characterization models. Category I indicates the precise random variables with only aleatory uncertainty. Category II represents the interval variables with only epistemic uncertainty. Category III implies the imprecise random variables with mixed aleatory and epistemic uncertainties. In this paper, there are two main differences of the variable setting with the initial released version. The first difference is on the five inputs of the first discipline analysis. In the initial setting, the categories of the five input variables are the same as those set in Table 2, but the bounds of epistemic intervals are much larger. In the first released version, the first discipline analysis is used for the subproblem of “model updating”, and it is required that the other subproblems should be solved based on the results of this subproblem. Thus, instead of using the initial setting, we use the results of model updating in Ref. [34], for the first five input variables, as shown in Table 2. The second difference is on the support of the three interval variables p_6 , p_{12} and p_{16} . In the initial setting, the support of each variable is $[0, 1]$, however, this paper, it is changed to $[0.2, 0.8]$, as shown in Table 2. The reason is that, the simulation models don't allow the value of each input variable to exceed the bounds $[0, 1]$, however, as

indicated by the toy example, the support of auxiliary distribution of each interval variable should better be larger than its real support so that better convergence can be obtained around the end point of real bound. One should note that this modification is not due the limitation of the NISS method, but is due to the limit of the setting of this problem. In other real-world applications, the physically allowed interval of one interval variable is commonly wider than the uncertainty support, making it possible to set the support of the auxiliary distribution wider than the uncertainty support. As shown in Table 2, with the above setting, we have 31 epistemic parameters, and they are denoted as $\theta_1 \sim \theta_{31}$, and then the system failure probability will be a function on these 31 parameters, and the purpose of this example is to estimate this failure probability function as well as the related failure probability bounds. It should be noted that for the sake of compactness, all epistemic parameters in Table 2 are labeled as $\theta_i, i = 1, \dots, 31$; nonetheless, parameters $\theta_3, \theta_9, \theta_{16}$ and θ_{23} should have been actually labeled as y_1, y_2, y_3 and y_4 , respectively.

With the simple random sampling, we generate 5×10^4 joint samples for $(p_1, \dots, p_{21}, \theta_1, \dots, \theta_{31})$, and compute the response value of limit state function $\omega(\mathbf{p}, d_{baseline})$ for each joint sample, to implement the NISS procedure in a bootstrap manner. The number of bootstrap replication is set to be 30. Thus the total number of function calls is 5×10^4 . With these samples, the constant RS-HDMR component of the failure probability is computed as 0.2319 with the STD being 0.0017.

With the same set of samples, the non-normalized first-order Sobol' indices are computed, and the results are shown in Figure 7, together with the STD of each estimate. As can be seen, all the sensitivity indices are robustly estimated. The results show that, among the 31 epistemic parameters, only a small number of them are influential, and the six most influential components are those of $\theta_{16}, \theta_1, \theta_3, \theta_{23}, \theta_9$ and θ_5 . The summation of the sensitivity indices of the other 25 first-order component functions is smaller than one percent of the summation of the sensitivity indices of these six most influential components. Thus, we need only to consider the six most influential first-order component functions. The sensitivity indices also reveals that, among the

31 epistemic parameters, the epistemic uncertainty of θ_{16} (i.e., p_{12}) contributes the most to the epistemic uncertainty of failure probability. Thus, for reducing the bounds of the failure probability, one should collect more information on p_{12} . Based on the same set of samples, the six first-order components are estimated, and the estimates with the 95.45% confidence intervals are shown in Figure 8. It is shown that the confidence interval of each component function is narrow enough, indicating that each component function is accurately estimated by NISS.

Table 2 Uncertain parameters of the NASA UQ challenge, where $\theta_1 \sim \theta_{31}$ indicates the epistemic parameters.

Input variables	Category	Uncertainty model
p_1	III	Unimodal Beta, $0.6783 \leq \theta_1 = \mu_1 \leq 0.7097$, $0.0387 \leq \theta_2^2 = \sigma_1^2 \leq 0.0397$
p_2	II	Interval, $\theta_3 = p_2 \in [0.9399, 0.9902]$
p_3	I	Uniform, $[0, 1]$
p_4, p_5	III	Normal, $3.4493 \leq \theta_4 = \mu_4 \leq 4.5812$, $0.4190 \leq \theta_5^2 = \sigma_4^2 \leq 2.7209$, $-1.5306 \leq \theta_6 = \mu_5 \leq -0.9106$, $0.2157 \leq \theta_7^2 = \sigma_5^2 \leq 0.6914$, $-0.4370 \leq \theta_8 = \rho \leq 0.7008$
p_6	II	Interval, $\theta_9 = p_6 \in [0.2, 0.8]$
p_7	III	Beta, $0.982 \leq \theta_{10} = a \leq 3.537$, $0.619 \leq \theta_{11} = b \leq 1.080$
p_8	III	Beta, $7.450 \leq \theta_{12} = a \leq 14.093$, $4.285 \leq \theta_{13} = b \leq 7.864$
p_9	I	Uniform, $[0, 1]$
p_{10}	III	Beta, $1.520 \leq \theta_{14} = a \leq 4.513$, $1.536 \leq \theta_{15} = b \leq 4.750$
p_{11}	I	Uniform, $[0, 1]$
p_{12}	II	Interval, $\theta_{16} = p_{12} \in [0.2, 0.8]$
p_{13}	III	Beta, $0.412 \leq \theta_{17} = a \leq 0.737$, $1.000 \leq \theta_{18} = b \leq 2.068$
p_{14}	III	Beta, $0.931 \leq \theta_{19} = a \leq 2.169$, $1.000 \leq \theta_{20} = b \leq 2.407$
p_{15}	III	Beta, $5.435 \leq \theta_{21} = a \leq 7.095$, $5.287 \leq \theta_{22} = b \leq 6.945$
p_{16}	II	Interval, $\theta_{23} = p_{16} \in [0.2, 0.8]$
p_{17}	III	Beta, $1.060 \leq \theta_{24} = a \leq 1.662$, $1.000 \leq \theta_{25} = b \leq 1.488$
p_{18}	III	Beta, $1.000 \leq \theta_{26} = a \leq 4.266$, $0.553 \leq \theta_{27} = b \leq 1.000$
p_{19}	I	Uniform, $[0, 1]$
p_{20}	III	Beta, $7.530 \leq \theta_{28} = a \leq 13.492$, $4.711 \leq \theta_{29} = b \leq 8.148$
p_{21}	III	Beta, $0.421 \leq \theta_{30} = a \leq 1.000$, $7.772 \leq \theta_{31} = b \leq 29.621$

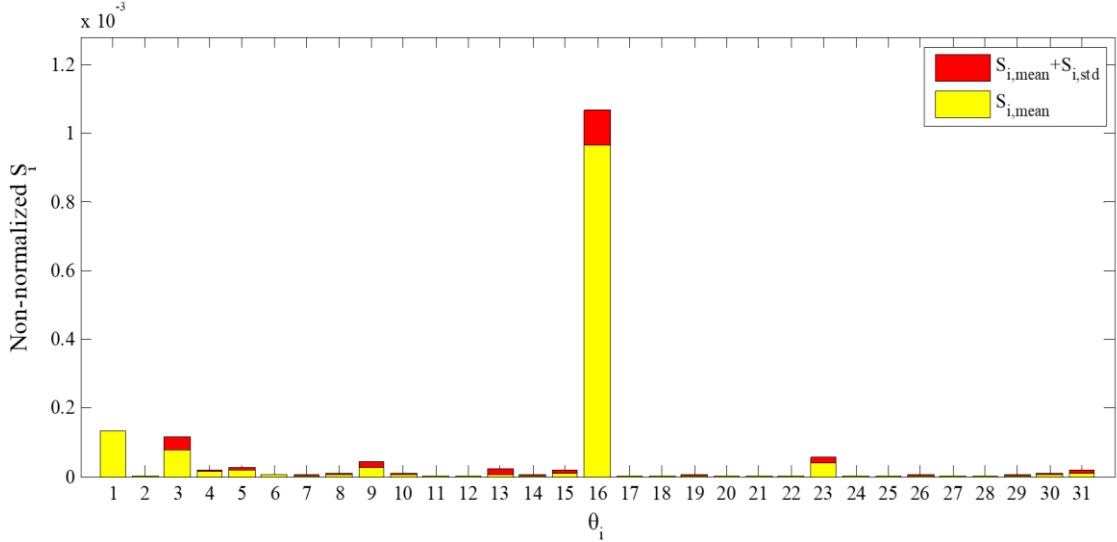


Figure 7 The first-order normalized sensitivity indices computed by NISS procedure

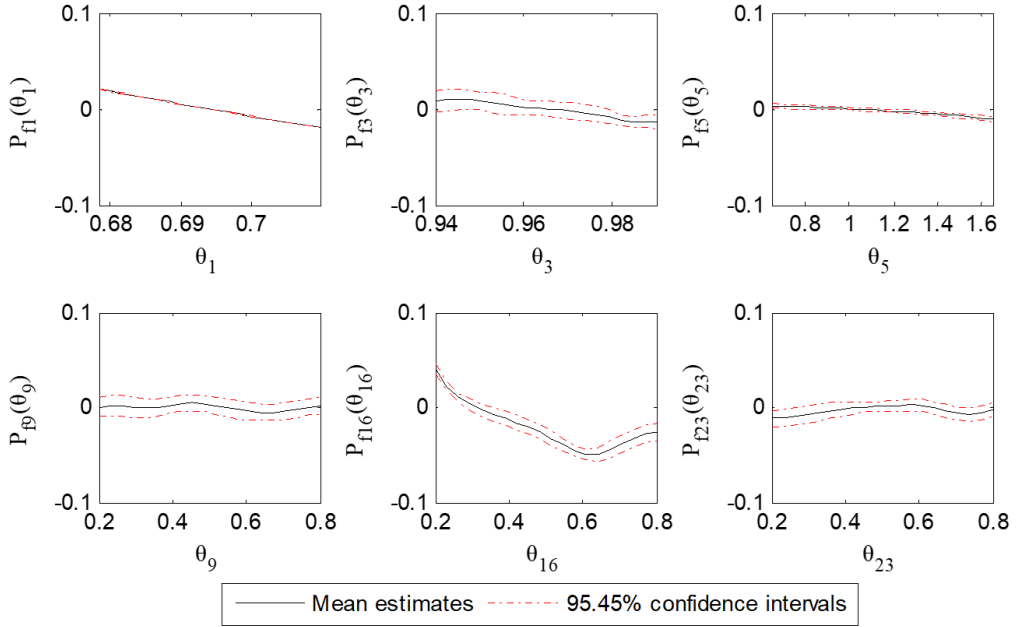


Figure 8 The first-order component functions of the NASA UQ challenge

Next, we go into the second-order component functions. As has been discussed in subsection 3.3, for the second-order component function of two interval input variables, we need to estimate their joint PDF based on their samples belonging to the failure domain. We randomly select 10^3 sample points for each pair of interval variables from their failure samples, and transform these data into copula scale by using the function ‘ksdensity’ in Matlab, and then plot the samples in pair in Figure 9. As can be seen, for each pair of interval variables, the sample points are

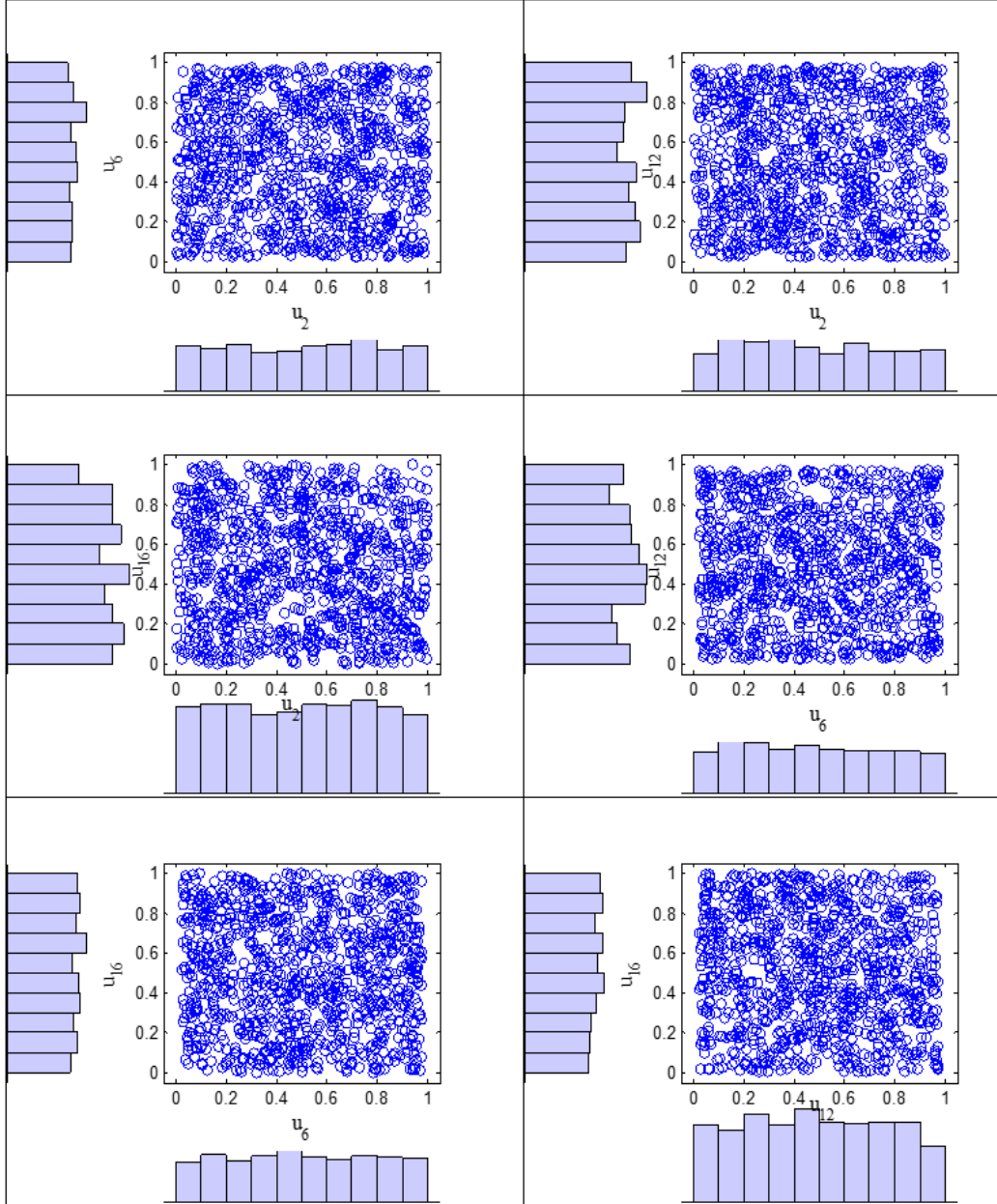


Figure 9 Pairwise scatter and histogram plots of the failure data of the four interval variables p_2 , p_6 , p_{12} and p_{16} in copula scale (unit square), where the transformation to copula scale is realized by the “ksdensity” function.

uniformly distributed in the unit square space $[0, 1]^2$, indicating that each pair of interval variables are independent in the failure domain. Then, based on the discussion in subsection 3.3, the second-order component functions of each pair of interval variables can be easily estimated by their first-order component functions, and we don't need to estimate the joint PDF. The six most influential second-order component functions are then estimated with the same set of

samples, and the estimates as well as the 95.45% confidence intervals are displayed in Figure 10. As can be seen, compared with the first-order component functions, all the second-order component functions can be neglected.

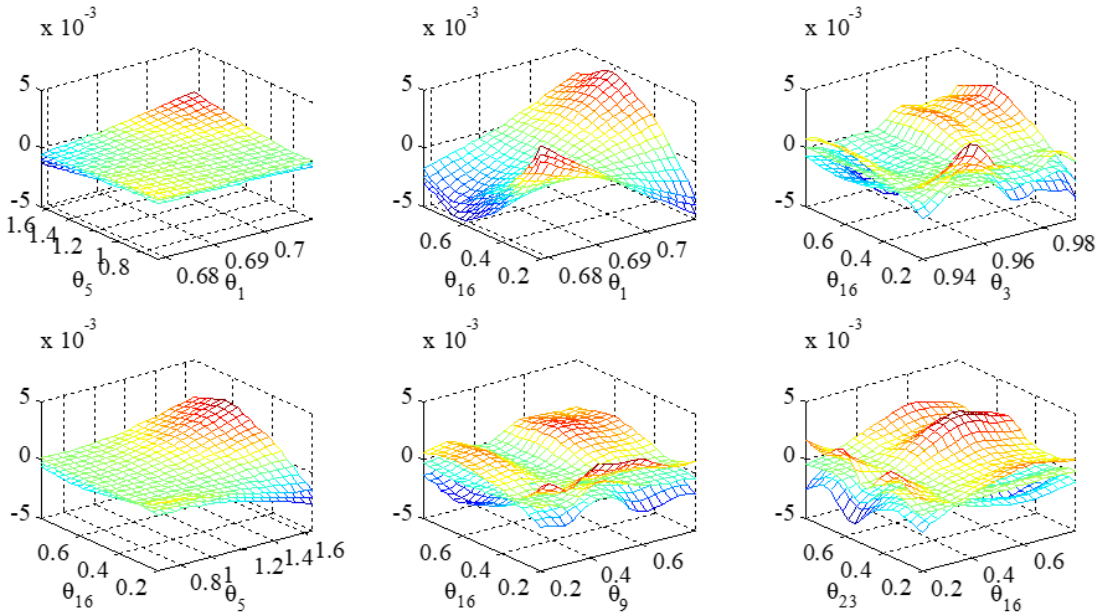


Figure 10 The six most influential second-order component functions

Based on mean estimate of the failure probability function synthesized with the six influential first-order component functions and the two most influential second-order component functions, the bounds of failure probability are estimated to be [0.1221, 0.3121]. Since the settings of the interval variables are different to the original ones, and the results of model updating of the first discipline vary from paper to paper, thus it is not possible to compare the results with the published results in, e.g., Refs. [11] and [35]. To demonstrate the correctness of our result, we also estimate the failure probability bounds by the interval Monte Carlo simulation (IMCS) developed in Ref. [13], which has also been utilized in Ref. [35] for estimating the failure probability bounds of the NASA challenge. This method involves a double-loop procedure. In the outer loop, the interval samples are generated for the input variables, while in the inner loop, the interval analysis is performed for generating the bounds of limit state function for each interval sample. The failure probability bounds are then estimated based on the samples of response bounds. Due to the large computational cost, this procedure is

implemented in a parallel scheme on a 48-core computer station. One should note that, the bounds estimated by IMCS in this example are more conservative since in this method, the parameterized p -box model is by default replaced by a non-parameterized p -box model with the bounds as the parameterized ones. This simplification is necessary in IMCS for generating interval samples in the outer loop. Similar to Ref. [35], 1000 interval samples are generated in the outer loop, and the genetic algorithm is utilized in the inner loop, to implement the IMCS method. The reference bounds are estimated to be [0.055, 0.337], which exactly include the bounds generated by NISS. Based on the above analysis, it should be believed that the bounds computed by NISS are correct.

5. Conclusions and discussions

This paper has developed a strategy for generalizing the NISS method, recently developed for efficiently propagating the imprecise probability models, to the general case where three categories of characterization models (i.e., precise probability models, non-probabilistic models, and imprecise probability models) are all involved, and specifically, the estimation of failure probability function and bounds are exemplified. The truncation errors of estimates are quantified by Sobol' sensitivity indices, which are also found to be useful for measuring the relative importance of the component functions as well as each epistemic parameter. Both the toy test example and the NASA Langley challenge have demonstrated the effectiveness of the proposed method.

The NISS method owns many advantages, and the most appealing one is that only one set of function calls are needed for implementing the whole analysis, and both types of estimation errors are properly addressed without extra computational cost. Being a pure stochastic simulation procedure, it is easy to implement it in a parallel scheme, making it more efficient for large-scale real-world applications. The only limitation of the generalization of the NISS reported here is that, for the component functions of interval variables, there is a need to do non-parametric density estimation, which, for first-order component functions, can be addressed with kernel density estimation, but for higher order component functions, may face challenge.

However, the estimation of bivariate density functions can be properly addressed by statistic dependence or parameterized Copula, as has been shown in subsection 3.3 and 4.2.

The success of NISS for high-dimensional problems is supported by the following facts. For most real physic processes, the model behavior is mainly governed by a low-dimensional manifold, and this manifold is mostly governed by individual and/or low-order interaction effects. The introduction of the RS-HDMR decomposition as well as the Sobol' sensitivity indices enables to identify this manifold and the influential effects without extra computational cost. Further, the RS-HDMR decomposition makes it possible to derive NISS estimators for the component functions of the epistemic parameters presented in both category II and category III models.

Open problems still exist. For example, the distribution-free category III models such as non-parametric *p*-box model are also widely used when the distribution type is not known due to lack of knowledge; the multivariate dependence may exist in category II model due to the natural constraints of model parameters; time-variant and spatial inputs are also commonly in real-world applications. There is a need to extend the method to the above situations. Besides, the uncertainty-based design optimization problem, e.g., the robust optimization subproblem in the NASA Langley UQ challenge [11], and the sensitivity analysis under mixed uncertain environment [36], can also be addressed by the NISS method, which will be presented in the future work.

Acknowledgments

This work is supported by the National Natural Science Foundation of China (NSFC 51905430) and the Aerospace Science and Technology Foundation of China. The first author is supported by the program of China Scholarships Council (CSC). The second to fourth authors are all supported by the Alexander von Humboldt Foundation of Germany. The second author is also supported by the Top International University Visiting Program for Outstanding Young Scholars of Northwestern Polytechnical University. The third author acknowledges the support by CONICYT (National Commission for Scientific and Technological Research) under grant

number 1180271. The authors also appreciate the two anonymous reviewers for their very useful comments and suggestions.

Reference

- [1] Der Kiureghian, A., & Ditlevsen, O. (2009). Aleatory or epistemic? Does it matter?. *Structural safety*, 31(2), 105-112.
- [2] Faes, M., & Moens, D. (2019). Recent trends in the modeling and quantification of non-probabilistic uncertainty. *Archives of Computational Methods in Engineering*, 1-39.
- [3] Jiang, C., Bi, R. G., Lu, G. Y., & Han, X. (2013). Structural reliability analysis using non-probabilistic convex model. *Computer Methods in Applied Mechanics and Engineering*, 254, 83-98.
- [4] Beer, M., Ferson, S., & Kreinovich, V. (2013). Imprecise probabilities in engineering analyses. *Mechanical systems and signal processing*, 37(1-2), 4-29.
- [5] Crespo, L. G., Kenny, S. P., & Giesy, D. P. (2014). The NASA Langley multidisciplinary uncertainty quantification challenge. In 16th AIAA Non-Deterministic Approaches Conference (p. 1347).
- [6] Li, J., Chen, J., Sun, W., & Peng, Y. (2012). Advances of the probability density evolution method for nonlinear stochastic systems. *Probabilistic Engineering Mechanics*, 28, 132-142.
- [7] Au, S. K., & Beck, J. L. (1999). A new adaptive importance sampling scheme for reliability calculations. *Structural safety*, 21(2), 135-158.
- [8] Au, S. K., & Beck, J. L. (2001). Estimation of small failure probabilities in high dimensions by subset simulation. *Probabilistic engineering mechanics*, 16(4), 263-277.
- [9] Schuëller, G. I., Pradlwarter, H. J., & Koutsourelakis, P. S. (2004). A critical appraisal of reliability estimation procedures for high dimensions. *Probabilistic engineering mechanics*, 19(4), 463-474.
- [10] Wei, P., Liu, F., & Tang, C. (2018). Reliability and reliability-based importance analysis of structural systems using multiple response Gaussian process model. *Reliability Engineering & System Safety*, 175, 183-195.

- [11] de Angelis, M., Patelli, E., & Beer, M. (2015). Advanced line sampling for efficient robust reliability analysis. *Structural safety*, 52, 170-182.
- [12] Pedroni, N., & Zio, E. (2015). Hybrid uncertainty and sensitivity analysis of the model of a twin-jet aircraft. *Journal of Aerospace Information Systems*, 12(1), 73-96.
- [13] Zhang, H., Dai, H., Beer, M., & Wang, W. (2013). Structural reliability analysis on the basis of small samples: an interval quasi-Monte Carlo method. *Mechanical Systems and Signal Processing*, 37(1-2), 137-151.
- [14] Wang, C., Zhang, H., & Beer, M. (2018). Computing tight bounds of structural reliability under imprecise probabilistic information. *Computers & Structures*, 208, 92-104.
- [15] Bi, S., Broggi, M., Wei, P., & Beer, M. (2019). The Bhattacharyya distance: Enriching the P-box in stochastic sensitivity analysis. *Mechanical Systems and Signal Processing*, 129, 265-281.
- [16] Gao, W., Wu, D., Gao, K., Chen, X., & Tin-Loi, F. (2018). Structural reliability analysis with imprecise random and interval fields. *Applied Mathematical Modelling*, 55, 49-67.
- [17] Wu, D., & Gao, W. (2017). Hybrid uncertain static analysis with random and interval fields. *Computer Methods in Applied Mechanics and Engineering*, 315, 222-246.
- [18] Feng, J., Wu, D., Gao, W., & Li, G. (2018). Hybrid uncertain natural frequency analysis for structures with random and interval fields. *Computer Methods in Applied Mechanics and Engineering*, 328, 365-389.
- [19] Wei, P., Lu, Z., & Song, J. (2014). Extended Monte Carlo simulation for parametric global sensitivity analysis and optimization. *AIAA journal*, 52(4), 867-878..F.
- [20] Zhang, J., & Shields, M. D. (2018). On the quantification and efficient propagation of imprecise probabilities resulting from small datasets. *Mechanical Systems and Signal Processing*, 98, 465-483.
- [21] Wei, P., Song, J., Bi, S., Broggi, M., Beer, M., Lu, Z., & Yue, Z. (2019). Non-intrusive stochastic analysis with parameterized imprecise probability models: I. Performance estimation. *Mechanical Systems and Signal Processing*, 124, 349-368.
- [22] Wei, P., Song, J., Bi, S., Broggi, M., Beer, M., Lu, Z., & Yue, Z. (2019). Non-intrusive

- stochastic analysis with parameterized imprecise probability models: II. Reliability and rare events analysis. *Mechanical Systems and Signal Processing*, 126, 227-247.
- [23] Li, G., Wang, S. W., & Rabitz, H. (2002). Practical approaches to construct RS-HDMR component functions. *The Journal of Physical Chemistry A*, 106(37), 8721-8733.
- [24] Tarantola, S., Gatelli, D., Kucherenko, S. S., & Mauntz, W. (2007). Estimating the approximation error when fixing unessential factors in global sensitivity analysis. *Reliability Engineering & System Safety*, 92(7), 957-960.
- [25] Wei, P., Lu, Z., & Song, J. (2015). Variable importance analysis: a comprehensive review. *Reliability Engineering & System Safety*, 142, 399-432.
- [26] Wang, P., Lu, Z., Zhang, K., Xiao, S., & Yue, Z. (2018). Copula-based decomposition approach for the derivative-based sensitivity of variance contributions with dependent variables. *Reliability Engineering & System Safety*, 169, 437-450.
- [27] Helton, J. C., Johnson, J. D., Oberkampf, W. L., & Sallaberry, C. J. (2010). Representation of analysis results involving aleatory and epistemic uncertainty. *International Journal of General Systems*, 39(6), 605-646.
- [28] Yun, W., Lu, Z., Zhang, Y., & Jiang, X. (2018). An efficient global reliability sensitivity analysis algorithm based on classification of model output and subset simulation. *Structural Safety*, 74, 49-57.
- [29] Wei, P., Lu, Z., Hao, W., Feng, J., & Wang, B. (2012). Efficient sampling methods for global reliability sensitivity analysis. *Computer Physics Communications*, 183(8), 1728-1743.
- [30] Au, S. K. (2005). Reliability-based design sensitivity by efficient simulation. *Computers & structures*, 83(14), 1048-1061.
- [31] Ching, J., & Hsieh, Y. H. (2007). Local estimation of failure probability function and its confidence interval with maximum entropy principle. *Probabilistic Engineering Mechanics*, 22(1), 39-49.
- [32] Botev, Z. I., Grotowski, J. F., & Kroese, D. P. (2010). Kernel density estimation via diffusion. *The annals of Statistics*, 38(5), 2916-2957.
- [33] Wei, P., Lu, Z., & Song, J. (2014). Moment-independent sensitivity analysis using

- copula. *Risk Analysis*, 34(2), 210-222.
- [34] Bi, S., Broggi, M., & Beer, M. (2019). The role of the Bhattacharyya distance in stochastic model updating. *Mechanical Systems and Signal Processing*, 117, 437-452.
- [35] Patelli, E., Alvarez, D. A., Broggi, M., & Angelis, M. D. (2015). Uncertainty management in multidisciplinary design of critical safety systems. *Journal of Aerospace Information Systems*, 12(1), 140-169.
- [36] Wei, P., Liu, F., Lu, Z., & Wang, Z. (2018). A probabilistic procedure for quantifying the relative importance of model inputs characterized by second-order probability models. *International Journal of Approximate Reasoning*, 98, 78-95.

Research article 2: Non-intrusive imprecise stochastic simulation by line sampling

This article concerns another specific area of applying NISS, which is the rare event analysis. For simplicity, we assume that the input variables of the structures are characterized by either the precise probability mode (category I) or the distributional *p*-box model (category III). In risk and reliability, the analysis of rare events is of great importance. Although the probability of these events is extremely small (typically less than 10^{-3}), once happen, it commonly results in huge commercial consequences and/or serious casualties.

In the classical NISS framework, the subset simulation has already been injected for tackling this type of problem, but it is still computationally challenging due to the low efficiency of the Markov Chain Monte Carlo simulation. The advantage of the subset simulation driven NISS is that it is applicable for highly nonlinear problems. In practical application, the nonlinearity of the model response functions may show linear or weak nonlinear behavior, and for this type of problem, the efficiency of NISS can be further improved by, e.g., injecting the stochastic simulation methods, which is more efficient for linear or weakly nonlinear problems, into the NISS framework, and this is the focus of this article.

For the classical rare event analysis with input variables characterized by only precise probability models, the line sampling (LS) is also a popular stochastic simulation technique, which has been shown to be especially efficient for high-dimensional problems with low nonlinearity. The LS method involves first generating an importance direction pointing to the failure point with (approximately) highest probability mass from the origin, then

performing random sampling in on the hyperplane which is vertical to the important direction, and for each random sample perform one dimensional integral along the importance direction, and this way to estimate the failure probability. Owing to the high efficiency of one-dimensional search, the LS is extremely efficient for the rare failure event analysis. There are two different philosophies for understanding the LS method, and based on which, this article will develop two strategies for injecting the classical LS method to the NISS framework.

First, by regarding the LS estimator as the combination of repeated first-order reliability analysis, a hyperplane-based strategy for injecting the LS to the local NISS method is proposed, it can estimate the cut-HDMR component functions of failure probability function with respect to the input epistemic parameters. Second, by understanding the LS method as the combination of a Monte Carlo simulation in an $(n-1)$ -dimensional subspace, and a one-dimensional integral along each line, a weighting scheme is developed for deriving the LS estimators of the cut-HDMR components of the failure probability function. Both the above two schemes require implementing the LS analysis for the constant cut-HDMR component for only one time, thus the computational cost keeps the same level as the classical LS method for precise reliability analysis.

In this article, we only consider the local NISS method, but the two developed two schemes are also applicable to global NISS. Considering the LS method can still be computationally expensive, and is not suitable for highly nonlinear problems, in the next article, an active learning scheme will be developed for further improvements of the LS method.

Non-intrusive imprecise stochastic simulation by line sampling

Jingwen Song^{a,c}, Marcos Valdebenito^{b,c}, Pengfei Wei^{a,c}, Michael Beer^{c,d,e}, Zhenzhou Lu^a

^a Northwestern Polytechnical University, West Youyi Road 127, Xi'an 710072, Shaanxi, China

^b Departamento de Obras Civiles, Universidad Tecnica Federico Santa Maria, Av. Espana 1680,

Valparaiso, Chile

^c Institute for Risk and Reliability, Leibniz University Hannover, Callinstr. 34, 30167 Hannover,

Germany

^d Institute for Risk and Uncertainty, University of Liverpool, Peach Street, L69 7ZF, Liverpool,

United Kingdom

^e International Joint Research Center for Engineering Reliability and Stochastic Mechanics,

Tongji University, Shanghai 200092, China

Published in *Structural Safety*, available online in February 2020

Abstract: The non-intrusive imprecise stochastic simulation (NISS) is a general framework for the propagation of imprecise probability models and analysis of reliability. The most appealing character of this methodology framework is that, being a pure simulation method, only one precise stochastic simulation is needed for implementing the method, and the requirement of performing optimization analysis on the response functions can be elegantly avoided. However, for rare failure events, the current NISS methods are still computationally expensive. In this paper, the classical line sampling developed for precise stochastic simulation is injected into the NISS framework, and two different imprecise line sampling (ILS) methods are developed based on two different interpretations of the classical line sampling procedure. The first strategy is devised based on the set of hyperplanes introduced by the line sampling analysis, while the second strategy is developed based on an integral along each individual line. The truncation errors of both methods are measured by sensitivity indices, and the variances of all estimators are derived for indicating the statistical errors. A test example and three engineering problems of different types are introduced for comparing and demonstrating the effectiveness of the two ILS

methods.

Keywords: Uncertainty quantification; Imprecise probability models; Line sampling; Sensitivity analysis; Aleatory uncertainty; Epistemic Uncertainty

1. Introduction

Uncertainty quantification (UQ) is the process of quantitatively characterizing the uncertainty of any non-deterministic quantities of interest in numerical simulation. Generally, two kinds of UQ tasks are concerned. The first task is forward UQ (also called uncertainty propagation), which aims at propagating the uncertainty characterization models from model inputs to outputs, so as to properly characterizing the uncertainties of model outputs, and further to perform risk and reliability analysis. The second task is backward UQ (also called model updating), which focuses on inferring and updating the uncertainty characterization models of model inputs based on experimental measurements of responses [1]. To implement the above UQ tasks, three groups of uncertainty characterization models have been developed, i.e., the precise probability model, the non-probabilistic models and the imprecise probability models.

Forward UQ based on precise probability models has been widely studied, and a plenty of numerical methods, such as the analytical methods based on Taylor series [2], the spectral representations [3], the stochastic simulation methods [4], and the probability density evolution method [5], have been developed, and shown to be effective for both response uncertainty characterization and reliability analysis. However, for generating precise probability models, plenty of accurate data is commonly required, which is almost impossible in real-world applications. To deal with this challenge, several kinds of non-probabilistic models, such as the interval/convex models and the fuzzy set theory, have been proposed, and numerical methods, such as the intrusive interval finite element analysis as well as the non-intrusive optimization methods [6]. The non-probabilistic models are simple but can be especially useful when the available data is extremely scarce and/or imprecise. The criticisms of non-probabilistic models are commonly twofold. Firstly, in terms of forward UQ, the intrusive methods are commonly

problem-dependent and can be of limited application, while the non-intrusive optimization-based methods may be computationally expensive and perhaps impractical, especially when the limit state functions (LSF) are not convex [6]. Secondly, due to scarcity, incompleteness, imprecision of available data, two kinds of uncertainties, termed as aleatory uncertainty and epistemic uncertainty, are commonly present for each model parameter, and plenty of studies have shown that it is necessary to distinguish between these two kinds of uncertainties [7], however, non-probabilistic models commonly fail to realize this.

To fill the above-mentioned gap, the imprecise probability models such as the probability-box (*p*-box) model, evidence theory, and fuzzy probability model, have been devised [8], and shown to be able to separately and correctly characterize the two kinds of uncertainties in a unified model framework, thus attracting substantial attention. The numerical methods which have been developed for propagating imprecise probability models can also be divided into two groups depending on whether they are intrusive or non-intrusive. The most well-known intrusive method is the interval Monte Carlo simulation (MCS) [9], which is based on firstly generating interval samples, and then estimating the bounds of model responses for each interval sample based on, e.g., interval finite element analysis. The non-intrusive optimization-based methods have also been developed. For example, in Ref. [10], the subset simulation combined with optimization has been extended for estimating the failure probability bound; in Ref. [11], the first-order and second-order reliability methods combined with an optimization procedure have been extended to reliability analysis associated with evidence theory. All these methods need to perform double-loop optimization solver on model response function, thus compared with the propagation of precise probability models, they are computationally much more expensive, and sometimes the global convergence cannot be achieved especially when the LSFs are non-convex and/or non-differentiable.

The non-intrusive imprecise stochastic simulation (NISS) is a non-intrusive methodology framework for efficiently propagating the imprecise probability models [12][13], which has been recently developed based on the extended Monte Carlo simulation [14] and high-dimensional model representation (HDMR) [15][16]. Two groups of NISS methods, i.e., the local NISS and

the global NISS, have been developed, and the subset simulation has been injected into both methods so as to perform reliability analysis subjected to rare failure events [13]. The NISS owns several advantages. Firstly, the computational cost is the same as the one involved in precise stochastic simulation, thus is much lower than the above-mentioned methods. Secondly, two kinds of potential estimation errors are properly assessed. Thirdly, there is no need to perform optimization on LSF. Thus, the NISS is an appealing method for forward UQ of imprecise probability models.

The aim of this work is to inject the line sampling [18][19], originally proposed as a generalization of axis-parallel importance sampling method for reliability analysis in precise probability models [20][21], to the local NISS framework, so as to efficiently estimate the failure probability functions associated with rare failure events. Based on the different interpretations of the classical line sampling, we developed two imprecise line sampling (ILS) procedures to achieve this target. The first strategy is motivated by the rationale that the line sampling can be regarded as repeated first-order reliability analysis, and the developed method is termed as hyperplane-based ILS. The second strategy is based on the interpretation that a line sampling analysis can be regarded as the combination of a Monte Carlo simulation in an $(n-1)$ -dimensional space and a one-dimensional integral along each line, and the corresponding proposed method is called Weighted-integral ILS. The two developed ILS methods are presented in detail and compared with both analytical and real-world engineering examples. Results show that both methods are highly efficient when the LSF is weakly or mildly non-linear.

The rest of this paper is organized as follows. Section 2 briefly reviews the backgrounds of imprecise stochastic simulation and line sampling, followed by the developments of the two ILS methods in section 3. A numerical test example and three real-world civil engineering examples are introduced in section 4 for demonstrating and comparing the proposed methods. Section 5 gives conclusions.

2. Background of imprecise stochastic simulation and line sampling

2.1 Problem statement

The performance function of the structure of interest is denoted by $G = g(\mathbf{x})$ with $\mathbf{x} = (x_1, \dots, x_n)$ being the n -dimensional input variables. For reliability analysis, the failure domain is defined as $F = \{\mathbf{x}: g(\mathbf{x}) < 0\}$, and the failure indicator function $I_F(\mathbf{x})$ is defined by $I_F(\mathbf{x}) = 1$ if $\mathbf{x} \in F$; else, $I_F(\mathbf{x}) = 0$. Let $f_{\mathbf{x}}(\mathbf{x}|\boldsymbol{\theta})$ denote the joint probability density function (PDF) of \mathbf{x} , and $\boldsymbol{\theta} = (\theta_1, \dots, \theta_i, \dots, \theta_m)$ refers to the vector of distribution parameters.

In classical reliability analysis, $\boldsymbol{\theta}$ is precisely determined as constant values, and the failure probability P_f can be formulated by the n -dimensional integral $P_f = \int I_F(\mathbf{x}) f_{\mathbf{x}}(\mathbf{x}) d\mathbf{x}$. For imprecise probability models, the distribution parameters are uncertain, and their uncertainty representing the epistemic uncertainty (lack of knowledge) on \mathbf{x} can be characterized, for example, by intervals. In this situation, the failure probability will be a function of $\boldsymbol{\theta}$, which is called failure probability function with the following expression

$$P_f(\boldsymbol{\theta}) = \int I_F(\mathbf{x}) f_{\mathbf{x}}(\mathbf{x}|\boldsymbol{\theta}) d\mathbf{x} \quad (1)$$

For simplification, suppose the input variables \mathbf{x} are characterized by parameterized p -box, then $\boldsymbol{\theta}$ will be characterized by interval variables (usually obtained with interval estimation method). Note that the above assumption doesn't imply that the proposed methods are restricted to p -box. In fact, they are applicable for any parameterized imprecise probability models. In this paper, all the input variables are assumed to be independent, and the joint PDF is expressed as $f_{\mathbf{x}}(\mathbf{x}|\boldsymbol{\theta}) = \prod_{d=1}^n f_{X_d}(x_d|\boldsymbol{\theta}_d)$, where $\boldsymbol{\theta}_d$ refers to the vector of the distribution parameters of x_d . Note that the independence assumption is not crucial for the implementation of our proposed methods. They are also applicable cases with dependent inputs, which will be discussed later.

2.2 Imprecise stochastic simulation

The NISS developed in Refs. [12][13] is a non-intrusive simulation methodology framework for propagating any parameterized imprecise probability model. This framework consists of two

groups of methods, where the first group of methods is termed as local NISS, and are developed based on the cut-HDMR decomposition and extended MCS procedure, while the second group of methods are global methods, and are developed based on random sampling (RS)-HDMR and a global version of extended MCS procedure. This paper is restricted to local methods.

Motivated by importance sampling, the extended MCS is based on formulating the failure probability function as [14]

$$P_f(\boldsymbol{\theta}) = \int I_F(\mathbf{x}) \frac{f(\mathbf{x}|\boldsymbol{\theta})}{f(\mathbf{x}|\boldsymbol{\theta}^*)} f(\mathbf{x}|\boldsymbol{\theta}^*) d\mathbf{x} \quad (2)$$

where $f(\mathbf{x}|\boldsymbol{\theta}^*)$ is the sampling PDF with the distribution parameters being fixed in a pre-specified point $\boldsymbol{\theta}^*$. One can refer to Ref. [14] and [22] for the specification of $\boldsymbol{\theta}^*$. Based on Eq.(2), the failure probability function can be estimated with only one set of g -function calls.

For improving the performance of Eq.(2) in high dimensional space and reducing the estimation errors, the HDMR is utilized to decompose the failure probability function as the sum of a series of component functions. The general HDMR formula of $P_f(\boldsymbol{\theta})$ is as follows

$$P_f(\boldsymbol{\theta}) = P_{f0} + \sum_{i=1}^m P_{fi}(\theta_i) + \sum_{i=1}^m \sum_{j=i+1}^m P_{fij}(\theta_i, \theta_j) + \dots + P_{f1, \dots, m}(\boldsymbol{\theta}) \quad (3)$$

By using cut-HDMR method [15] to expand $P_f(\boldsymbol{\theta})$ at the fixed point $\boldsymbol{\theta}^*$, the component probability functions on the right side of Eq.(3) can be specified as

$$\begin{aligned} P_{f0} &= P_f(\boldsymbol{\theta}^*) \\ P_{fi}(\theta_i) &= P_f(\theta_i, \boldsymbol{\theta}_{-i}^*) - P_{f0} \\ P_{fij}(\theta_i, \theta_j) &= P_f(\theta_i, \theta_j, \boldsymbol{\theta}_{-i,j}^*) - P_{fi}(\theta_i) - P_{fj}(\theta_j) - P_{f0} \end{aligned} \quad (4)$$

where $\boldsymbol{\theta}^*$ is the aforementioned fixed point chosen within the support domain $\boldsymbol{\Theta}$, $\boldsymbol{\theta}_{-i}^*$ denotes the $m-1$ dimensional vector containing all elements in $\boldsymbol{\theta}^*$ except θ_i^* , and $\boldsymbol{\theta}_{-i,j}^*$ refers to the $m-2$ dimensional vector containing all elements in $\boldsymbol{\theta}^*$ except θ_i^* and θ_j^* . Based on our study, in many applications, the higher-order effects of distribution parameters are commonly not as important as the first few order effects [17][23], and representing $P_f(\boldsymbol{\theta})$ up to second-order can usually provide a satisfactory estimation, i.e.

$$P_f(\boldsymbol{\theta}) \approx P_{f0} + \sum_{i=1}^m P_{fi}(\theta_i) + \sum_{i=1}^m \sum_{j=i+1}^m P_{fij}(\theta_i, \theta_j) \quad (5)$$

It is obvious that the components above can be directly estimated with classical MCS method which is actually a double-loop procedure with a heavy computational burden. NISS method [12]

enables to estimate the component functions in Eq.(5) with only one set of g -function evaluations, such estimation procedure is briefly described below.

Generate N sample points $\mathbf{x}^{(s)} = (x_1^{(s)}, \dots, x_n^{(s)})$ ($s = 1, \dots, N$) from $f_{\mathbf{x}}(\mathbf{x}|\boldsymbol{\theta}^*)$ and evaluate the corresponding values of $I_F(\mathbf{x}^{(s)})$ ($s = 1, \dots, N$). Then, the unbiased estimators for the first-order and second-order component functions are as follows

$$\begin{aligned}\hat{P}_{f0} &= \frac{1}{N} \sum_{s=1}^N I_F(\mathbf{x}^{(s)}) \\ \hat{P}_{fi}(\theta_i) &= \frac{1}{N} \sum_{s=1}^N I_F(\mathbf{x}^{(s)}) r_i(\mathbf{x}^{(s)}|\theta_i, \boldsymbol{\theta}^*) \\ \hat{P}_{fij}(\theta_i, \theta_j) &= \frac{1}{N} \sum_{s=1}^N I_F(\mathbf{x}^{(s)}) r_{ij}(\mathbf{x}^{(s)}|\theta_i, \theta_j, \boldsymbol{\theta}^*)\end{aligned}\quad (6)$$

where $r_i(\mathbf{x}^{(s)}|\theta_i, \boldsymbol{\theta}^*)$ and $r_{ij}(\mathbf{x}^{(s)}|\theta_i, \theta_j, \boldsymbol{\theta}^*)$ are weight coefficients of density, and are defined as

$$\begin{aligned}r_i(\mathbf{x}^{(s)}|\theta_i, \boldsymbol{\theta}^*) &= \frac{f_{\mathbf{x}}(\mathbf{x}^{(s)}|\theta_i, \boldsymbol{\theta}_{-i}^*)}{f_{\mathbf{x}}(\mathbf{x}^{(s)}|\boldsymbol{\theta}^*)} - 1 \\ r_{ij}(\mathbf{x}^{(s)}|\theta_i, \theta_j, \boldsymbol{\theta}^*) &= \frac{f_{\mathbf{x}}(\mathbf{x}^{(s)}|\theta_i, \theta_j, \boldsymbol{\theta}_{-ij}^*)}{f_{\mathbf{x}}(\mathbf{x}^{(s)}|\boldsymbol{\theta}^*)} - \frac{f_{\mathbf{x}}(\mathbf{x}^{(s)}|\theta_i, \boldsymbol{\theta}_{-i}^*)}{f_{\mathbf{x}}(\mathbf{x}^{(s)}|\boldsymbol{\theta}^*)} - \frac{f_{\mathbf{x}}(\mathbf{x}^{(s)}|\theta_j, \boldsymbol{\theta}_{-j}^*)}{f_{\mathbf{x}}(\mathbf{x}^{(s)}|\boldsymbol{\theta}^*)} + 1\end{aligned}\quad (7)$$

Based on Eq.(3), the estimator $\hat{P}_f(\boldsymbol{\theta})$ is the sum of all the components in Eq.(6). In fact, higher-order component functions can also be estimated with the same set g -function evaluations if needed.

The above procedure introduces two types of errors, truncation error due to cut-HDMR truncation (e.g., Eq.(5)) and statistical error due to MCS. The statistical error, which is also a function of $\boldsymbol{\theta}$, can be estimated by computing the variances of estimators in Eq.(6) using the following expressions

$$\begin{aligned}Var(\hat{P}_{f0}) &= \frac{1}{N(N-1)} \sum_{s=1}^N (I_F^{(s)} - \hat{P}_{f0})^2 \\ Var(\hat{P}_{fi}) &= \frac{1}{N(N-1)} \sum_{s=1}^N (I_F^{(s)} r_i - \hat{P}_{fi})^2 \\ Var(\hat{P}_{fij}) &= \frac{1}{N(N-1)} \sum_{s=1}^N (I_F^{(s)} r_{ij} - \hat{P}_{fij})^2\end{aligned}\quad (8)$$

On the other hand, HDMR can be used to measure the relative importance of component functions, also called sensitivity analysis [24]. Ref. [17] shows the definition of sensitivity index $S_{i_1 i_2 \dots i_k}$ of component functions for measuring the effect of uncertainties in distribution

parameters on failure probability,

$$S_{i_1 i_2 \dots i_k} = \frac{\int_{\boldsymbol{\Theta}_{i_1 i_2 \dots i_k}} P_{f_{i_1 \dots i_k}}^2(\boldsymbol{\theta}_{i_1 \dots i_k}) f_{\boldsymbol{\Theta}_{i_1 i_2 \dots i_k}}(\boldsymbol{\theta}_{i_1 \dots i_k}) d\boldsymbol{\theta}_{i_1 \dots i_k}}{\sum_{i_1 \dots i_k \in \{1 \dots, m\}} \int_{\boldsymbol{\Theta}_{i_1 i_2 \dots i_k}} P_{f_{i_1 \dots i_k}}^2(\boldsymbol{\theta}_{i_1 \dots i_k}) f_{\boldsymbol{\Theta}_{i_1 i_2 \dots i_k}}(\boldsymbol{\theta}_{i_1 \dots i_k}) d\boldsymbol{\theta}_{i_1 \dots i_k}} | \{i_1 i_2 \dots i_k\} | \leq M \quad (9)$$

where M refers to the highest order under consideration, $f_{\boldsymbol{\Theta}_{i_1 i_2 \dots i_k}}(\boldsymbol{\theta}_{i_1 \dots i_k})$ denotes the instrumental joint PDF for $\boldsymbol{\theta}_{i_1 \dots i_k}$, for p -box case, $f_{\boldsymbol{\Theta}_{i_1 i_2 \dots i_k}}(\boldsymbol{\theta}_{i_1 \dots i_k})$ is uniform type of PDF defined with the upper and lower bound of $\boldsymbol{\theta}_{i_1 \dots i_k}$. In our previous developments, both local and global NISS methods have been developed, and in the global NISS, the Sobol' indices are used, while in the local NISS, the sensitivity indices as shown in this paper were used since it is derived based on cut-HDMR decomposition. While cut-HDMR decomposition is utilized, the sensitivity indices utilized in this paper in fact measure the average L^2 distance of component functions to the expansion points, and the larger this distance is, the more important is this component. If the sensitivity index equals zero, then it implies that the corresponding component function always takes zero value, thus of course has no effect on the failure probability function, thus it can be eliminated in searching for the extreme values of failure probability.

Although the above procedure enables to estimate failure probability function with only one set of samples, it is still computationally intensive, especially when estimating probabilities associated with rare failure events. In Ref. [13], the subset simulation has been extended for solving this problem. However, for problems involving moderately nonlinear performance functions, line sampling can be more efficient than subset simulation from a numerical viewpoint. This motivates us to inject the line sampling into the NISS framework so that the computational cost for mildly nonlinear problems can be further reduced.

2.3 Line sampling

In precise probability framework of structural reliability analysis (epistemic uncertainty is not yet involved), line sampling is an efficient simulation method especially developed for solving a wide range applications with high-dimensional inputs and rare failure events [25]. It formulates a reliability problem as a number of conditional one-dimensional reliability problems which are

analyzed in standard normal space [18]. In line sampling procedure, the important direction, which is usually defined as the negative of the steepest descent direction of LSF, must be firstly approximated. This assumption arouses one limitation that line sampling is not suitable for strong nonlinear performance functions, especially when the important direction cannot be easily estimated [26].

As mentioned above, the original space of random variables \mathbf{x} must be transformed to standard normal space where the new variables are denoted by $\mathbf{z} = (z_1, \dots, z_n)$, similarly, the LSF $g(\mathbf{x})$ is then transformed to $h(\mathbf{z})$. The probability integral transformation (PIT) formula from original random space to standard normal space is expressed as

$$\mathbf{z} = \Phi^{-1}(F_{\mathbf{x}}(\mathbf{x})) \quad (10)$$

where $F_{\mathbf{x}}(\mathbf{x})$ is the cumulative density function (CDF) of \mathbf{x} , $\Phi^{-1}(\cdot)$ is the inverse CDF of standard normal distribution. For simplification, denote the transformation as $\mathbf{z} = T(\mathbf{x})$ and the inverse transformation as $\mathbf{x} = T^{-1}(\mathbf{z})$. Let $\boldsymbol{\alpha}$ denote the optimal important direction, and the normalized important direction $\mathbf{e}_{\boldsymbol{\alpha}}$ (which is a unit vector) is defined as follows

$$\mathbf{e}_{\boldsymbol{\alpha}} = \boldsymbol{\alpha} / \|\boldsymbol{\alpha}\| \quad (11)$$

Once $\mathbf{e}_{\boldsymbol{\alpha}}$ is determined, the standard normal space is orthogonally decomposed to a 1-dimensional and $n - 1$ dimensional space [27], and vector \mathbf{z} can be written as

$$\mathbf{z} = \mathbf{z}^{\parallel} + \mathbf{z}^{\perp} \quad (12)$$

where \mathbf{z}^{\parallel} is parallel to $\mathbf{e}_{\boldsymbol{\alpha}}$, and \mathbf{z}^{\perp} is orthogonal to $\mathbf{e}_{\boldsymbol{\alpha}}$, expressed as

$$\begin{aligned} \mathbf{z}^{\parallel} &= \bar{z} \mathbf{e}_{\boldsymbol{\alpha}} \\ \mathbf{z}^{\perp} &= \mathbf{z} - \langle \mathbf{e}_{\boldsymbol{\alpha}}, \mathbf{z} \rangle \mathbf{e}_{\boldsymbol{\alpha}} \end{aligned} \quad (13)$$

where $\langle \cdot, \cdot \rangle$ is the symbol of inner product. Since the standard Gaussian PDF is isotropic [27], the scalar \bar{z} and vector \mathbf{z}^{\perp} are also standard normally distributed.

The direct MCS is carried out by generating N_z samples $\mathbf{z}^{(s)} = (z^{(1)}, \dots, z^{(n)})$ ($s = 1, \dots, N_z$) from its joint PDF $\phi_{\mathbf{z}}(\mathbf{z})$, then the $n - 1$ dimensional sample vector $\mathbf{z}^{\perp(s)}$ can be derived with the formula $\mathbf{z}^{\perp(s)} = \mathbf{z}^{(s)} - \langle \mathbf{e}_{\boldsymbol{\alpha}}, \mathbf{z}^{(s)} \rangle \mathbf{e}_{\boldsymbol{\alpha}}$. Figure 1 provides the rationale of line sampling procedure for the s th sample in 2-dimensional standard normal space. As shown

in Figure 1, the conditional failure probabilities are determined where $\mathbf{z} = \bar{\mathbf{z}}\mathbf{e}_\alpha + \mathbf{z}^{\perp(s)}$ varies randomly along the line $l^{(s)}(\bar{\mathbf{z}}, \mathbf{e}_\alpha)$. The failure probability corresponding to $\mathbf{z}^{(s)}$ can be computed by

$$P_f^{(s)} = \Phi(-\tilde{c}^{(s)}) \quad (14)$$

where $\tilde{c}^{(s)}$ is the reliability index which is actually the value of \bar{z} at intersection point between the LSF $h(\mathbf{z}) = 0$ and the line $l^{(s)}(\bar{\mathbf{z}}, \mathbf{e}_\alpha)$. Different methods can be used for this one-dimensional reliability analysis task [28]. One popular way is to consider three specific values c_1, c_2, c_3 of \bar{z} so as that three points $(c_1, h(c_1\mathbf{e}_\alpha + \mathbf{z}^{\perp(s)}))$, $(c_2, h(c_2\mathbf{e}_\alpha + \mathbf{z}^{\perp(s)}))$ and $(c_3, h(c_3\mathbf{e}_\alpha + \mathbf{z}^{\perp(s)}))$ are evaluated. Then $\tilde{c}^{(s)}$ can be easily determined by fitting them with second-order polynomial and determine the point $(\tilde{c}^{(s)}, h(\tilde{c}^{(s)}\mathbf{e}_\alpha + \mathbf{z}^{\perp(s)})) = 0$ [29]. According to the theory of advanced first order second moment method (AFOSM) [26], in standard normal space, the reliability index $\tilde{c}^{(s)}$ is in fact the minimum distance between the origin point and the failure boundary approximated by a hyperplane.

By collecting all the values of $\tilde{c}^{(s)}$, the MCS estimator of failure probability is

$$\hat{P}_f = \frac{1}{N_z} \sum_{s=1}^{N_z} P_f^{(s)} = \frac{1}{N_z} \sum_{s=1}^{N_z} \Phi(-\tilde{c}^{(s)}) \quad (15)$$

And the variance of the above estimator is

$$V(\hat{P}_f) = \frac{1}{N_z(N_z - 1)} \sum_{s=1}^{N_z} (P_f^{(s)} - \hat{P}_f)^2 = \frac{1}{N_z(N_z - 1)} \left(\sum_{s=1}^{N_z} P_f^{(s)2} - N \hat{P}_f^2 \right) \quad (16)$$

Note that LSF is evaluated only when searching the value of $\tilde{c}^{(s)}$ along each line. To sum up, line sampling is an efficient simulation method based on a series of conditional one-dimensional reliability analysis, and each one-dimensional reliability analysis is implemented on MC samples from $n - 1$ dimensional standard normal space orthogonal to \mathbf{e}_α . From the geometric point of view, line sampling can also be regarded as carrying out N times of AFOSM reliability analysis and taking the mean of all the AFOSM results. Although the estimator of failure probability is unbiased independent from the choice of important direction, its quality (measured in terms of its variance) strongly depends on the selection of an appropriate important direction. Since the

determination of important direction is not the focus of this paper, it is assumed to be known in the following part.

Further advances has been made in recent years for improving the efficiency of line sampling, such as advanced line sampling [30] to adaptively searching the important direction, and the use of surrogate model [31] to approximate the original LSF.

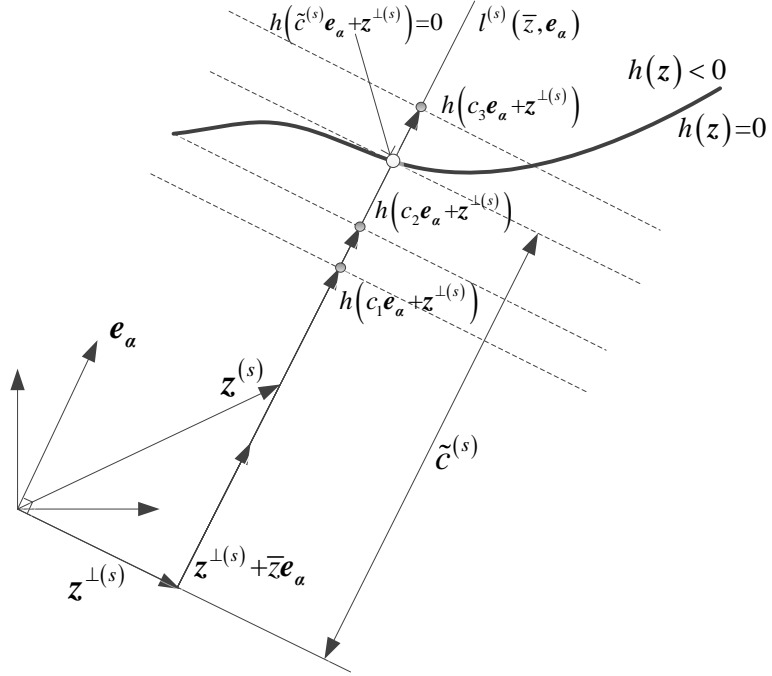


Figure 1 Rationale of Line sampling procedure in standard normal space.

3. Imprecise line sampling method

In this section, we develop two different strategies for injecting the line sampling into the NISS framework for estimating the failure probability function. The first strategy is devised based on the geometric interpretation of the reliability index $\tilde{c}^{(s)}$, and is denoted as hyperplane-approximation based imprecise line sampling (HA-ILS), while the second one is developed based on the mathematical interpretation of the probability computed by integration along each line, and is called weighted-integral based imprecise line sampling (WI-ILS).

3.1 Hyperplane-approximation based imprecise line sampling

As mentioned in subsection 2.1, $\boldsymbol{\theta}^*$ is a fixed point chosen from the support domain of $\boldsymbol{\theta}$. In this strategy, the important direction is determined by fixing $\boldsymbol{\theta}$ at $\boldsymbol{\theta}^*$, and will be kept

unchanged during the whole analysis process. This utilizes the merit of line sampling that it is unbiased, independent of the choice of important direction. As for choosing $\boldsymbol{\theta}^*$, we propose to use the same concept in Ref.[14], i.e., the support domain of \mathbf{x} determined by the optimal $\boldsymbol{\theta}^*$ should be the same with \mathbf{x} at the whole range of $\boldsymbol{\theta}$. In fact, $\boldsymbol{\theta}^*$ can also be specified at the point around any value of interest, as it is expected that the proposed method always performs well close to $\boldsymbol{\theta}^*$.

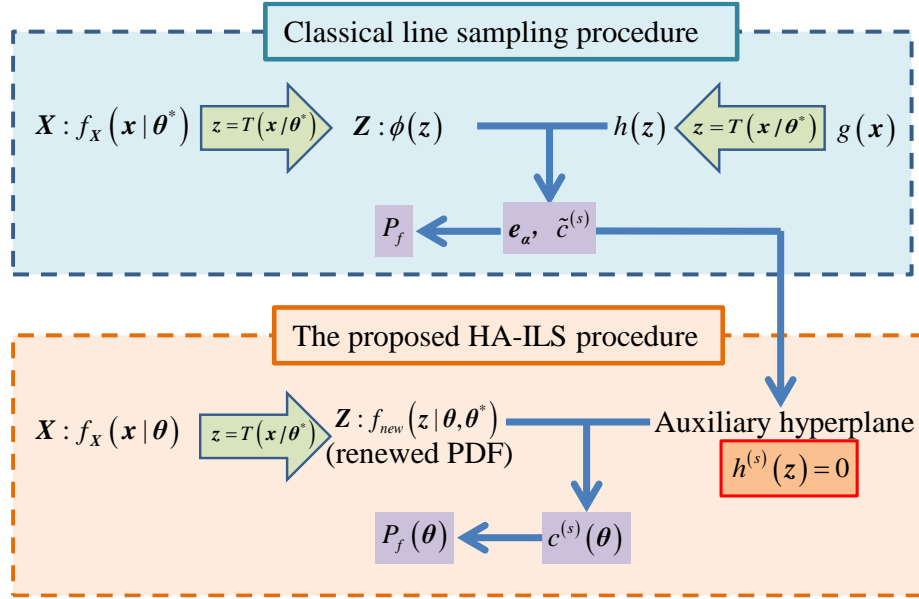


Figure 2 Sketch of the concept of hyperplane-approximation method.

Figure 2 shows the general concept of the proposed HA-ILS method. First of all, classical line sampling method is applied with $\boldsymbol{\theta}$ being fixed at $\boldsymbol{\theta}^*$, shown as the upper blue box. Note that, $h(\mathbf{z})$ is the LSF transformed by $\mathbf{z} = T(\mathbf{x} | \boldsymbol{\theta}^*)$ from the original physical model, which keeps unchanged as long as the formula $\mathbf{z} = T(\mathbf{x} | \boldsymbol{\theta}^*)$ is fixed. There are two key concepts of the proposed method, as shown in the lower red box in Figure 2. One is to introduce auxiliary hyperplane $h^{(s)}(\mathbf{z}) = 0$ to approximate the LSF, which can be established based on the reliability index $\tilde{c}^{(s)}$ and the important direction e_α (a detailed procedure for establishing $h^{(s)}(\mathbf{z})$ will be discussed later). The other is to renew (update) the probability distribution of \mathbf{z} when the distribution parameters of \mathbf{x} changes from $\boldsymbol{\theta}^*$ to $\boldsymbol{\theta}$ but the input variables \mathbf{x} remains being transformed by the same formula $\mathbf{z} = T(\mathbf{x} | \boldsymbol{\theta}^*)$. For example, when x follows a normal distribution such that $N(2, 2^2)$, $z = (x - 2)/2$ follows standard normal distribution.

If the distribution of x changes to $N(4, 4^2)$, then $z = (x - 2)/2$ no longer follows standard normal distribution, but a new distribution such that $z \sim N(1, 2^2)$. As a consequence of the renewal (update) of the probability distribution, \mathbf{x} and $g(\mathbf{x})$ are guaranteed to be consistently transformed by the same formula $T(\cdot|\boldsymbol{\theta}^*)$ and can be used for the following reliability analysis. When the analytical formula of the auxiliary LSF as well as the new probability distribution of \mathbf{z} w.r.t. $\boldsymbol{\theta}$ are precisely known, the failure probability value at $\boldsymbol{\theta}$ corresponding to the s th sample can be easily computed.

Actually, an analytical formula of $h^{(s)}(\mathbf{z}) = 0$ can be easily derived based on the hyperplane equation. In n -dimensional space of \mathbf{z} , the equation of a hyperplane is determined by $\boldsymbol{\omega}^T \mathbf{Z} = \beta$, where $\boldsymbol{\omega} = (\omega_1 \cdots \omega_n)^T$ refers to the normalized unit vector orthogonal to the hyperplane, and β refers to the distance from the origin point to the hyperplane. Hence, when the normalized unit vector and the distance are known, the hyperplane can be uniquely determined. In the classical line sampling, the reliability index $\tilde{c}^{(s)}$ indicates the distance β and the unit important direction \mathbf{e}_α represents the normalized unit vector $\boldsymbol{\omega}$. As shown in Figure 3, for each sample $\mathbf{z}^{(s)}$, the corresponding hyperplane is orthogonal to the important direction \mathbf{e}_α , and contains the intersection point $\mathbf{z}^{\perp(s)} + \tilde{c}^{(s)}\mathbf{e}_\alpha$. Based on the rationale of the first-order reliability method, the failure probability of Eq.(14) actually equals to the probability mass of the failure domain specified by the auxiliary hyperplane. As a consequence, the original failure domain $F_z = \{\mathbf{z}: h(\mathbf{z}) \leq 0\}$ can be approximated by a series of hyperplanes orthogonal to the important direction. Thus for the s th line sample, the analytical formula of auxiliary hyperplane is expressed as

$$h^{(s)}(\mathbf{z}) = \tilde{c}^{(s)} - \mathbf{e}_\alpha \mathbf{z} = 0 \quad (17)$$

As mentioned above, the model structure $h(\mathbf{z})$ stays unchanged since the transformation $\mathbf{z} = T(\mathbf{x}|\boldsymbol{\theta}^*)$ is fixed, and the model structure itself has no relation to the uncertainty characterization of model inputs from a theoretical point of view. In fact, the probability mass of failure domain determined by the established hyperplane will change w.r.t. $\boldsymbol{\theta}$. Hence the

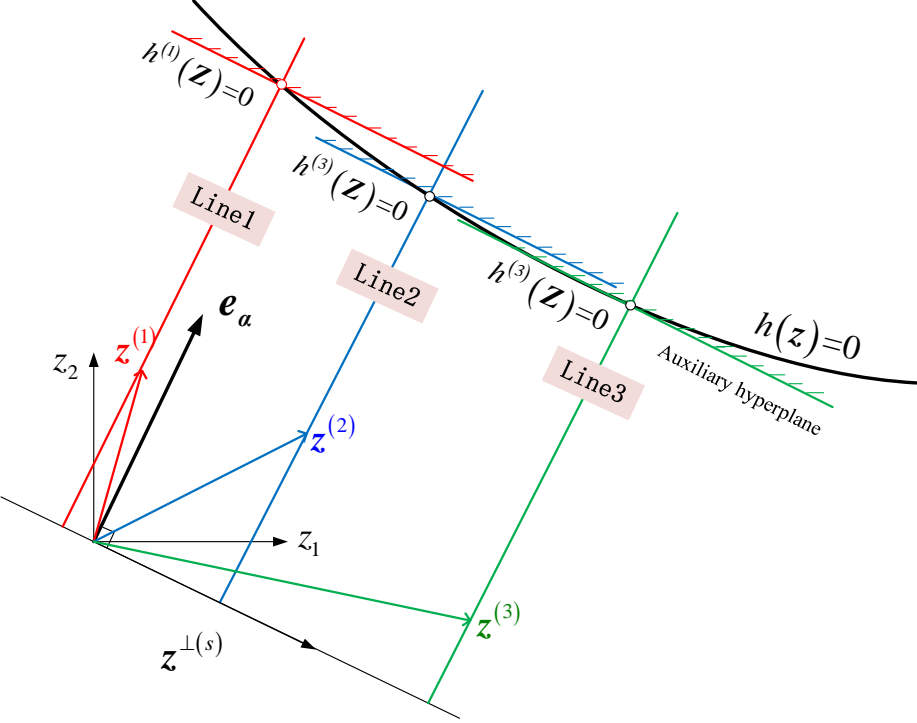


Figure 3 Interpretation of the auxiliary hyperplane for each line sample in standard normal space.

approximated formula $h^{(s)}(\mathbf{z})$ can be utilized for estimating failure probability function $P_f(\boldsymbol{\theta})$ by averaging the failure probability function $P_f^{(s)}(\boldsymbol{\theta})$ across all hyperplanes. $P_f^{(s)}(\boldsymbol{\theta})$ can be estimated by using reliability index, for imprecise variables, the new reliability index becomes a function of $\boldsymbol{\theta}$, denoted by $c^{(s)}(\boldsymbol{\theta})$. If $h^{(s)}(\mathbf{z})$ follows Gaussian distribution, the definition of reliability index can be expressed as

$$c^{(s)}(\boldsymbol{\theta}) = \frac{\mu_{h^{(s)}}(\boldsymbol{\theta})}{\sigma_{h^{(s)}}(\boldsymbol{\theta})} = \frac{\tilde{c}^{(s)} - \sum_{d=1}^n e_{\alpha,d} \mu_{z_d}(\boldsymbol{\theta})}{\sqrt{\sum_{d=1}^n e_{\alpha,d}^2 \sigma_{z_d}^2(\boldsymbol{\theta})}} \quad (18)$$

where $e_{\alpha,d}$ is the d th element in e_α , $\mu_{z_d}(\boldsymbol{\theta})$ and $\sigma_{z_d}(\boldsymbol{\theta})$ refer to the renewed mean and standard deviation of z_d corresponding to the new value $\boldsymbol{\theta}$ (the derivation of renewed mean and standard variation will be discussed later). Specifically, when $\boldsymbol{\theta} = \boldsymbol{\theta}^*$, $\mu_{z_d} = 0$, $\sigma_{z_d} = 1$ and $c^{(s)}(\boldsymbol{\theta}) = \tilde{c}^{(s)}$. Then the estimator of $P_f(\boldsymbol{\theta})$ is as follows

$$\hat{P}_f(\boldsymbol{\theta}) = \frac{1}{N} \sum_{s=1}^N P_f^{(s)}(\boldsymbol{\theta}) = \frac{1}{N} \sum_{s=1}^N \Phi(-c^{(s)}(\boldsymbol{\theta})) \quad (19)$$

, and the variance of the estimator is

$$Var[\hat{P}_f(\boldsymbol{\theta})] = \frac{1}{N(N-1)} \sum_{s=1}^N [\Phi(-c^{(s)}(\boldsymbol{\theta})) - \hat{P}_f(\boldsymbol{\theta})]^2 \quad (20)$$

In the above procedure, we only need to call the LSF when establishing each auxiliary hyperplane, thus the computational cost is the same as that of the classical line sampling. Note that the estimator in Eq.(19) is biased due to the approximation of limit state function through auxiliary hyperplane, the closer $\boldsymbol{\theta}$ is to $\boldsymbol{\theta}^*$, the less biased the estimator will be.

Based on the rationale of NISS reviewed in subsection 2.1, Eq.(19) can be further decomposed with the cut-HDMR, and the estimators of the first two order components are derived as

$$\begin{aligned} \hat{P}_{f0} &= \frac{1}{N} \sum_{s=1}^N \Phi(-\tilde{c}^{(s)}) \\ \hat{P}_{fi}(\theta_i) &= \frac{1}{N} \sum_{s=1}^N (\Phi(-c^{(s)}(\theta_i, \boldsymbol{\theta}_{-i}^*)) - \Phi(-\tilde{c}^{(s)})) \\ \hat{P}_{fij}(\theta_i, \theta_j) &= \frac{1}{N} \sum_{s=1}^N \left(\begin{array}{c} \Phi(-c^{(s)}(\theta_i, \theta_j, \boldsymbol{\theta}_{-i,j}^*)) - \Phi(-c^{(s)}(\theta_i, \boldsymbol{\theta}_{-i}^*)) \\ -\Phi(-c^{(s)}(\theta_j, \boldsymbol{\theta}_{-j}^*)) + \Phi(-\tilde{c}^{(s)}) \end{array} \right) \end{aligned} \quad (21)$$

where $c^{(s)}(\theta_i, \boldsymbol{\theta}_{-i}^*)$ and $c^{(s)}(\theta_i, \theta_j, \boldsymbol{\theta}_{-i,j}^*)$ indicate the first-order and second-order reliability index functions, respectively. Note that those reliability index functions can be easily derived by Eq.(18), therefore, the component functions can also analytically derived with no additional limit function evaluations. The statistical error due to Monte Carlo simulation, which is also a function of $\boldsymbol{\theta}$, can be estimated by the variances of the estimators derived as

$$\begin{aligned} Var(\hat{P}_{f0}) &= \frac{1}{N(N-1)} \sum_{s=1}^N (\Phi(-\tilde{c}^{(s)}) - \hat{P}_{f0})^2 \\ Var(\hat{P}_{fi}) &= \frac{1}{N(N-1)} \sum_{s=1}^N (\Phi(-c^{(s)}(\theta_i, \boldsymbol{\theta}_{-i}^*)) - \Phi(-\tilde{c}^{(s)}) - \hat{P}_{fi})^2 \\ Var(\hat{P}_{fij}) &= \frac{1}{N(N-1)} \sum_{s=1}^N \left(\begin{array}{c} \Phi(-c^{(s)}(\theta_i, \theta_j, \boldsymbol{\theta}_{-i,j}^*)) - \Phi(-c^{(s)}(\theta_i, \boldsymbol{\theta}_{-i}^*)) \\ -\Phi(-c^{(s)}(\theta_j, \boldsymbol{\theta}_{-j}^*)) + \Phi(-\tilde{c}^{(s)}) - \hat{P}_{fij} \end{array} \right)^2 \end{aligned} \quad (22)$$

With those explicit component functions, parametric sensitivity analysis can be applied based on the definition in Eq.(9). The above procedure solves imprecise reliability problems by the auxiliary hyperplane approximation of failure boundary, thus is denoted by hyperplane-approximation based approach.

Note that the accuracy of reliability index function given in Eq.(18) depends on the distribution type of input variables. For normal and lognormal distributions, $h^{(s)}(\mathbf{z})$ follows the Gaussian distribution, then the definition in Eq.(18) is accurate. However, for other distribution types, a change of $\boldsymbol{\theta}$ may result to a non-Gaussian distribution of $h^{(s)}(\mathbf{z})$, then this definition is not accurate anymore. A more detailed discussion about this is given below with normal, lognormal and general cases, separately.

(1) Normal distribution

First, we discuss the analytical formulation of the renewed mean function $\mu_{z_d}(\boldsymbol{\theta})$ and variance function $\sigma_{z_d}^2(\boldsymbol{\theta})$ utilized in Eq.(18). For normal variable x_d , the chosen distribution parameters $\boldsymbol{\theta}_d^*$ are specified as μ_d^* and σ_d^* , the varying parameters $\boldsymbol{\theta}_d$ are specified as μ_d and σ_d , the transformation formula is then specified as $T(x_d|\boldsymbol{\theta}_d^*) = (x_d - \mu_d^*)/\sigma_d^* = z_d$. Then z_d is regarded as a linear transformation of x_d , it is obvious that z_d still follows normal distribution with mean parameter $\mu_{z_d}(\mu_d) = E(z_d) = (\mu_d - \mu_d^*)/\sigma_d^*$ and standard deviation parameter $\sigma_{z_d}(\sigma_d) = \sqrt{Var(z_d)} = \sigma_d/\sigma_d^*$, where $E(\cdot)$ and $Var(\cdot)$ represent the expectation and variance operators respectively.

When all input variables follow normal distribution, the analytical expression of first-order reliability indices $c^{(s)}(\theta_i, \boldsymbol{\theta}_{-i}^*)$ w.r.t. μ_i and σ_i in Eq.(21) can be derived as

$$\begin{cases} c^{(s)}(\mu_i) = \tilde{c}^{(s)} - e_{\alpha,i} \frac{(\mu_i - \mu_i^*)}{\sigma_i^*} \\ c^{(s)}(\sigma_i) = \frac{\tilde{c}^{(s)}}{\sqrt{e_{\alpha,i}^2 \frac{\sigma_i^2}{\sigma_i^{*2}} + \sum_{d=1, d \neq i}^n e_{\alpha,d}^2}} \end{cases} \quad (23)$$

The second-order reliability index $c^{(s)}(\theta_i, \theta_j, \boldsymbol{\theta}_{-i,j}^*)$ in Eq.(21) is expressed as

$$\begin{cases} c^{(s)}(\mu_i, \mu_j) = \tilde{c}^{(s)} - e_{\alpha,i} \frac{(\mu_i - \mu_i^*)}{\sigma_i^*} - e_{\alpha,j} \frac{(\mu_j - \mu_j^*)}{\sigma_j^*} \quad (i \neq j) \\ c^{(s)}(\sigma_i, \sigma_j) = \frac{\tilde{c}^{(s)}}{\sqrt{e_{\alpha,i}^2 \frac{\sigma_i^2}{\sigma_i^{*2}} + e_{\alpha,j}^2 \frac{\sigma_j^2}{\sigma_j^{*2}} + \sum_{d=1, d \neq i, d \neq j}^n e_{\alpha,d}^2}} \\ c^{(s)}(\mu_i, \sigma_j) = \frac{\tilde{c}^{(s)} - e_{\alpha,i} \frac{(\mu_i - \mu_i^*)}{\sigma_i^*}}{\sqrt{e_{\alpha,j}^2 \frac{\sigma_j^2}{\sigma_j^{*2}} + \sum_{d=1, d \neq j}^n e_{\alpha,d}^2}} \end{cases} \quad (24)$$

The estimators of the component failure probability functions are then accordingly specified. For

example, $\hat{P}_{fi}(\mu_i) = \frac{1}{N} \sum_{s=1}^N \left(\Phi\left(e_{\alpha,i} \frac{(\mu_i - \mu_i^*)}{\sigma_i^*}\right) - \Phi(-\tilde{c}^{(s)}) \right)$.

(2) Lognormal distribution

For lognormal distribution $x_d \sim \log N(\mu_d, \sigma_d^2)$, the PDF of x_d is known as

$$f(x_d) = \frac{1}{\sigma_d x_d \sqrt{2\pi}} \exp\left(-\frac{(\ln x_d - \mu_d)^2}{2\sigma_d^2}\right) \quad (25)$$

where μ_d and σ_d are the expected value and standard deviation of the normal distribution associated with x_d . The mean value and variance of x_d are calculated as $m = \exp(\mu_d + \sigma_d^2/2)$, and $v = (\exp(\sigma_d^2) - 1)\exp(2\mu_d + \sigma_d^2)$, respectively. The transformation formula is specified as $T(x_d|\boldsymbol{\theta}_d^*) = (\ln x_d - \mu_d^*)/\sigma_d^* = z_d$. z_d can be regarded as a linear transformation of $\ln x_d$, and as $\ln x_d$ is following normal distribution $N(\mu_d, \sigma_d^2)$, then z_d also follows normal distribution with its mean and standard variance as $\mu_{z_d}(\mu_d) = (\mu_d - \mu_d^*)/\sigma_d^*$ and $\sigma_{z_d}(\sigma_d) = \sigma_d/\sigma_d^*$, respectively. The formulas of renewed mean and standard variance are actually the same with the case of normal distribution type. As a consequence, the subsequent procedure of estimating failure probability function is also the same. Since the approximated LSF $h^{(s)}(\mathbf{z})$ is a linear combination of \mathbf{z} , thus it follows a Gaussian distribution for normal and lognormal input variables.

(3) General case

When x_d follows general distribution types with the PDF $f_{X_d}(x_d|\boldsymbol{\theta}_d)$, the translation formula is $T(x_d|\boldsymbol{\theta}_d^*) = \Phi^{-1}(F_{X_d}(x_d|\boldsymbol{\theta}_d^*)) = z_d$. For general case, z_d might be non-Gaussian distribution, we propose to do classical Monte Carlo simulation to estimate $P_f(\boldsymbol{\theta})$ instead of using reliability index. For any value of $\boldsymbol{\theta}$, generating M samples $(x_1^{(r)}, \dots, x_n^{(r)})$ ($r = 1, \dots, M$), then evaluating the corresponding samples $(z_1^{(r)}, \dots, z_n^{(r)})$ ($r = 1, \dots, M$) by using transformation formula. Then failure probability can be easily estimated by

$$P_f^{(s)} = \frac{1}{M} \sum_{r=1}^M I_F^h(\mathbf{z}^{(r)}) \quad I_F^h(\mathbf{z}^{(r)}) = \begin{cases} 1 & h^{(s)}(\mathbf{z}^{(r)}) < 0 \\ 0 & h^{(s)}(\mathbf{z}^{(r)}) \geq 0 \end{cases} \quad (26)$$

Although it requires resampling for each $\boldsymbol{\theta}$ value, but it will not require additional evaluation of real LSF since the formula $h^{(s)}(\mathbf{z})$ is analytically known. And the following steps for estimating

$P_f(\boldsymbol{\theta})$ are the same as those with the case of normal distribution. Note that for dependent input variables, it is also necessary to firstly transform the input variables from correlated distribution space into standard Gaussian space, then the residual procedures will be almost the same with the independent case.

3.2 Weighted-integral based imprecise line sampling

In this subsection, we develop another strategy based on the formula of line sampling integral, denoted as weighted-integral ILS (WI-ILS), for injecting the line sampling into the NISS framework.

Like HA-ILS method, the first step of WI-ILS is also to perform the classical line sampling method for the constant cut-HDMR component with the distribution parameters $\boldsymbol{\theta}$ being fixed at $\boldsymbol{\theta}^*$, and all the following discussions and developments are based on the standard normal space obtained by the fixed transformation $\mathbf{z} = T(\mathbf{x}|\boldsymbol{\theta}^*)$. By differentiating both sides of $\Phi(\mathbf{z}) = F_{\mathbf{x}}(\mathbf{x}|\boldsymbol{\theta}^*)$, one can obtain $\phi(\mathbf{z})d\mathbf{z} = f_{\mathbf{x}}(\mathbf{x}|\boldsymbol{\theta}^*)d\mathbf{x}$. Thus the integral of failure probability function in Eq.(2) can be rewritten as

$$P_f(\boldsymbol{\theta}) = \int_{g(x) \leq 0} \frac{f_{\mathbf{x}}(\mathbf{x}|\boldsymbol{\theta})}{f_{\mathbf{x}}(\mathbf{x}|\boldsymbol{\theta}^*)} f_{\mathbf{x}}(\mathbf{x}|\boldsymbol{\theta}^*) d\mathbf{x} = \int_{g(T^{-1}(\mathbf{z}|\boldsymbol{\theta}^*)) \leq 0} \frac{f_{\mathbf{x}}(T^{-1}(\mathbf{z}|\boldsymbol{\theta}^*)|\boldsymbol{\theta})}{f_{\mathbf{x}}(T^{-1}(\mathbf{z}|\boldsymbol{\theta}^*)|\boldsymbol{\theta}^*)} \phi(\mathbf{z}) d\mathbf{z} \quad (27)$$

Based on the rationale of line sampling, decomposing \mathbf{z} as $\mathbf{z} = \mathbf{z}^\perp + \bar{z}\mathbf{e}_\alpha$ can reshape the n -dimensional integral of Eq.(27) orthogonally into a double-loop integral, where the outer loop is a $(n-1)$ -dimensional integral in the space of \mathbf{z}^\perp , and the inner loop is a one-dimensional integral in the space of \bar{z} , thus $P_f(\boldsymbol{\theta})$ can be expressed as

$$P_f(\boldsymbol{\theta}) = \int_{g(T^{-1}(\mathbf{z}^\perp + \bar{z}\mathbf{e}_\alpha|\boldsymbol{\theta}^*)) \leq 0} \eta(\mathbf{z}^\perp + \bar{z}\mathbf{e}_\alpha, \boldsymbol{\theta}, \boldsymbol{\theta}^*) \phi(\bar{z}) d\bar{z} \phi(\mathbf{z}^\perp) d\mathbf{z}^\perp \quad (28)$$

where $\eta(\mathbf{z}^\perp + \bar{z}\mathbf{e}_\alpha, \boldsymbol{\theta}, \boldsymbol{\theta}^*)$ denotes the PDF weight, and is expressed as

$$\eta(\mathbf{z}^\perp + \bar{z}\mathbf{e}_\alpha, \boldsymbol{\theta}, \boldsymbol{\theta}^*) = \frac{f_{\mathbf{x}}(T^{-1}(\mathbf{z}^\perp + \bar{z}\mathbf{e}_\alpha|\boldsymbol{\theta}^*)|\boldsymbol{\theta})}{f_{\mathbf{x}}(T^{-1}(\mathbf{z}^\perp + \bar{z}\mathbf{e}_\alpha|\boldsymbol{\theta}^*)|\boldsymbol{\theta}^*)} \quad (29)$$

With the set of samples of $\mathbf{z}^{\perp(s)} (s=1, \dots, N)$ following $(n-1)$ -dimensional PDF $\phi(\mathbf{z}^\perp)$, the estimator of $P_f(\boldsymbol{\theta})$ is derived as

$$\hat{P}_f(\boldsymbol{\theta}) = \frac{1}{N} \sum_{s=1}^N \int_{g(T^{-1}(\mathbf{z}^{\perp(s)} + \bar{z}\mathbf{e}_{\alpha}|\boldsymbol{\theta}^*)) \leq 0} \eta(\mathbf{z}^{\perp(s)} + \bar{z}\mathbf{e}_{\alpha}, \boldsymbol{\theta}, \boldsymbol{\theta}^*) \phi(\bar{z}) d\bar{z} \quad (30)$$

Note that the one-dimensional failure domain defined by $g(T^{-1}(\mathbf{z}^{\perp(s)} + \bar{z}\mathbf{e}_{\alpha}|\boldsymbol{\theta}^*)) \leq 0$ is actually the same failure domain along the line $l^{(s)}(\bar{z}, \mathbf{e}_{\alpha})$ which has been discussed in section 2.2. Hence, the integral boundary can be replaced by $[\tilde{c}^{(s)}, +\infty)$, where $\tilde{c}^{(s)}$ corresponds to the intersection point between the line and limit state boundary. Let $L^{(s)}(\boldsymbol{\theta})$ denote the integral in Eq.(30) as

$$L^{(s)}(\boldsymbol{\theta}) = \int_{\tilde{c}^{(s)}}^{\infty} \eta(\mathbf{z}^{\perp(s)} + \bar{z}\mathbf{e}_{\alpha}, \boldsymbol{\theta}, \boldsymbol{\theta}^*) \phi(\bar{z}) d\bar{z} \quad (31)$$

Specifically, when $\boldsymbol{\theta} = \boldsymbol{\theta}^*$, $\eta = 1$ and $L^{(s)}(\boldsymbol{\theta}) = \Phi(-\tilde{c}^{(s)})$. Thus the estimator of failure probability function can be represented as

$$\hat{P}_f(\boldsymbol{\theta}) = \frac{1}{N} \sum_{s=1}^N L^{(s)}(\boldsymbol{\theta}) \quad (32)$$

Similar with the HA-ILS method in subsection 3.1 (see Eq.(20)-(22)), the variance of the above estimator, the estimator of cut-HDMR component functions as well as the variance of each component can be easily derived, which is omitted here. Actually, the computation of Eq.(31) does not require any additional performance function evaluations, thus making it possible that the computational cost of line sampling for the estimation of $P_f(\boldsymbol{\theta})$ is the same with $P_f(\boldsymbol{\theta}^*)$. Note that, all the expressions above can be easily evaluated through one-dimensional numerical integration and do not involve any other approximations.

Now the main problem is to estimate the value of integral $L^{(s)}(\boldsymbol{\theta})$, which can be derived analytically for some specific distribution types, and a detailed discussion is given below.

(1) Normal distribution

For the d th variable, $X_d \sim N(\mu_d, \sigma_d^2)$, and $x_d = T^{-1}(z_d|\boldsymbol{\theta}_d^*)$ can be specified as

$$x_d = \mu_d^* + \sigma_d^* z_d = \mu_d^* + \sigma_d^* z_d^{\perp(s)} + \sigma_d^* \bar{z} e_{\alpha,d} \quad (33)$$

Then the PDF weight in Eq.(29) can be derived analytically as

$$\eta = \left(\prod_{d=1}^n \frac{\sigma_d^*}{\sigma_d} \right) \exp \left(\sum_{d=1}^n \left(\frac{(\mu_d^* + \sigma_d^* z_d^{\perp(s)} + \sigma_d^* \bar{z} e_{\alpha,d} - \mu_d^*)^2}{2\sigma_d^{*2}} - \frac{(\mu_d^* + \sigma_d^* z_d^{\perp(s)} + \sigma_d^* \bar{z} e_{\alpha,d} - \mu_d)^2}{2\sigma_d^2} \right) \right) \quad (34)$$

Then substituting Eq.(34) into Eq.(31) analytically, the integral is expressed as

$$L^{(s)}(\boldsymbol{\mu}, \boldsymbol{\sigma}) = \frac{\xi}{\sqrt{1-2\zeta}} \exp\left(\lambda^{(s)} + \frac{(\kappa^{(s)})^2}{2-4\zeta}\right) \Phi\left(\frac{\kappa^{(s)} - (1-2\zeta)c^{(s)}}{\sqrt{1-2\zeta}}\right) \quad (35)$$

One can refer to **Appendix A** for detailed definition of parameters ξ , ζ , $\lambda^{(s)}$, $\kappa^{(s)}$, as well as the derivations of the analytical formula in Eq.(35). After that, the estimator of failure probability function and the corresponding variance of estimator can be derived accordingly.

Furtherly, the first-order and second-order failure probability functions can be derived with cut-HDMR decomposition, and the integral functions in $P_f(\theta_i, \boldsymbol{\theta}_{-i}^*)$ and $P_f(\theta_i, \theta_j, \boldsymbol{\theta}_{-i,j}^*)$ are denoted by $L^{(s)}(\mu_i)$, $L^{(s)}(\mu_j)$, $L^{(s)}(\mu_i, \mu_j)$, $L^{(s)}(\sigma_i, \sigma_j)$, $L^{(s)}(\mu_i, \sigma_j)$, respectively. The corresponding self-defined parameters ξ , ζ , $\lambda^{(s)}$, $\kappa^{(s)}$ within integral functions are given in Table 1.

Table 1 Analytical expressions of parameters ξ , ζ , $\lambda^{(s)}$, $\kappa^{(s)}$ in component integral functions.

Integrals	ξ	ζ	$\lambda^{(s)}$	$\kappa^{(s)}$
$L^{(s)}(\mu_i)$	1	0	$\frac{(z_i^{\perp(s)})^2}{2} - \frac{(\mu_i^* + \sigma_i^* z_i^{\perp(s)} - \mu_i)^2}{2\sigma_i^{*2}}$	$\frac{(\mu_i - \mu_i^*)e_{\alpha,i}}{\sigma_i^*}$
$L^{(s)}(\sigma_i)$	$\frac{\sigma_i^*}{\sigma_i}$	$\frac{e_{\alpha,i}^2}{2} \left(1 - \frac{\sigma_i^{*2}}{\sigma_i^2}\right)$	$\frac{(z_i^{\perp(s)})^2}{2} \left(1 - \frac{\sigma_i^{*2}}{\sigma_i^2}\right)$	$z_i^{\perp(s)} e_{\alpha,i} \left(1 - \frac{\sigma_i^{*2}}{\sigma_i^2}\right)$
$L^{(s)}(\mu_i, \mu_j)$	1	0	$\sum_{k=i,j} \frac{(z_k^{\perp(s)})^2}{2} - \frac{(\mu_k^* + \sigma_k^* z_k^{\perp(s)} - \mu_k)^2}{2\sigma_k^{*2}}$	$\sum_{k=i,j} \frac{(\mu_k - \mu_k^*)e_{\alpha,k}}{\sigma_k^*}$
$L^{(s)}(\sigma_i, \sigma_j)$	$\frac{\sigma_i^* \sigma_j^*}{\sigma_i \sigma_j}$	$\sum_{k=i,j} \frac{e_{\alpha,k}^2}{2} \left(1 - \frac{\sigma_k^{*2}}{\sigma_k^2}\right)$	$\sum_{k=i,j} \frac{(z_k^{\perp(s)})^2}{2} \left(1 - \frac{\sigma_k^{*2}}{\sigma_k^2}\right)$	$\sum_{k=i,j} z_k^{\perp(s)} e_{\alpha,k} \left(1 - \frac{\sigma_k^{*2}}{\sigma_k^2}\right)$
$L^{(s)}(\mu_i, \sigma_i)$	$\frac{\sigma_i^*}{\sigma_i}$	$\frac{e_{\alpha,i}^2}{2} \left(1 - \frac{\sigma_i^{*2}}{\sigma_i^2}\right)$	$\frac{(z_i^{\perp(s)})^2}{2} - \frac{(\mu_i^* + \sigma_i^* z_i^{\perp(s)} - \mu_i)^2}{2\sigma_i^2}$	$z_i^{\perp(s)} e_{\alpha,i} - \frac{(\mu_i^* + \sigma_i^* z_i^{\perp(s)} - \mu_i)\sigma_i^* e_{\alpha,i}}{\sigma_i^2}$
$L^{(s)}(\mu_i, \sigma_j)$ ($i \neq j$)	$\frac{\sigma_j^*}{\sigma_j}$	$\frac{e_{\alpha,j}^2}{2} \left(1 - \frac{\sigma_j^{*2}}{\sigma_j^2}\right)$	$\frac{(z_i^{\perp(s)})^2}{2} - \frac{(\mu_i^* + \sigma_i^* z_i^{\perp(s)} - \mu_i)^2}{2\sigma_i^{*2}}$ $+ \frac{(z_j^{\perp(s)})^2}{2} \left(1 - \frac{\sigma_j^{*2}}{\sigma_j^2}\right)$	$\frac{(\mu_i - \mu_i^*)e_{\alpha,i}}{\sigma_i^*} + z_j^{\perp(s)} e_{\alpha,j} \left(1 - \frac{\sigma_j^{*2}}{\sigma_j^2}\right)$

(2) Lognormal distribution

For the lognormal type of distribution, the transformation formula is specified as

$$T(\mathbf{x}|\boldsymbol{\theta}^*) = (\ln x_d - \mu_d^*)/\sigma_d^* \quad , \quad \text{decomposing } z_d \text{ with } z_d = z_d^{\perp(s)} + \bar{z} e_{\alpha,d} \text{ , the relation}$$

between x_d and z_d can be expressed as

$$\ln x_d = \mu_d^* + \sigma_d^* z_d^{\perp(s)} + \sigma_d^* \bar{z} e_{\alpha,d} \quad (36)$$

Then the PDF weight η has the following expression

$$\eta = \left(\prod_{d=1}^n \frac{\sigma_d^*}{\sigma_d} \right) \exp \left(\sum_{d=1}^n \left(\frac{(\ln x_d - \mu_d^*)^2}{2\sigma_d^{*2}} - \frac{(\ln x_d - \mu_d)^2}{2\sigma_d^2} \right) \right) \quad (37)$$

Replacing $\ln x_d$ with $\mu_d^* + \sigma_d^* z_d^{\perp(s)} + \sigma_d^* \bar{z} e_{\alpha,d}$, we can find that the analytical expression of η turns out to be completely the same as in Eq.(34), obviously, the following procedure for estimating integral function $L^{(s)}(\boldsymbol{\theta})$ as well as the failure probability functions is also the same as normal distribution type.

(3) General case

When x_d follows general distribution with the PDF $f_{X_d}(x_d|\boldsymbol{\theta}_d)$, the relationship between x_d and z_d becomes $x_d = F_{X_d}^{-1}(\Phi(z_d^{\perp(s)} + \bar{z} e_{\alpha,d})|\boldsymbol{\theta}_d^*)$, then PDF weight is

$$\eta = \prod_{d=1}^n \frac{f_{X_d}(F_{X_d}^{-1}(\Phi(z_d^{\perp(s)} + \bar{z} e_{\alpha,d})|\boldsymbol{\theta}_d^*)|\boldsymbol{\theta}_d)}{f_{X_d}(F_{X_d}^{-1}(\Phi(z_d^{\perp(s)} + \bar{z} e_{\alpha,d})|\boldsymbol{\theta}_d^*)|\boldsymbol{\theta}_d^*)} \quad (38)$$

And the integral $L^{(s)}(\boldsymbol{\theta})$ is generally expressed as

$$L^{(s)}(\boldsymbol{\theta}) = \int_{-\infty}^{\infty} \prod_{d=1}^n \frac{f_{X_d}(F_{X_d}^{-1}(\Phi(z_d^{\perp(s)} + \bar{z} e_{\alpha,d})|\boldsymbol{\theta}_d^*)|\boldsymbol{\theta}_d)}{f_{X_d}(F_{X_d}^{-1}(\Phi(z_d^{\perp(s)} + \bar{z} e_{\alpha,d})|\boldsymbol{\theta}_d^*)|\boldsymbol{\theta}_d^*)} \phi(\bar{z}) d\bar{z} \quad (39)$$

The accuracy of the above one-dimensional integral depends on the specific formula of PDF and CDF, of course, the best way is to derive analytically as normal and lognormal. The following steps for estimating $P_f(\boldsymbol{\theta})$ are all the same with the former cases.

4. Case studies

4.1 Analytical example

Consider a simple analytical example where the LSF is a parabola. The expression for the performance function is

$$g(x_1, x_2) = \beta - x_1 + \kappa x_2^2 \quad (40)$$

, where $X_1 \sim N(\mu_1, \sigma_1^2)$, $X_2 \sim N(\mu_2, \sigma_2^2)$. The constant β controls the failure probability level and κ controls the degree of nonlinearity of performance function. The failure probability

function can be calculated analytically by solving numerically the following one dimensional integral (see Appendix B).

$$P_f(\mu_1, \mu_2, \sigma_1, \sigma_2) = \int_{-\infty}^{+\infty} \Phi\left(-\frac{\beta - \mu_1}{\sigma_1} - \frac{\kappa}{\sigma_1} (\mu_2 + \sigma_2 z_2)^2\right) \phi(z_2) dz_2 \quad (41)$$

Let $\beta = 3.5$ and $\kappa = 0.2$ such that the failure is a rare event and the failure surface is mildly nonlinear. The imprecisions of distribution parameters are defined by intervals $\mu_1 \in [-0.5, 0.5]$, $\mu_2 \in [-0.5, 0.5]$, $\sigma_1 \in [0.6, 1]$, $\sigma_2 \in [0.8, 1]$.

The fixed distribution parameters $\boldsymbol{\theta}^*$ are chosen to be $(\mu_1^*, \mu_2^*, \sigma_1^*, \sigma_2^*) = (0, 0, 1, 1)$. For this case, it is straightforward to locate the important direction as $\mathbf{e}_\alpha = (1, 0)^T$. Figure 4 shows the plot of the first-order component functions estimated by HA-ILS and WI-ILS methods, together with the analytical results (denoted as ANA) for comparison, where 100 lines with a total of 300 times of performance function evaluations are used in both ILS procedures. Figure 4 shows that first-order component functions of μ_1 and σ_1 are accurately estimated by both methods, however, for the component of μ_2 and σ_2 , the results generated by WI-ILS is in good agreement with the analytical solutions, but those generated by HA-ILS show some differences. Thus, WI-ILS shows a better performance than HA-ILS in this case. However, it is important to recall that $\mathbf{e}_\alpha = (1, 0)^T$ with the second element equals to zero, indicating that x_2 may not be important for reliability analysis. According to Eq.(17), x_2 is not involved in hyperplane formula, then the parameter change associated with x_2 will not be detected. However, one should note that this does not mean HA-ILS method is not applicable for this case. In Figure 4, the orders of magnitude of μ_2 and σ_2 are much smaller than those of μ_1 and σ_1 , thus it does not affect considerably the result of the final synthesized estimation of the failure probability function if it fails to capture the non-influential behavior. The sensitivity indices shown in Table 2 can also validate this conclusion.

The first- and second-order sensitivity indices computed by the HA-ILS and WI-ILS methods are listed in Table 2, together with their standard deviations (SDs) computed by on Eq.(22) as well as the analytical results for comparison. It is shown that the results generated by both HA-ILS and WI-ILS methods have good consistency with the analytical results, illustrating

the effectiveness of the proposed two methods. All sensitivity indices associated with x_2 are close to zero, indicating the parameters of x_2 are non-influential to failure probability. As a result, the parameters of x_2 can be fixed at any point in the imprecise intervals for subsequent reliability design and optimization. One should note that all the first- and second-order component functions are estimated with one set of samples, and higher- order components can also be estimated by this set of samples.

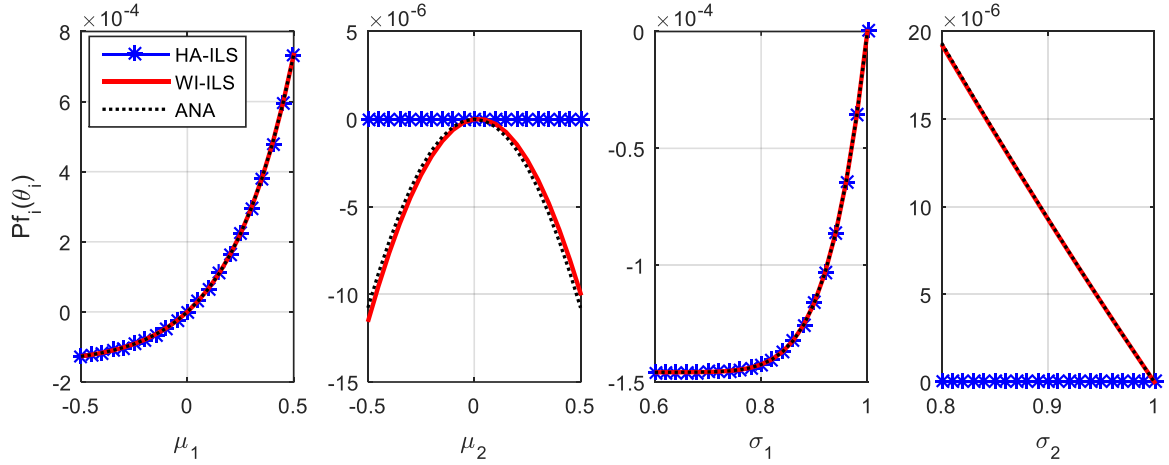


Figure 4 The plot of first-order component functions in the analytical example.

Table 2 The sensitivity indices of the parabolic LSF in the analytical example.

Methods	HA-ILS	WI-ILS	ANA
N_{call}	300	300	/
$P_f(\boldsymbol{\theta}^*)$	$1.4585e-4^{(7.5e-6)}$	$1.4585e-4^{(7.5e-6)}$	$1.4584e-4$
S_i	μ_1	$0.5033^{(0.0012)}$	$0.4866^{(0.0011)}$
	μ_2	$0.0000^{(0.0000)}$	$0.0002^{(4e-5)}$
	σ_1	$0.1339^{(0.0003)}$	$0.1295^{(0.0003)}$
	σ_2	$0.00000^{(0.0000)}$	$0.0009^{(1e-5)}$
S_{ij}	(μ_1, μ_2)	$0.0000^{(0.0001)}$	$0.0005^{(0.0001)}$
	(σ_1, σ_2)	$0.0000^{(0.0000)}$	$0.0007^{(1e-5)}$
	(μ_1, σ_1)	$0.3628^{(0.0008)}$	$0.3790^{(0.0008)}$
	(μ_1, σ_2)	$0.0000^{(0.0000)}$	$0.0024^{(4e-5)}$
	(μ_2, σ_1)	$0.0000^{(0.0000)}$	$0.0001^{(3e-5)}$
	(μ_2, σ_2)	$0.0000^{(0.0000)}$	$0.0000^{(0.0000)}$

Next, we slightly modify the setting of the test example. The parabola is rotated 45 degrees anticlockwise and the g -function becomes

$$g = 3.5 - \frac{\sqrt{2}}{2} (X_1 + X_2) + \frac{0.2}{4} (X_1 - X_2)^2 \quad (42)$$

The uncertainty characterization of each input variable as well as the fixed parameters $\boldsymbol{\theta}^*$ remain the same. The important direction then is calculated to be $\mathbf{e}_\alpha = (\sqrt{2}/2, \sqrt{2}/2)^T$. In this case, the reference results are all calculated by double-loop Monte Carlo method (denoted as DL) with the sample size of each inner loop being 10^7 .

Table 3 The sensitivity indices after rotation of the parabola LSF in the analytical example.

Methods	HA-ILS	WI-ILS	DL
N_{call}	300	300	/
$P_f(\boldsymbol{\theta}^*)$	1.7457e-4 ^(6.1e-6)	1.7457e-4 ^(6.1e-6)	1.7450e-4
S_i	μ_1	0.2012 ^(0.0002)	0.1742 ^(0.0003)
	μ_2	0.2012 ^(0.0002)	0.1842 ^(0.0003)
	σ_1	0.1102 ^(0.0000)	0.1086 ^(0.0001)
	σ_2	0.0556 ^(0.0000)	0.0557 ^(0.0001)
S_{ij}	(μ_1, μ_2)	0.1425 ^(0.0001)	0.1414 ^(0.0002)
	(σ_1, σ_2)	0.0263 ^(0.0000)	0.0295 ^(0.0001)
	(μ_1, σ_1)	0.0905 ^(0.0001)	0.1040 ^(0.0002)
	(μ_1, σ_2)	0.0410 ^(0.0000)	0.0437 ^(0.0001)
	(μ_2, σ_1)	0.0905 ^(0.0001)	0.0965 ^(0.0001)
	(μ_2, σ_2)	0.0410 ^(0.0000)	0.0610 ^(0.0002)
			0.0347

For this case, the sensitivity indices are displayed in Table 3 and the results of the proposed two methods match well with the reference solutions. Figure 5 displays the plot of first-order component functions. Compared with Figure 4 of the previous case, HA-ILS behaves much better in Figure 5 because the two components in important direction \mathbf{e}_α become equal. Besides, the plot of HA-ILS w.r.t σ_1 and σ_2 show a small deviation from the reference results when σ_i is far from σ_i^* , although the corresponding SDs are already smaller than WI-ILS. It indicates HA-ILS converges faster but may go to a biased result because of the approximation of LSF. The component functions always equal to zero at the expansion point $\boldsymbol{\theta}^*$ due to the

definition of cut-HDMR components. All the first-order component functions are monotonically increasing w.r.t the respective parameters, then all the maximum and minimum values of the first-order component functions locate at the upper and lower bound of imprecise parameters, respectively.

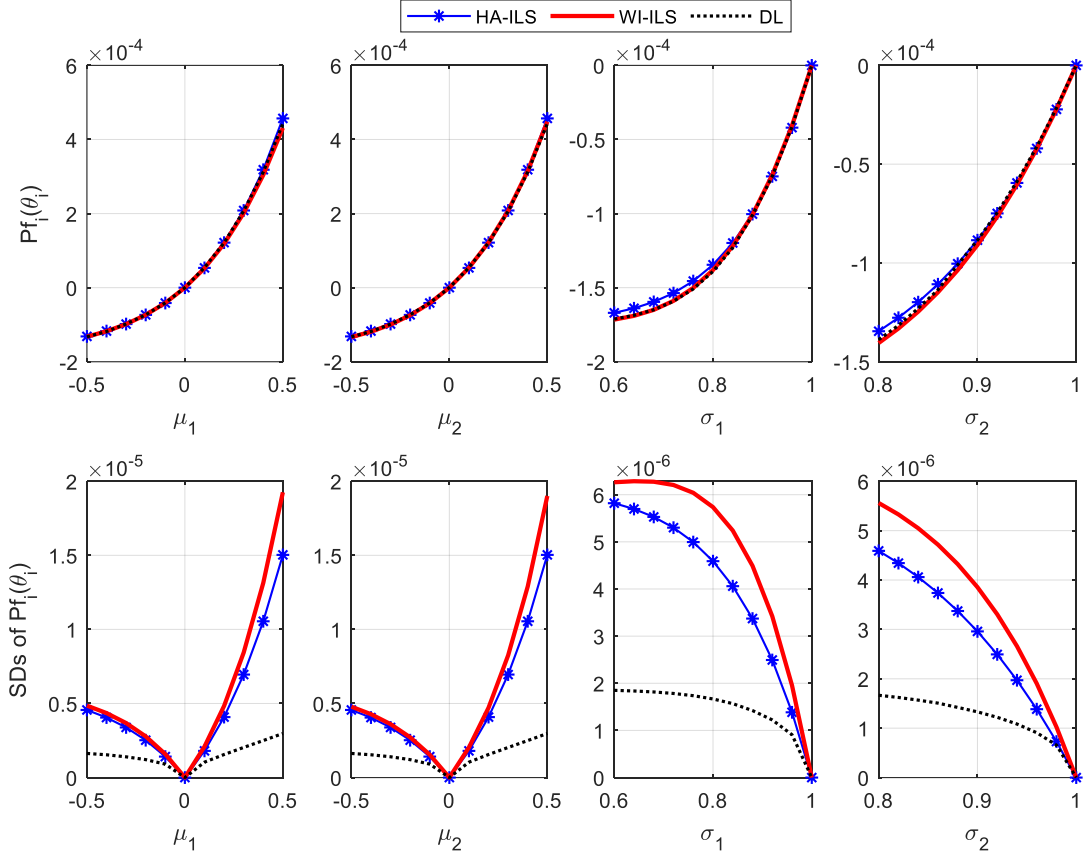


Figure 5 The plot of first-order component functions after rotation of the parabola LSF in the analytical example.

4.2 A shallow foundation model

To illustrate the effectiveness of the proposed method to engineering applications, a shallow foundation resting over elastic soil is considered [32], and a finite element model considering of 320 quadrilateral elements is established for simulating the structure [3]. The schematic representation is shown in Figure 6. The elastic soil is composed of two layers. The first layer is a sand layer of 9 [m] thickness while the second is a gravel layer of 21 [m] thickness resting over a rock bed which is assumed as infinitely rigid.

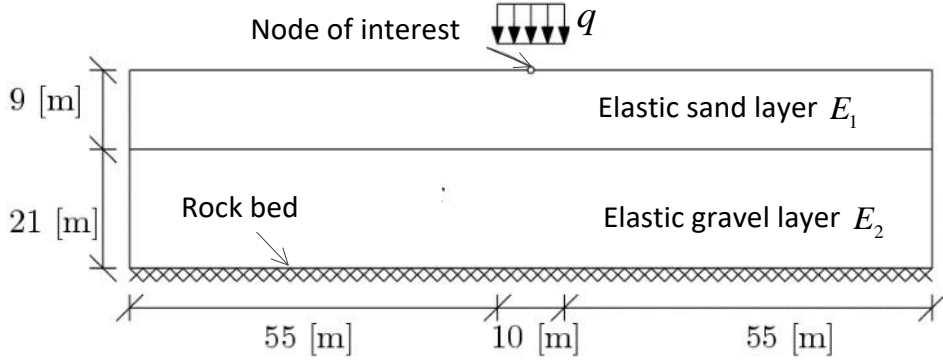


Figure 6 The schematic representation of elastic soil layer of shallow foundation model.

The Young's modulus of the sand and gravel layers are characterized by random variables obeying lognormal distribution, denoted as E_1 and E_2 , respectively. The shallow foundation of 10 [m] width applies a distributed load q of over the elastic soil layer. The load intensity q is characterized by means of a lognormal variable as well. The mean value (denoted by m_{E_1} , m_{E_2} and m_q) of the three random variables are imprecisely known varying within intervals, and the COV (coefficient of variance) are all assumed to be 0.1, as given in Table 4, thus three mean value are modeled as imprecise parameters. The performance function is defined as the threshold level $b=0.055$ [m] minus the vertical displacement at the center of the shallow foundation.

Table 4 Distribution parameters of input variables for shallow foundation model.

Variables	Description	Distribution type	Mean	COV
E_1 [kPa]	Young's modulus of sand layer	Lognormal	[27000,33000]	10%
E_2 [kPa]	Young's modulus of gravel layer	Lognormal	[90000,110000]	10%
q [kPa]	Load density	Lognormal	[90,110]	10%

The expansion point $\boldsymbol{\theta}^*$ are chosen to be $(E_1^*, E_2^*, q^*) = (30000, 100000, 100)$ [kPa], the important direction is $\mathbf{e}_\alpha = (-0.6270, -0.1394, 0.7664)^T$ by implementing AFOSM method in standard normal space with 42 times of model evaluation. We firstly plot the components for the failure probability function with the proposed HA-ILS and WI-ILS procedure in which 100 lines with a total of 342 times of model evaluations are involved, as shown in Figure 7. Since the finite element model of shallow foundation is not very cost-demanding, DL method is also

plotted as reference results with $N = 10^6$ for each failure probability evaluation. It shows that the results of both HA-ILS and WI-ILS match well with DL method except that the plot of m_{E_2} by WI-ILS has a slight difference with the reference results. The plots of HA-ILS keep quite close to the reference plots within the whole range of parameters, showing that not too much bias is introduced by LSF approximations when the values of parameters move away from the expansion point. This indicates that the real LSF of the shallow foundation model may be approximately linear. The plot of SDs shows HA-ILS converges much faster than WI-ILS; specifically, when the value of m_{E_1} is close to the lower bound 27000, the SD of WI-ILS increases sharply while SD of HA-ILS stays at a low value, that means when the values of parameters are far away from the expansion point, HA-ILS shows a much better performance. On the other hand, all the component values vary monotonous with the corresponding parameters, furtherly, it is incremental for q and diminishing for E_1 and E_2 .

The sensitivity indices estimated by HA-ILS and WI-ILS are listed in Table 5, as well as the value of constant component $P_f(\boldsymbol{\theta}^*)$. Among the first-order components, m_{E_1} and m_q are much more influential than m_{E_2} , and among all orders of components, (m_{E_1}, m_q) is the most influential one, indicating that the interaction effect of m_{E_1} and m_q contributes most to failure probability of shallow foundation model. Note that the third-order index is also estimated in Table 5 with the value less than 0.02, that means the third-order component is non-influential in estimating $P_f(\boldsymbol{\theta})$, so truncation up to second order will not introduce significant errors. Figure 8 shows the 3D plot of the most influential second-order component function $P_{f_{ij}}(m_{E_1}, m_q)$ as well as its SDs by the proposed two methods. In Figure 8 the second-order plots by both methods match well with each other, and the SDs show that WI-ILS converges slower than HA-ILS especially in those points far away from $\boldsymbol{\theta}^*$. The maximum value of $P_{f_{ij}}(m_{E_1}, m_q)$ locates in $(2.7 \times 10^4, 110)$, which is also the maximum point of the corresponding first-order plot shown in Figure 7.

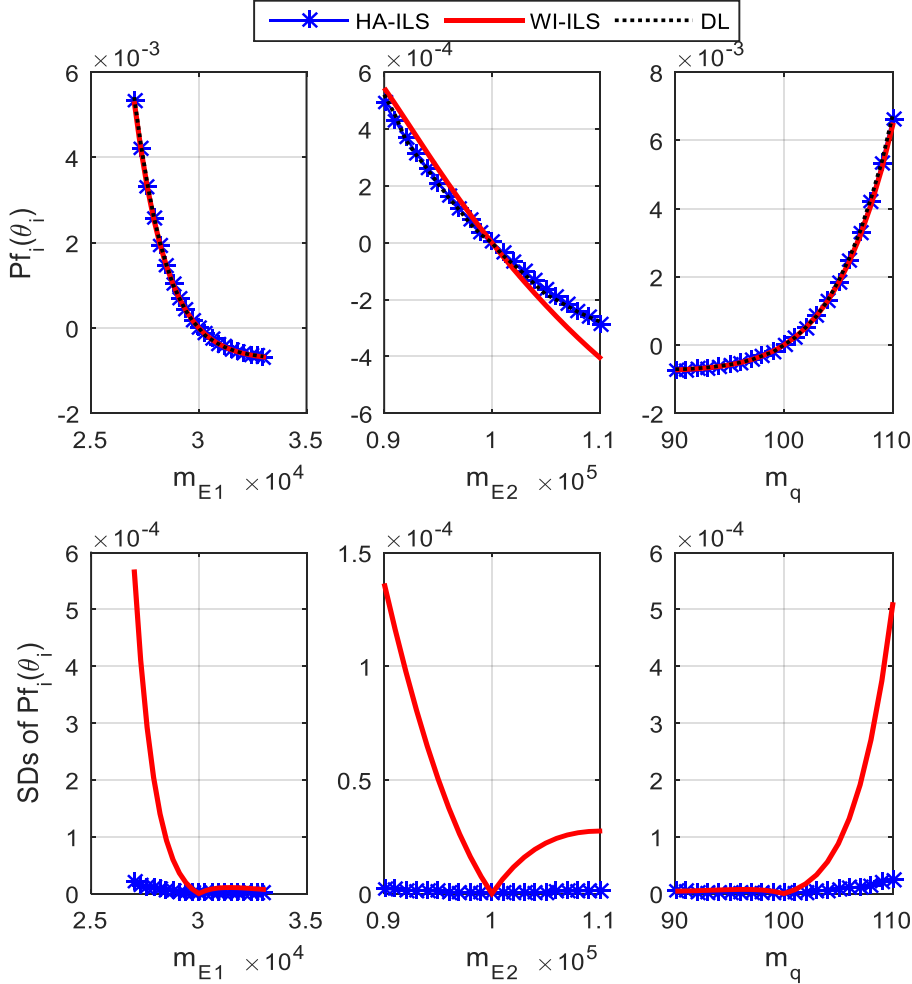


Figure 7 The plot of first-order component functions for shallow foundation model.

Table 5 Sensitivity indices for shallow foundation model.

Methods	HA-ILS	WI-ILS
N_{call}	342	342
$P_f(\boldsymbol{\theta}^*)$	$7.6609e-4^{(2.4e-6)}$	$7.6609e-4^{(2.4e-6)}$
m_{E_1}	$0.1732^{(1e-6)}$	$0.1815^{(0.0006)}$
S_i	m_{E_2}	$0.0028^{(2e-7)}$
	m_q	$0.2341^{(1e-6)}$
(m_{E_1}, m_{E_2})	$0.0101^{(5e-8)}$	$0.0094^{(0.0010)}$
S_{ij}	(m_{E_1}, m_q)	$0.5489^{(2e-6)}$
	(m_{E_2}, m_q)	$0.0133^{(6e-8)}$
S_{ijk}	(m_{E_1}, m_{E_2}, m_q)	$0.0175^{(2e-8)}$
		$0.0173^{(0.0014)}$

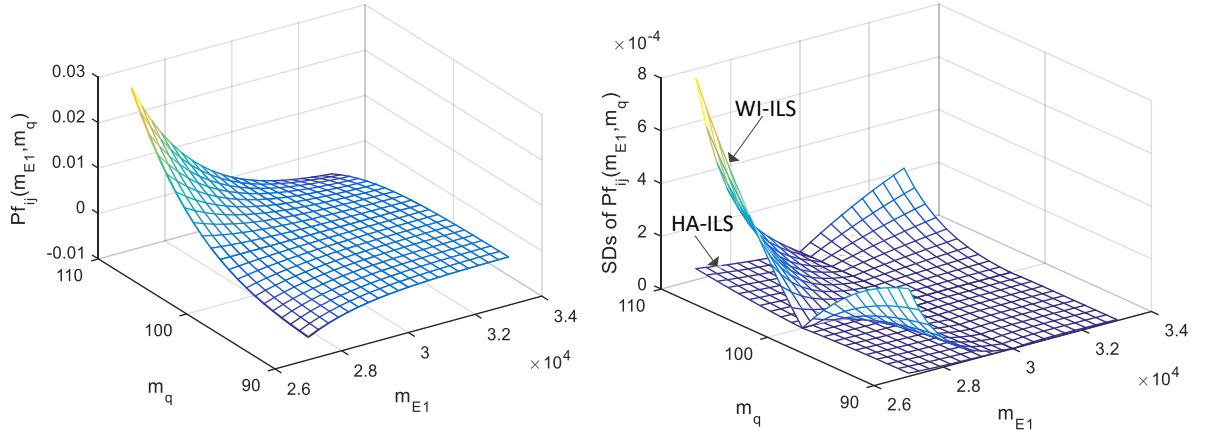


Figure 8 The plot of the most influential second-order component function with both HA-ILS and WI-ILS for shallow foundation model.

4.3 Confined seepage model

Consider a steady state of confined seepage below a dam discussed in Ref. [33], the elevation of the dam is shown in Figure 9. The dam rests over soil composed of two permeable layers and one impermeable layer, and a cutoff wall is designed in the bottom of the dam for preventing excessive seepage. The water height in the upstream side of the dam is denoted by h_D (m) which is modeled as a random variable following uniform distribution of $U(7[m], 10[m])$. The hydraulic head h_W over the segment AB with respect to the impermeable layer is equal to $h_W = h_D + 20[m]$. The water flows through two permeable soil layers towards the downstream side of the dam (see segment CD in Figure 9). It is assumed that there is no water flow on any of the boundaries excepted the segments AB and CD. The first permeable layer is silty sand,

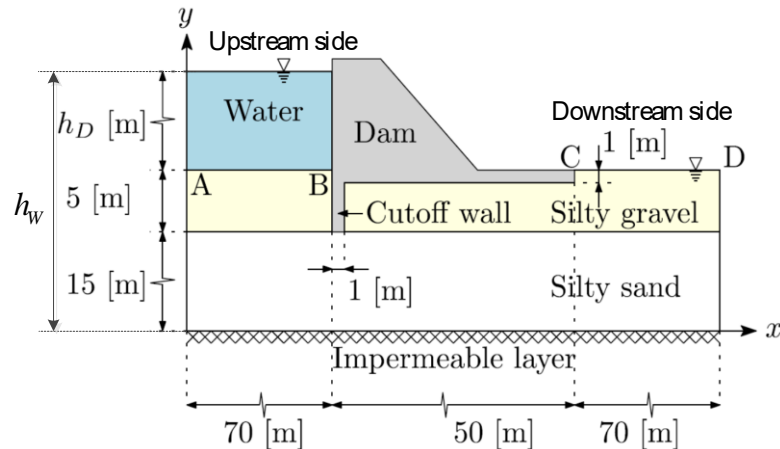


Figure 9 The elevation of the dam in confined seepage model.

while the second one is composed of silty gravel. The permeability of them are modeled as anisotropic and characterized by lognormal random variables, the mean (denoted by m , i.e., $m_{k_{xx,i}}$) and COV of the horizontal (denoted by $k_{xx,i}$) and vertical permeability (denoted by $k_{yy,i}$) of the two soil layers are provided in Table 6. Note that the COV associated with each permeability is equal to 100%, indicating a high degree of uncertainty when estimating the parameters in engineering applications. The governing partial differential equation of the seepage problem is

$$k_{xx,i} \frac{\partial^2 h_W}{\partial x^2} + k_{yy,i} \frac{\partial^2 h_W}{\partial y^2} = 0 \quad (i=1, 2) \quad (43)$$

The boundary conditions are the hydraulic head over segments AB and CD. A finite element mesh comprising 3413 nodes and 1628 quadratic triangular elements is established for solving the above equation. And the seepage q at the downstream side is measured in volume over time (hour) over distance (meter), i.e., the units of q is $[L/h/m]$, it can be calculated by

$$q = - \int_{CD} k_{yy,2} \frac{\partial h_W}{\partial y} dx \quad (44)$$

The failure event of interest is defined when seepage q exceeds a prescribed threshold 33 $[L/h/m]$. Summarily, the permeability of the permeable layers are modeled as imprecise random variables, while water height h_D is modeled as a precise uniform random variable, and LSF is $g(\mathbf{x}) = 33 - q(\mathbf{x})$.

Table 6 Distribution parameters of input variables for confined seepage model.

Inputs	Description	Distribution type	Means	COV	Bounds
$k_{xx,1}$ $[10^{-7}\text{m/s}]$	Horizontal permeability of sand soil layer	Lognormal	[4.5,5.5]	100%	/
$k_{yy,1}$ $[10^{-7}\text{m/s}]$	Vertical permeability of sand soil layer	Lognormal	[1.8,2.2]	100%	/
$k_{xx,2}$ $[10^{-6}\text{m/s}]$	Horizontal permeability of gravel soil layer	Lognormal	[4.5,5.5]	100%	/
$k_{yy,2}$ $[10^{-6}\text{m/s}]$	Vertical permeability of gravel soil layer	Lognormal	[1.8,2.2]	100%	/
h_D [m]	water height in upstream side of dam	Uniform	/	/	[7,10]

First, we set the fixed point $\boldsymbol{\theta}^*$ as $(k_{xx,1}^*, k_{yy,1}^*, k_{xx,2}^*, k_{yy,2}^*) = (5, 2, 50, 20)[10^{-7}\text{m/s}]$ and implementing AFOSM method after transforming into standard normal space, the important direction is $\mathbf{e}_\alpha = (0.8094, 0.3949, 0.2826, 0.2491, 0.2168)^T$ corresponding to the five variables in Table 6 by using 152 times of model evaluations. The proposed HA-ILS and WI-ILS are implemented by sampling 100 lines in which the total number of model evaluation is 452. The computational results of first-order component functions are plotted in Figure 10. It is shown that the results of both methods match well with each other and there is a clear trend of linear increase among all the first-order functions. The SDs in Figure 10 vary in the magnitude of 10^{-6} which is two orders of magnitude smaller than the corresponding component functions, revealing that all the first-order estimators are robustly estimated. Since WI-ILS does not involve approximations, so its plot is a relatively more accurate result, and the small deviation in the third subplot of $P_{fi}(m_{k_{xx,2}})$ confirms the bias in HA-ILS method. Additionally, the plots of SDs also show a slower convergence speed away from $\boldsymbol{\theta}^*$, this indicates that the utilized important direction is suboptimal for estimating the actual values of the components as the distance between $\boldsymbol{\theta}$ and $\boldsymbol{\theta}^*$ increases.

The first- and second-order parametric sensitivity indices as well as their SDs and constant component $P_f(\boldsymbol{\theta}^*)$ are provided in Table 7. Comparing the values of indices one can find that $m_{k_{xx,1}}$ is the most influential parameter among all the indices, and first-order indices are much larger than second-order indices, indicating that the four parameters have a weak interaction effect on failure probability. Figure 11 shows the 3D plot of $P_{fij}(m_{k_{xx,1}}, m_{k_{yy,1}})$ and the corresponding SDs for illustrating the trend of second-order components with the proposed two methods. By comparing it with Figure 8 in shallow foundation model, there exist two maximum points in Figure 11 while there is only one in Figure 8. Overall, the plot of first-order and second-order component functions provide a deeper insight into the relationship between failure probability and distribution parameters.

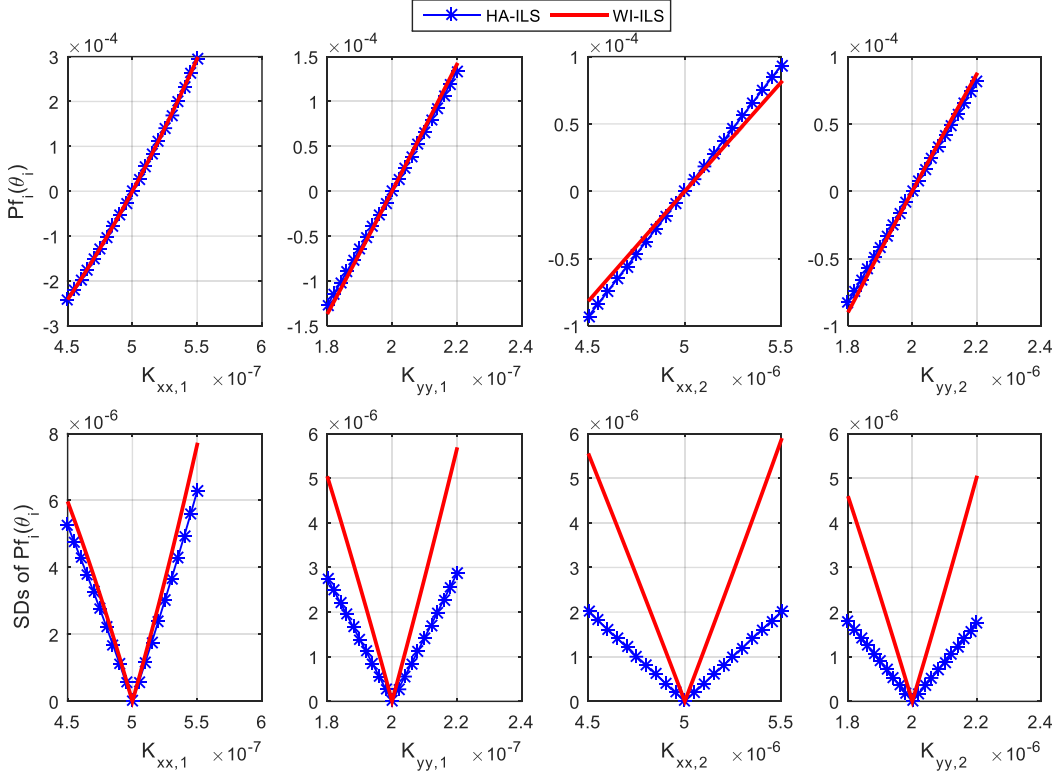


Figure 10 Plots of first-order component functions for confined seepage model.

Table 7 The first- and second-order sensitivity indices for confined seepage model.

Methods	HA-ILS	WI-ILS
N_{call}	452	452
$P_f(\boldsymbol{\theta}^*)$	$8.088e-4^{(1.8e-5)}$	$8.088e-4^{(1.8e-5)}$
$m_{k_{xx,1}}$	$0.6796^{(0.0003)}$	$0.6714^{(0.0004)}$
$m_{k_{yy,1}}$	$0.1618^{(0.0001)}$	$0.1812^{(0.0002)}$
$m_{k_{xx,2}}$	$0.0831^{(3e-5)}$	$0.0612^{(0.0003)}$
$m_{k_{yy,2}}$	$0.0646^{(2e-5)}$	$0.0735^{(0.0002)}$
$(m_{k_{xx,1}}, m_{k_{yy,1}})$	$0.0050^{(2e-6)}$	$0.0060^{(9e-5)}$
$(m_{k_{xx,1}}, m_{k_{xx,2}})$	$0.0026^{(1e-6)}$	$0.0018^{(1e-5)}$
$(m_{k_{xx,1}}, m_{k_{yy,2}})$	$0.0020^{(8e-7)}$	$0.0024^{(8e-6)}$
$(m_{k_{yy,1}}, m_{k_{xx,2}})$	$0.0006^{(2e-7)}$	$0.0006^{(4e-6)}$
$(m_{k_{yy,1}}, m_{k_{yy,2}})$	$0.0005^{(2e-7)}$	$0.0007^{(4e-6)}$
$(m_{k_{xx,2}}, m_{k_{yy,2}})$	$0.0002^{(9e-8)}$	$0.0002^{(3e-6)}$

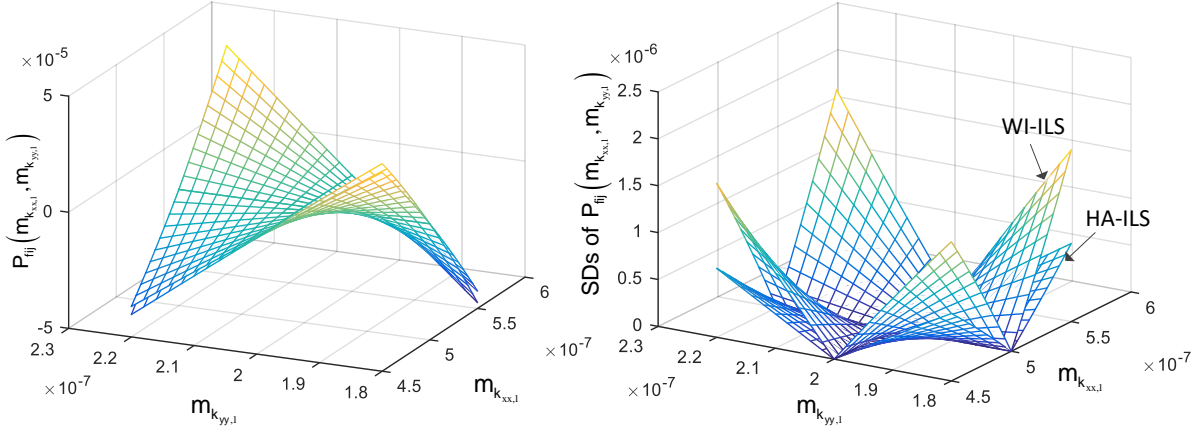


Figure 11 Plots of the two most influential second-order component function with both HA-ILS and WI-ILS method for confined seepage model.

4.4 Transmission tower

A model partially based on the example in Ref.[34] is considered, which comprises a considerable number of uncertain parameters. It consists of a truss structure with 80 bars representing a transmission tower (see Figure 12) that behaves within the linear elastic range, and it withstands four static loads in its top nodes. The four loads are applied in direction $[\sin(\pi/3), \cos(\pi/3), 0]$ and are characterized as deterministic with magnitude $F=200$ [kN]. Each of the 80 bars contains two random variables, Young's modulus, and the cross-section area, so the total number of random variables is 160. The Young's modulus in each bar is modeled by a lognormal distribution, denoted by (E_1, \dots, E_{80}) . The cross-section area is also modeled considering a lognormal distribution, the area for the corner bars is denoted by (A_1^c, \dots, A_{20}^c) , while the cross-section area for the rest 60 bars is denoted by (A_{21}, \dots, A_{80}) .

The COV of 10% is considered for all the 160 lognormal random variables, the mean value of both Young's modulus and cross-section area of corner bars are modeled as 40 imprecise parameters (denoted by $m_{E_1}, \dots, m_{E_{20}}$ and $m_{A_1^c}, \dots, m_{A_{20}^c}$), while the mean value of the rest random variables are precisely known. All the parameters of the random variables are listed in Table 8. The response of interest is the displacement of node A located at the top of the transmission tower, which should not exceed a prescribed threshold of 0.06 [m].

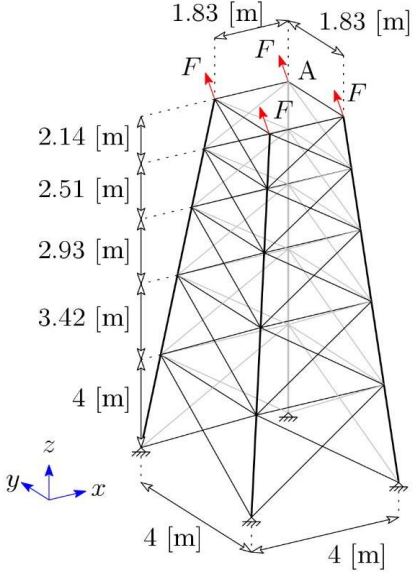


Figure 12 Sketch of transmission tower.

Table 8 Distribution parameters of 160 imprecise random variables in transmission tower model.

Variable	Description	Distribution	Mean	COV
(E_1, \dots, E_{20})	Young's modulus of bars 1~20	Lognormal	$[1.89, 2.31] \times 10^{11}$ [Pa]	10%
(E_{21}, \dots, E_{80})	Young's modulus of bars 21~80	Lognormal	2.1×10^{11} [Pa]	10%
(A_1^c, \dots, A_{20}^c)	Cross-section area of 20 corner bars	Lognormal	$[6700, 8200] [\text{mm}^2]$	10%
(A_{21}, \dots, A_{80})	Cross-section area of the rest 60 bars	Lognormal	4350 $[\text{mm}^2]$	10%.

The expansion points $\boldsymbol{\theta}^*$ of the 40 imprecise parameters are all set at the middle value of the intervals. Both methods are implemented with the same set 5000 lines with the total number of g -function calls being 15056. Note that line sampling is implemented considering a relatively high number of lines; such number is selected in order to verify and compare the behavior of the proposed two methods with crude MCS. The constant HDMR component is estimated by both methods as 0.0016 with SD being $8.085e^{-5}$, and the reference result computed by crude MCS is 0.0015 with SD computed to be $7.145e^{-5}$, indicating that the results computed by LS are accurate and robust. With the same set of samples, the first-order sensitivity indices as well as the corresponding plots of component functions are reported in Figure 13 and Figure 14, respectively.

The sensitivity indices are normalized by the summation of the first two order non-normalized sensitivity indices.

As can be seen from Figure 13, the first-order sensitivity indices computed by HA-ILS and WI-ILS methods show some differences, which is caused by the failure of computing the indices of the two less important components of E_{17} and A_{17}^c by HA-ILS. The first-order influential components computed by DL are also reported in Figure 14 for comparison. It is shown that all the first-order influential components are accurately estimated by the WI-ILS method. However, while HA-ILS is utilized, the estimates of the two most influential components of E_{16} and A_{16}^c are accurate, but those of the two less important components of E_{17} and A_{17}^c are not. The reason has been reported in the analytical example, which is due to the inability of identifying these two less influential dimensions in the important direction. However, this can be improved by utilizing some other advanced method for searching another more accurate MPP, instead of the AFOSM method which does not identify all the influential dimensions in this implementation with high accuracy. This indicates that the performance of HA-ILS is highly dependent on the identified important direction, to which WI-ILS is much less sensitive.

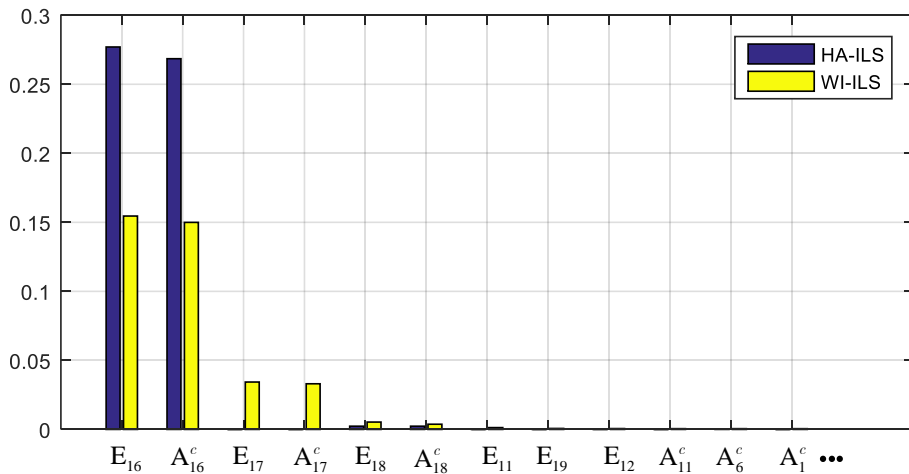


Figure 13 Barplot of the influential first-order sensitivity indices for transmission tower model.

The six most important second-order component functions computed by WI-ILS method with the same set of samples are then reported in Figure 15. The SDs of all estimates are very small and are not reported here. The sensitivity indices of all the influential components

reported in Figure 13 and Figure 15 sum up to 0.86, indicating that it is accurate to approximate the failure probability function with these components. For higher accuracy, the residual less influential components can be added, and we don't give more details for simplicity.

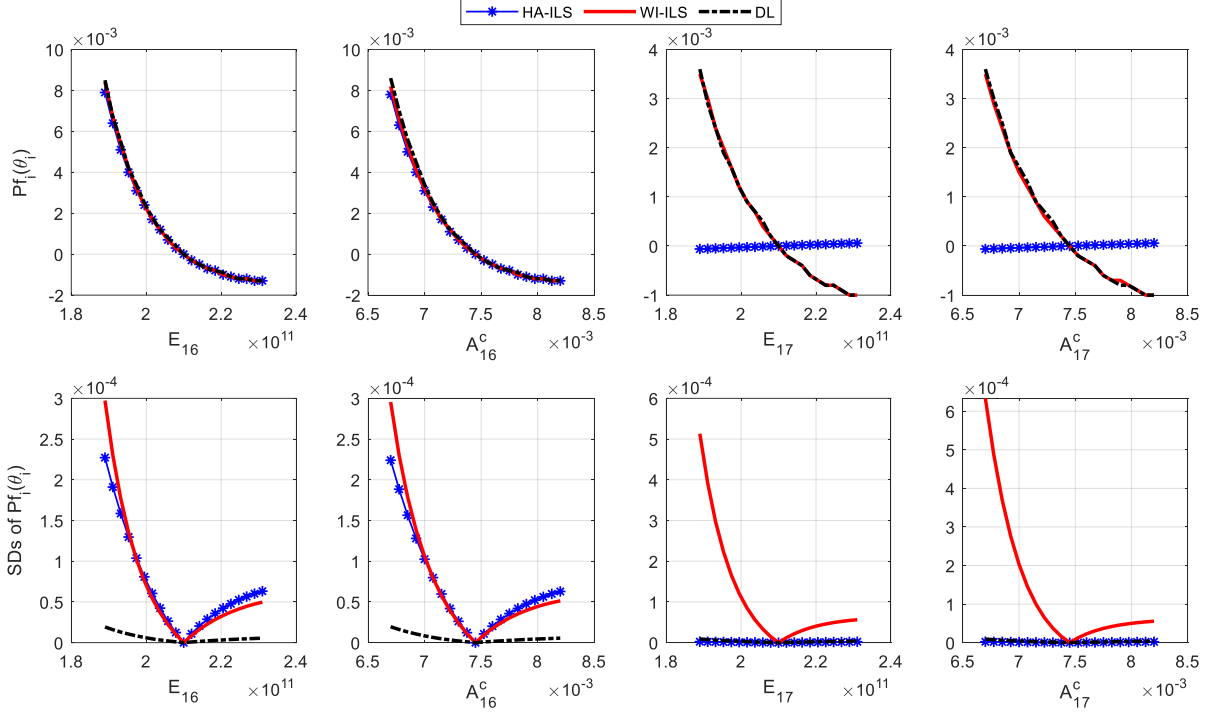


Figure 14 Plots of the four most influential first-order component functions for transmission tower model.

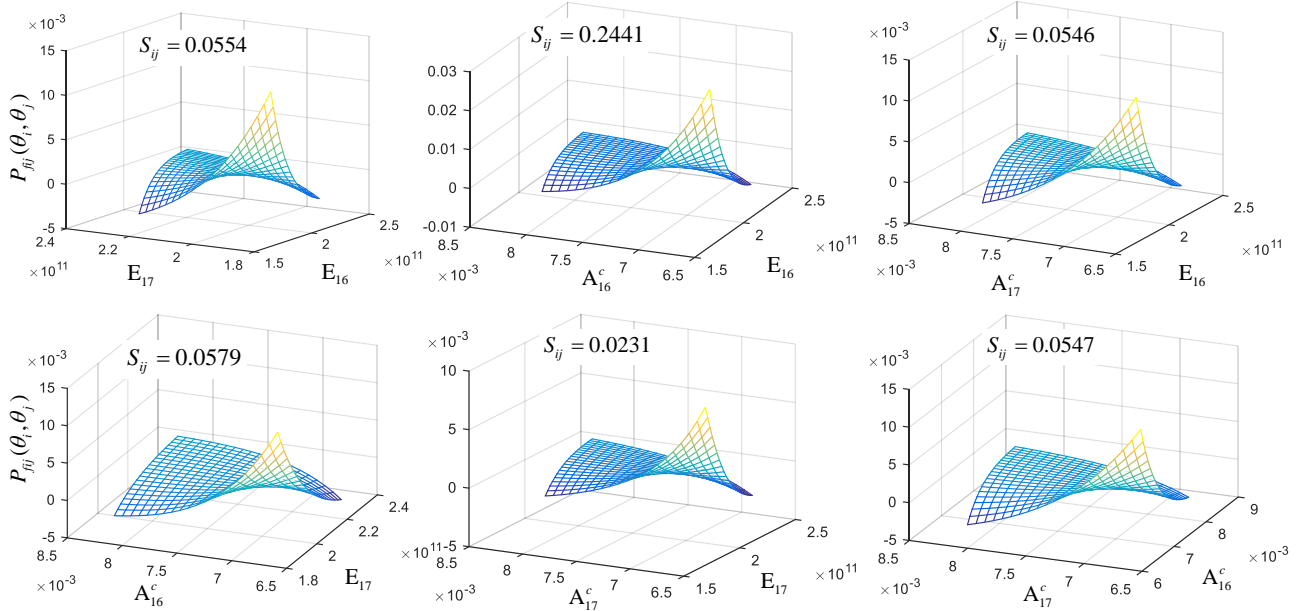


Figure 15 Plots of the six most influential second-order component functions by WI-ILS for transmission tower model.

5. Conclusions

The present study was designed to develop efficient simulation methods for reliability analysis subjected to rare failure events when the model input variables are characterized by imprecise probabilities due to the imperfect knowledge. It is realized by developing two strategies for injecting the classical line sampling into the newly developed NISS framework. The first strategy, denoted as HA-ILS, is based on establishing a series of auxiliary hyperplanes for approximating the real LSF with the input distribution parameters being fixed, and then evaluating the probability mass of the failure domain specified by each hyperplane when the distribution parameters vary. The second strategy, abbreviated as WI-ILS, is developed based on the combination of the simulation in $(n-1)$ -dimensional subspace and the one-dimensional integral along each line. Analytical formulas of failure probability component functions associated with the proposed two methods are discussed in detail when the distribution of model inputs are specified as normal or lognormal independent distributions.

An analytical example and three engineering examples are introduced for demonstrating the two proposed methods, and the main conclusions are as follows. Firstly, the results estimated by HA-ILS and WI-ILS all match well with the reference results by sharing only one small set of samples, indicating that both methods are effective and highly efficient for real applications. Secondly, for weakly or mildly non-linear models with small parameter ranges, HA-ILS has generally a faster convergence speed than WI-ILS, but in the meantime, it may produce a biased result caused by LSF approximations. Thirdly, as $\boldsymbol{\theta}$ is far away from $\boldsymbol{\theta}^*$, the hyperplane approximation of LSF used in HA-ILS might become worse especially for non-linear models. As for WI-ILS, although it doesn't involve approximations, but the utilized important direction will become more and more suboptimal which will undoubtedly lead to a slower convergence speed of the estimators (that is, larger variance). Besides, our method can also evaluate the high-order component functions based on the same set of LS samples, and their relative importance is measured by the sensitivity indices. Thus, in our development, it really doesn't matter whether the higher-order effects are influential or not. The only difference is that, for higher-order

component functions, the statistical errors (measured by variances of estimators) can be larger. But for linear or moderately nonlinear problems, the statistical errors increases slowly w.r.t to the orders of components.

Results of the transmission tower show that, for high-dimensional problems with a small number of dimensions being influential, the WI-ILS method is still efficient and accurate for all cut-HDMR components, whereas, the HA-ILS may be ineffective for estimating the less influential components due to the inability of including these dimensions in the important directions. This indicates that, the HA-ILS method is highly dependent on the identified directions, while WI-ILS is not.

Future extensions of the two approaches reported herein, that is HA-ILS and WI-ILS, involve two main aspects. The first one is the analysis of problems involving several failure criteria, which in turn may demand identifying several important directions. Such issue has not been fully addressed in the literature, even when applying Line Sampling to purely aleatoric reliability problems. The second one is addressing the loss of precision (that is, increased variability) of the cut-HDMR estimators when evaluating probabilities for values of the parameter vector $\boldsymbol{\theta}$ that are far away from the reference value $\boldsymbol{\theta}^*$. It is envisioned that such problems could be addressed by performing a more exhaustive exploration of the uncertain parameter space, by switching from a local NISS to its global counterpart.

Acknowledgment

This work is supported by National Natural Science Foundation of China (NSFC) under grant number 51905430. The first author is supported by the program of China Scholarship Council (CSC). The second and third authors are both supported by the Alexander von Humboldt Foundation of Germany. The second author also acknowledges the support by CONICYT (National Commission for Scientific and Technological Research) under grant number 1180271.

Appendix A : Derivation of failure probability function for Eq.(35)

The PDF weight η in Eq.(34) can be further expressed by

$$\begin{aligned}\eta(\mathbf{z}^{\perp(s)} + \bar{z}\mathbf{e}_{\alpha}, \boldsymbol{\theta}, \boldsymbol{\theta}^*) &= \left(\prod_{d=1}^n \frac{\sigma_d^*}{\sigma_d} \right) \times \\ &\exp \left(\sum_{d=1}^n \left(\frac{(z_d^{\perp(s)} + \bar{z}e_{\alpha,d})^2}{2} - \frac{(\mu_d^* + \sigma_d^* z_d^{\perp(s)} + \sigma_d^* \bar{z}e_{\alpha,d} - \mu_d)^2}{2\sigma_d^2} \right) \right)\end{aligned}\quad (\text{A.1})$$

Let ξ denote the first term above

$$\xi = \prod_{d=1}^n \frac{\sigma_d^*}{\sigma_d} \quad (\text{A.2})$$

As for the second term, it can be derived further as

$$\exp \left(\sum_{d=1}^n \left(\frac{(z_d^{\perp(s)})^2}{2} - \frac{(\mu_d^* + \sigma_d^* z_d^{\perp(s)} - \mu_d)^2}{2\sigma_d^2} \right) + \bar{z} \sum_{d=1}^n \left(z_d^{\perp(s)} e_{\alpha,d} - \frac{(\mu_d^* + \sigma_d^* z_d^{\perp(s)} - \mu_d) \sigma_d^* e_{\alpha,d}}{\sigma_d^2} \right) + \bar{z}^2 \sum_{d=1}^n \left(\frac{e_{\alpha,d}^2}{2} \left(1 - \frac{\sigma_d^{*2}}{\sigma_d^2} \right) \right) \right) \quad (\text{A.3})$$

Let $\lambda^{(s)}$, $\kappa^{(s)}$, ζ denote the above three terms, respectively, i.e.,

$$\begin{aligned}\lambda^{(s)} &= \sum_{d=1}^n \left(\frac{(z_d^{\perp(s)})^2}{2} - \frac{(\mu_d^* + \sigma_d^* z_d^{\perp(s)} - \mu_d)^2}{2\sigma_d^2} \right) \\ \kappa^{(s)} &= \sum_{d=1}^n \left(z_d^{\perp(s)} e_{\alpha,d} - \frac{(\mu_d^* + \sigma_d^* z_d^{\perp(s)} - \mu_d) \sigma_d^* e_{\alpha,d}}{\sigma_d^2} \right) \\ \zeta &= \sum_{d=1}^n \left(\frac{e_{\alpha,d}^2}{2} \left(1 - \frac{\sigma_d^{*2}}{\sigma_d^2} \right) \right)\end{aligned}\quad (\text{A.4})$$

Note that ξ , ζ , $\lambda^{(s)}$, $\kappa^{(s)}$ are all functions of distribution parameters $\boldsymbol{\mu}$ and $\boldsymbol{\sigma}$, and $\zeta \leq 1/2$. Additionally, $\lambda^{(s)}$, $\kappa^{(s)}$ vary according to the value of sample $z_d^{\perp(s)}$. Then the PDF weight is simplified as

$$\eta(\mathbf{z}^{\perp(s)} + \bar{z}\mathbf{e}_{\alpha}, \boldsymbol{\theta}, \boldsymbol{\theta}^*) = \xi \exp(\lambda^{(s)} + \bar{z}\kappa^{(s)} + \bar{z}^2\zeta) \quad (\text{A.5})$$

Taking it into Eq.(31) one derives

$$L^{(s)}(\boldsymbol{\mu}, \boldsymbol{\sigma}) = \xi e^{\lambda^{(s)}} \int_{\bar{c}^{(s)}}^{\infty} \exp(\bar{z}\kappa^{(s)} + \bar{z}^2\zeta) \phi(\bar{z}) d\bar{z} \quad (\text{A.6})$$

The integral $\int_{\bar{c}^{(s)}}^{\infty} \exp(\bar{z}\kappa^{(s)} + \bar{z}^2\zeta) \phi(\bar{z}) d\bar{z}$ can furtherly derived with an analytical solution

$$\begin{aligned}
 & \int_{\tilde{c}^{(s)}}^{\infty} \exp(\bar{z}\kappa^{(s)} + \bar{z}^2\zeta) \phi(\bar{z}) d\bar{z} \\
 &= \int_{\tilde{c}^{(s)}}^{\infty} \frac{1}{\sqrt{2\pi}} \exp\left(\left(\zeta - \frac{1}{2}\right)\bar{z}^2 + \kappa^{(s)}\bar{z}\right) d\bar{z} \\
 &= \int_{\tilde{c}^{(s)}}^{\infty} \frac{1}{\sqrt{2\pi}} \exp\left(-\frac{1}{2}\left((1-2\zeta)\bar{z}^2 - 2\kappa^{(s)}\bar{z} + \frac{(\kappa^{(s)})^2}{1-2\zeta}\right) + \frac{(\kappa^{(s)})^2}{2-4\zeta}\right) d\bar{z} \\
 &= \exp\left(\frac{(\kappa^{(s)})^2}{2-4\zeta}\right) \int_{\tilde{c}^{(s)}}^{\infty} \frac{1}{\sqrt{2\pi}} \exp\left(-\frac{1}{2}\left(\sqrt{1-2\zeta}\bar{z} - \frac{\kappa^{(s)}}{\sqrt{1-2\zeta}}\right)^2\right) d\bar{z}
 \end{aligned} \tag{A.7}$$

Let $\sqrt{1-2\zeta}\bar{z} - \kappa^{(s)}/\sqrt{1-2\zeta} = t$, where $t \in [\sqrt{1-2\zeta}\tilde{c}^{(s)} - \kappa^{(s)}/\sqrt{1-2\zeta}, +\infty)$, the above integral can be derived as

$$\begin{aligned}
 & \int_{\tilde{c}^{(s)}}^{\infty} \exp(\bar{z}\kappa^{(s)} + \bar{z}^2\zeta) \phi(\bar{z}) d\bar{z} \\
 &= \exp\left(\frac{(\kappa^{(s)})^2}{2-4\zeta}\right) \int_{\sqrt{1-2\zeta}\tilde{c}^{(s)} - \frac{\kappa^{(s)}}{\sqrt{1-2\zeta}}}^{\infty} \frac{1}{\sqrt{2\pi}} \exp\left(-\frac{1}{2}t^2\right) d\left(\frac{1}{\sqrt{1-2\zeta}}t + \frac{\kappa^{(s)}}{1-2\zeta}\right) \\
 &= \frac{1}{\sqrt{1-2\zeta}} \exp\left(\frac{(\kappa^{(s)})^2}{2-4\zeta}\right) \Phi\left(-\left(\sqrt{1-2\zeta}\tilde{c}^{(s)} - \frac{\kappa^{(s)}}{\sqrt{1-2\zeta}}\right)\right) \\
 &= \frac{1}{\sqrt{1-2\zeta}} \exp\left(\frac{(\kappa^{(s)})^2}{2-4\zeta}\right) \Phi\left(\frac{\kappa^{(s)} - (1-2\zeta)c^{(s)}}{\sqrt{1-2\zeta}}\right)
 \end{aligned} \tag{A.8}$$

Then the analytical expression of the integral is finally derived as

$$L^{(s)}(\boldsymbol{\mu}, \boldsymbol{\sigma}) = \frac{\xi}{\sqrt{1-2\zeta}} \exp\left(\lambda^{(s)} + \frac{(\kappa^{(s)})^2}{2-4\zeta}\right) \Phi\left(\frac{\kappa^{(s)} - (1-2\zeta)c^{(s)}}{\sqrt{1-2\zeta}}\right) \tag{A.9}$$

Appendix B: Derivation of analytical failure probability function of Eq.(41)

In standard normal space, the performance function in Eq.(40) is expressed as $h(z_1, z_2) = \beta - (\mu_1 + \sigma_1 z_1) + \kappa(\mu_2 + \sigma_2 z_2)^2$. The boundary of LSF $h(z_1, z_2) = 0$ can be drawn as shown in Figure B1. Assume that z_2' is a realization of z_2 , then search the value of z_1' that satisfies the equation $h(z_1, z_2') = 0$, i.e.,

$$z_1' = \frac{\beta - \mu_1}{\sigma_1} + \frac{\kappa}{\sigma_1} (\mu_2 + \sigma_2 z_2')^2 \tag{B.1}$$

From the view of line sampling, the reliability index associated with z_2' is actually the distance d_1 shown in Figure B1, and its value equals to z_1' . As a consequence, the failure probability can be expressed analytically with the following one-dimensional integral,

$$\begin{aligned}
 P_f(\mu_1, \mu_2, \sigma_1, \sigma_2) &= \int_{-\infty}^{+\infty} \Phi(-z_1') \phi(z_2) dz_2 \\
 &= \int_{-\infty}^{+\infty} \Phi\left(-\frac{\beta - \mu_1}{\sigma_1} - \frac{\kappa}{\sigma_1} (\mu_2 + \sigma_2 z_2)^2\right) \phi(z_2) dz_2
 \end{aligned} \tag{B.2}$$

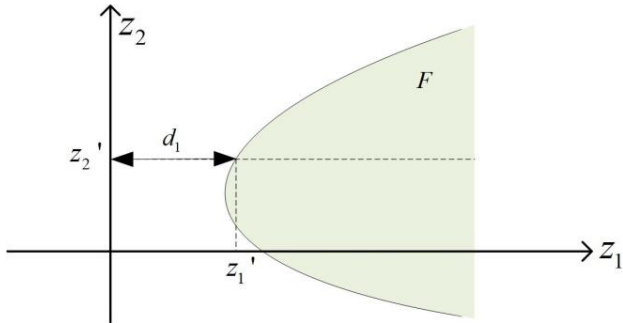


Figure B1 Geometric sketch for deriving analytical solution of failure probability

References

- [1]. Faes, M., Broggi, M., Patelli, E., Govers, Y., Mottershead, J., Beer, M., & Moens, D. (2019). A multivariate interval approach for inverse uncertainty quantification with limited experimental data. *Mechanical Systems and Signal Processing*, 118, 534-548.
- [2]. Hohenbichler, M., Gollwitzer, S., Kruse, W., & Rackwitz, R. (1987). New light on first-and second-order reliability methods. *Structural safety*, 4(4), 267-284.
- [3]. Ghanem, R. G., Spanos, P. D. (2003). Stochastic finite elements: a spectral approach. Courier Corporation.
- [4]. Au, S. K. & Beck, J. L. (2001). Estimation of small failure probabilities in high dimensions by subset simulation. *Probabilistic Engineering Mechanics*, 16(4), 263-277.
- [5]. Li, J., Chen, J. (2008). The principle of preservation of probability and the generalized density evolution equation. *Structural Safety*, 30(1), 65-77.
- [6]. Faes, M. & Moens, D. (2019). Recent Trends in the Modeling and Quantification of Non-probabilistic Uncertainty. *Archives of Computational Methods in Engineering*, 1-39.
- [7]. Der Kiureghian, A. & Ditlevsen, O. (2009). Aleatory or epistemic? Does it matter?. *Structural Safety*, 31(2), 105-112.
- [8]. Beer, M., Ferson, S. & Kreinovich, V. (2013). Imprecise probabilities in engineering analyses. *Mechanical systems and signal processing*, 37(1-2), 4-29.

- [9]. Zhang, H., Mullen, R. L. & Muhanna, R. L. (2010). Interval Monte Carlo methods for structural reliability. *Structural Safety*, 32(3), 183-190.
- [10]. Alvarez, D. A., Uribe, F. & Hurtado, J. E. (2018). Estimation of the lower and upper bounds on the probability of failure using subset simulation and random set theory. *Mechanical Systems and Signal Processing*, 100, 782-801.
- [11]. Zhang, Z., Jiang, C., Wang, G. G., & Han, X. (2015). First and second order approximate reliability analysis methods using evidence theory. *Reliability Engineering & System Safety*, 137, 40-49.
- [12]. Wei, P., Song, J., Bi, S., Broggi, M., Beer, M., Lu, Z., & Yue, Z. (2019). Non-intrusive stochastic analysis with parameterized imprecise probability models: I. Performance estimation. *Mechanical Systems and Signal Processing*, 124, 349-368.
- [13]. Wei, P., Song, J., Bi, S., Broggi, M., Beer, M., Lu, Z., & Yue, Z. (2019). Non-intrusive stochastic analysis with parameterized imprecise probability models: II. Reliability and rare events analysis. *Mechanical Systems and Signal Processing*, 126, 227-247.
- [14]. Wei, P., Lu, Z. & Song, J. (2014). Extended Monte Carlo simulation for parametric global sensitivity analysis and optimization. *AIAA Journal*, 52(4), 867-878.
- [15]. Li, G., Wang, S. W., Rosenthal, C., & Rabitz, H. (2001). High dimensional model representations generated from low dimensional data samples. I. mp-Cut-HDMR. *Journal of Mathematical Chemistry*, 30(1), 1-30.
- [16]. Li, G., & Rabitz, H. (2012). General formulation of HDMR component functions with independent and correlated variables. *Journal of Mathematical Chemistry*, 50(1), 99-130.
- [17]. Kaya, H., Kaplan, M., & Saygin, H. (2004). A recursive algorithm for finding HDMR terms for sensitivity analysis. *Computer Physics Communications*, 158(2), 106-112.
- [18]. Schuëller, G. I., Pradlwarter, H. J. & Koutsourelakis, P. S. (2004). A critical appraisal of reliability estimation procedures for high dimensions. *Probabilistic engineering mechanics*, 19(4), 463-474.
- [19]. Koutsourelakis, P. S., Pradlwarter, H. J. & Schuëller, G. I. (2004). Reliability of structures in high dimensions, part I: algorithms and applications. *Probabilistic Engineering*

- Mechanics, 19(4), 409-417.
- [20]. Hohenbichler, M. & Rackwitz, R. (1988). Improvement of second-order reliability estimates by importance sampling. *Journal of Engineering Mechanics*, 114(12), 2195-2199.
- [21]. Rackwitz, R. (2001). Reliability analysis—a review and some perspectives. *Structural safety*, 23(4), 365-395.
- [22]. Song, J., Lu, Z., Wei, P. & Wang, Y. (2015). Global sensitivity analysis for model with random inputs characterized by probability-box. *Proceedings of the Institution of Mechanical Engineers, Part O: Journal of Risk and Reliability*, 229(3), 237-253.
- [23]. Chen, L., Wang, H., Ye, F., & Hu, W. (2019). Comparative study of HDMRs and other popular metamodeling techniques for high dimensional problems. *Structural and Multidisciplinary Optimization*, 59(1), 21-42.
- [24]. Wei, P., Lu, Z. & Song, J. (2015). Variable importance analysis: a comprehensive review. *Reliability Engineering & System Safety*, 142, 399-432.
- [25]. Schueller, G. I. (2009). Efficient Monte Carlo simulation procedures in structural uncertainty and reliability analysis-recent advances. *Structural Engineering and Mechanics*, 32(1), 1-20.
- [26]. Lu, Z., Song, S., Li, H. & Yuan, X. (2009). The reliability and reliability sensitivity analysis for structural and mechanical system. Beijing, China: Science Press, pp. 179-181.
- [27]. Pradlwarter, H. J., Schueller, G. I., Koutsourelakis, P. S., & Charmpis, D. C. (2007). Application of line sampling simulation method to reliability benchmark problems. *Structural Safety*, 29(3), 208-221.
- [28]. Pradlwarter, H. J., Pellissetti, M. F., Schenk, C. A., Schueller, G. I., Kreis, A., Fransen, S., ... & Klein, M. (2005). Realistic and efficient reliability estimation for aerospace structures. *Computer Methods in Applied Mechanics and Engineering*, 194(12-16), 1597-1617.
- [29]. Lu, Z., Song, S., Yue, Z., & Wang, J. (2008). Reliability sensitivity method by line sampling. *Structural Safety*, 30(6), 517-532.
- [30]. de Angelis, M., Patelli, E., & Beer, M. (2015). Advanced line sampling for efficient robust

- reliability analysis. Structural safety, 52, 170-182.
- [31]. Depina, I., Le, T. M. H., Fenton, G., & Eiksund, G. (2016). Reliability analysis with metamodel line sampling. Structural Safety, 60, 1-15.
- [32]. Valdebenito M A, Valdebenito, M. A., Jensen, H. A., Beer, M., & Pérez, C. A. (2014). Approximation concepts for fuzzy structural analysis. In Vulnerability, Uncertainty, and Risk: Quantification, Mitigation, and Management (pp. 135-144).
- [33]. Valdebenito, M. A., Jensen, H. A., Hernández, H. B., & Mehrez, L. (2018). Sensitivity estimation of failure probability applying line sampling. Reliability Engineering & System Safety, 171, 99-111.
- [34]. Haukaas, T., & Der Kiureghian, A. (2006). Strategies for finding the design point in non-linear finite element reliability analysis. Probabilistic Engineering Mechanics, 21(2), 133-147.

Research article 3: Active Learning Line Sampling for Rare Event Analysis

As have been shown in the last chapter, the line sampling (LS) is not only effective for precise reliability analysis with small failure probability, but can also be elegantly injected to the NISS framework for analyzing the structure reliability with inputs characterized by *p*-box models. However, when applied to real-world engineering problems, there are still two limitations.

First, as shown by the test examples in the last article, the LS based NISS still requires at least hundreds of *g*-function calls for achieving estimation with high accuracy. For practical engineering applications involving computationally expensive computer simulators, one *g*-function call may take several minutes or even several hours, thus the computationally cost can still be too high. There is a requirement of further reducing the required number of *g*-function calls.

Second, the classical LS method is not suitable for problems highly nonlinear *g*-functions. The reasons behind this fact are twofold. On the one hand, the important direction need to be specified first, which requires more *g*-function calls for highly nonlinear problems. On the other hand, for highly nonlinear *g*-function, the high accuracy of LS estimator requires much more lines, each of which requires more *g*-function calls for accurately estimating its intersection points with the failure surface. The above two reasons make the LS method computationally extremely expensive for highly nonlinear problems.

For overcoming the above two limitations, this article develops an improved LS algorithm by combining the active learning and Gaussian process regression (GPR) with LS

method. This algorithm is driven by a newly developed learning function, which can inform the posterior probability of correctly estimating the intersection point for each line within a specified tolerance. Then, with this learning function, a GPR model is trained and/or updated, and the design point is specified one by one actively, with the target to accurately estimate the intersection point for each line, with the least g -function calls. All the g -function calls for specifying the important direction can be used for training the GPR model, so they are not wasted. For highly nonlinear problems, the algorithm adaptively produces more lines to promise the accuracy of failure probability estimation, but the required number of g -function calls does not increase too much as for the new lines, the intersection points have been correctly learned by the trained GPR model. The high efficiency of the proposed method is then demonstrated by numerical and engineering test cases.

Active Learning Line Sampling for Rare Event Analysis

Jingwen Song^{a,b}, Pengfei Wei^{a,b}, Marcos Valdebenito^c, Michael Beer^{b,d,e}

^a Northwestern Polytechnical University, West Youyi Road 127, Xi'an 710072, China

^b Institute for Risk and Reliability, Leibniz Universität Hannover, Callinstr. 34, Hannover 30167, Germany

^c Departamento de Obras Civiles, Universidad Tecnica Federico Santa Maria, Av. Espana 1680, Valparaiso, Chile

^d Institute for Risk and Uncertainty, University of Liverpool, Peach Street, L69 7ZF Liverpool, United Kingdom

^e International Joint Research Center for Engineering Reliability and Stochastic Mechanics, Tongji University, Shanghai 200092, China

Published in Mechanical Systems and Signal Processing in July 2020

Abstract: Line Sampling (LS) has been widely recognized as one of the most appealing stochastic simulation algorithms for rare event analysis, but when applying it to many real-world engineering problems, improvement of the algorithm with higher efficiency is still required. This paper aims to improve both the efficiency and accuracy of LS by active learning and Gaussian process regression (GPR). A new learning function is devised for informing the accuracy of the calculation of the intersection points between each line associated with LS and the failure surface. Then, an adaptive algorithm, with the learning function as an engine and a stopping criterion, is developed for adaptively training a GPR model to accurately estimate the intersection points for all lines in LS scheme, and the number of lines is actively increased if it is necessary for improving the accuracy of failure probability estimation. By introducing this adaptive GPR model, the number of required function calls has been largely reduced, and the accuracy for estimation of the intersection points has been largely improved, especially for highly nonlinear problems with extremely rare events. Numerical test examples and engineering applications show the superiority of the developed algorithm over the classical LS algorithm and some other active learning schemes.

Keywords: Rare Failure Event; Gaussian Process Regression; Line Sampling; Learning Function; Adaptive Experiment Design; Active learning

1 Introduction

Estimating the failure probability of complex structures has long been recognized as one of the most important tasks in civil engineering, mechanical engineering, and related areas. The rapid development of computational power has allowed the simulation of more large-scale structural systems and more complex failure mechanisms, resulting in the requirement of more efficient and accurate computational methods for structural reliability analysis, especially when it comes to rare failure event analysis [1].

From the 60s of last century on, the probabilistic uncertainty propagation and the reliability analysis of structural systems have been coming into the view of the academic community, and plenty of classical computational methods with their own relative merits have been developed. These available methods can be generally grouped into (i) analytical approximation methods, (ii) probability-conservation based methods, (iii) stochastic simulation methods, and (iv) surrogate model method especially equipped by active learning and stochastic simulation.

Analytical approximation methods, including the first-order reliability method (FORM) [2], the second-order reliability method (SORM) [3], etc., aims at approximating the failure probability by statistical moments of the performance function (or limit state function) approximated by Taylor series expansion expended at the most probable points (MPPs). This group of methods requires gradient information of the performance function and is commonly only applicable for problems with continuous performance function of low nonlinearity (around the MPP).

Probability-preservation based methods, including the probability density evolution [4], the direct probability integral method [5], etc., propagate the probabilistic uncertainty from model inputs to outputs and also estimate the failure probability based on the principle of probability conservation. This group of methods commonly rely on experiment design that involves some low-discrepancy sequence techniques. Compared with the first group of methods, the latter is

commonly computationally more expensive, but have wider applications, especially to dynamic problems.

Stochastic simulation, such as Monte Carlo simulation (MCS) and advanced MCS, are rooted in the classical probability theory, and the convergence and accuracy of the estimators are guaranteed by the central-limit theory and the law of larger numbers. For structural reliability analysis and especially rare event analysis, advanced MCS such as importance sampling (IS) [6][7], subset simulation (SS) [8][9], line sampling (LS) [10][11] and directional simulation (DS) [12] have been developed, and been comprehensively investigated from both theoretical and application aspects. These simulation methods have their advantages but also disadvantages. For example, SS is applicable for small failure probability estimation and high-dimensional problems, but the convergence is highly affected by the utilized Markov Chain Monte Carlo (MCMC) algorithms [9][13], and the estimation errors also increase with respect to the number of introduced intermediate failure events. LS can be especially efficient for small failure probability estimation, but the efficiency and estimation accuracy highly rely on the important direction and the accuracy of calculating the intersection points along each line with the failure event; furthermore, for highly nonlinear problems, LS requires more lines and more evaluations of the system's response on each line, thus can be less efficient. Generally, the stochastic simulation methods provide rigorous treatments of numerical errors but are still computationally expensive for real-world structures with time-consuming simulators.

The requirement of highly efficient reliability analysis has motivated the development and application of surrogate model methods, especially those relying on active learning strategies. In particular, methods that combine the advantages of the Gaussian Process Regression (GPR) model (also called Kriging model) with stochastic simulation methods have received considerable attention. One of the pioneering developments in this direction is the AK-MCS (active learning Kriging driven by MCS) proposed by Echard et al. in Ref. [14]. This method makes full use of the convergence property of MCS, but avoids its high computational cost by actively learning the signs of the performance function for each MCS sample based on the property of GPR model. During the past years, this scheme has received a lot of attention, and many improved versions

have been developed. There are two mainstreams of these new developments. The first line is focused on developing new learning functions for more effective learning. Some of the most well-known learning functions include the U-function [14], the expected improvement function (EIF) [15], the H-function [16], the least improvement function (LIF) [17], etc. Another line aims at combining the active learning scheme with advanced stochastic simulation to improve the applicability for small (typically less than 10^{-3}) or extremely small (less than 10^{-6}) failure probability estimation. Some of the representative developments in this direction include AK-IS methods that combine AK with (adaptive) IS method [18]-[21], AK-SS, or AK-MCMC methods combining AK with SS method [22]-[25], etc. Other developments based on AK-MCS also include the parallelization of the algorithm [26], the treatment of structural system reliability analysis [27][28], etc. The combination of GPR with LS has also been presented in Refs. [29] and [30], but neither of these references considers an active training scheme, and specifically, in Ref. [29] a large number of performance function evaluations are required for calculating a correction coefficient introduced for addressing the model error. Theoretically, the proper combination of LS and active learning Kriging (named as adaptive GPR (AGPR) in this paper) has the potential to substantially reduce the required performance function calls for extremely small failure probability estimation since they are complementary to one another, however, the current studies are still far from achieving this goal.

To make full use of the advantages of the AGPR model and LS method, we develop a new active learning scheme, which is named AGPR-LS, for efficiently estimating very small failure probabilities. A new active learning function is firstly developed for adaptively learning the intersection points between each line and the failure surface accurately, and which also serves as a stopping criterion. Then, based on this learning function, the adaptive learning scheme AGPR-LS is developed. Extensive numerical and engineering test cases show that the AGPR-LS algorithm is especially efficient and accurate for extremely rare event analysis.

The rest of this paper is organized as follows. Section 2 briefly reviews the classical LS method and highlights the aspects that could be improved by injecting the AGPR model. In section 3, the new learning function and the AGPR-LS algorithm are developed, followed by the

case studies in section 4. Section 5 gives conclusions.

2 Review of Line Sampling

LS method, as a classical advanced MCS method, formulates a reliability problem as a group of conditional one-dimensional reliability estimations, and each one-dimensional problem is solved by searching along the line parallel to the important direction [10][29]. The important direction is defined as a vector pointing from the origin to the most probable failure region in input space [10][11], and the performance of LS highly relies on the accuracy of specifying the important direction.

Assume that the n -dimensional input random variables are denoted by $\mathbf{x} = (x_1, x_2, \dots, x_n)$, and the performance function of a reliability problem is denoted as $y(\mathbf{x})$, where $y < 0$ indicates the failure of the structure. The classical LS method is established in the standard Gaussian space. However, in real-world applications, non-Gaussian input variables are ubiquitous, and these non-Gaussian input variables must be transformed into standard Gaussian variables. This can be realized by using an isoprobabilistic transformation such as Rosenblatt or Nataf transformation [31]. Here we briefly introduce the transformation for the independent case. Let $F(x_i)$ denote the cumulative distribution function (CDF) of any type of distribution, then the isoprobabilistic transformation is $z_i = \Phi^{-1}(F(x_i))$, where $\Phi^{-1}(\cdot)$ indicates the inverse CDF of the standard Gaussian variable z_i . Then the inverse transformation is given as $x_i = F^{-1}(\Phi(z_i))$. For the general case with dependent input variables, one can refer to Ref. [31] for details. For the general case, let $\mathbf{z} = T(\mathbf{x})$ denote the isoprobabilistic transformation (e.g., Rosenblatt transformation) of \mathbf{x} , and the inverse transformation is formulated as $\mathbf{z} = T^{-1}(\mathbf{x})$. Then the performance function with standard Gaussian arguments can be formulated as $g(\mathbf{z}) = y(T^{-1}(\mathbf{z}))$. For simplification, all the subsequent work will be discussed in standard Gaussian space with the performance function expressed by $g(\mathbf{z})$.

The normalized important direction associated with $g(\mathbf{z})$ is denoted by \mathbf{e}_α . Once \mathbf{e}_α has been estimated, the standard Gaussian space can be orthogonally decomposed into a one-dimensional subspace and a $(n - 1)$ -dimensional subspace, and the input vector can be

decomposed into two vectors:

$$\mathbf{z} = z^{\parallel} \mathbf{e}_{\alpha} + \mathbf{z}^{\perp} \quad (1)$$

, where z^{\parallel} is the one-dimensional standard Gaussian variable so that $z^{\parallel} \mathbf{e}_{\alpha}$ is parallel to \mathbf{e}_{α} , and \mathbf{z}^{\perp} is the $(n - 1)$ -dimensional standard Gaussian variables orthogonal to \mathbf{e}_{α} . For a given value of \mathbf{z} , the value of \mathbf{z}^{\perp} and z^{\parallel} can be calculated with the following expression

$$\begin{cases} z^{\parallel} = \langle \mathbf{e}_{\alpha}, \mathbf{z} \rangle \\ \mathbf{z}^{\perp} = \mathbf{z} - \langle \mathbf{e}_{\alpha}, \mathbf{z} \rangle \mathbf{e}_{\alpha} \end{cases} \quad (2)$$

, where $\langle \cdot, \cdot \rangle$ indicates inner product.

With the above decomposition, the failure probability p_f can be formulated as a double-loop integral, i.e.,

$$p_f = \int_{g(\mathbf{z}) \leq 0} \phi_n(\mathbf{z}) d\mathbf{z} = \int_{g(\mathbf{z}^{\perp} + z^{\parallel} \mathbf{e}_{\alpha}) \leq 0} \phi(z^{\parallel}) dz^{\parallel} \phi_{n-1}(\mathbf{z}^{\perp}) d\mathbf{z}^{\perp} \quad (3)$$

, with a $(n - 1)$ -dimensional integral of \mathbf{z}^{\perp} in the outer loop and one-dimensional integral of z^{\parallel} in the inner loop. Based on Eq.(3), the LS method involves first generating a set of N_z samples $(\mathbf{z}^{\perp(1)}, \dots, \mathbf{z}^{\perp(s)}, \dots, \mathbf{z}^{\perp(N_z)})$ in the $(n - 1)$ -dimensional subspace of \mathbf{z}^{\perp} based on Eq.(2), and then expressing the estimator of failure probability as:

$$\hat{p}_f = \frac{1}{N_z} \sum_{s=1}^{N_z} \int_{g(\mathbf{z}^{\perp(s)} + z^{\parallel} \mathbf{e}_{\alpha}) \leq 0} \phi(z^{\parallel}) dz^{\parallel}. \quad (4)$$

For estimating the failure probability based on Eq.(4), one only needs to estimate the N_z one-dimensional integrals, and this problem is schematically shown in Figure 1. As can be seen, given a fixed value $\mathbf{z}^{\perp(s)}$ of \mathbf{z}^{\perp} , $\mathbf{z}^{\perp(s)} + z^{\parallel} \mathbf{e}_{\alpha}$ varies along the line $l^{(s)}$ which is parallel to the important direction. The intersection point of this line with the failure surface is then denoted as $\mathbf{z}^{\perp(s)} + c^{(s)} \mathbf{e}_{\alpha}$. Clearly, if the value of z^{\parallel} exceeds $c^{(s)}$, then failure happens along this line, and since z^{\parallel} follows standard Gaussian distribution, the estimator in Eq.(4) can then be further derived as:

$$\hat{p}_f = \frac{1}{N_z} \sum_{s=1}^{N_z} \int_{c^{(s)}}^{+\infty} \phi(z^{\parallel}) dz^{\parallel} = \frac{1}{N_z} \sum_{s=1}^{N_z} \Phi(-c^{(s)}) \quad (5)$$

, and the variance of the estimator is

$$\mathbb{V}(\hat{p}_f) = \frac{1}{N_z(N_z-1)} \sum_{s=1}^{N_z} (\Phi(-c^{(s)}) - \hat{p}_f)^2. \quad (6)$$

Therefore, the estimation of the failure probability is equivalent to the estimation of the intersection point for each line sample. With the estimator in Eq.(5) and the variance of the estimator in Eq.(6), the Coefficient Of Variation (COV) of the estimate can be computed by:

$$\text{COV}(\hat{p}_f) = \frac{\sqrt{\mathbb{V}(\hat{p}_f)}}{\hat{p}_f}. \quad (7)$$

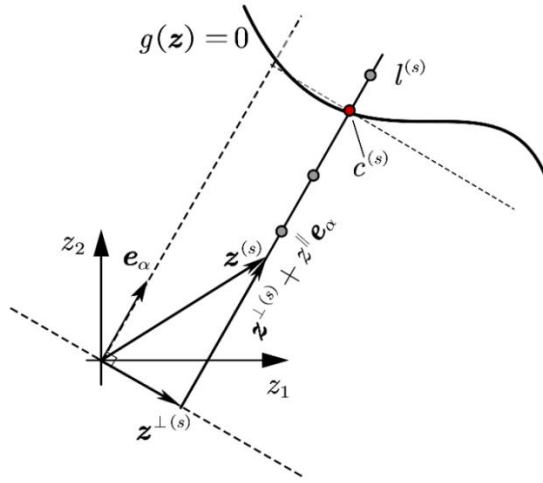


Figure 1 Geometric interpretation of LS in standard Gaussian space.

Many numerical methods can be used for calculating the value of $c^{(s)}$ associated with the intersection point on each line, and the most efficient way is to use the three-point-second-order (TPSO) polynomial interpolation method. This procedure involves first generating three values for z^{\parallel} , denoted as c_1 , c_2 , c_3 , and evaluating the performance function values at the three points on the s -th line, then the one-dimensional function $g(z^{\perp(s)} + z^{\parallel} e_{\alpha})$ can be approximated by TPSO polynomial interpolation, thus the value of $c^{(s)}$ is calculated by searching the root of this polynomial.

The above LS scheme has been widely known to be efficient for rare event analysis due to the high efficiency of one-dimensional searching in the most important direction. However, disadvantages also exist. For highly nonlinear problems, the TPSO method can be less effective for accurately estimating the intersection points, resulting in poor accuracy, and further, high

nonlinearity also increases the number of required lines for generating sufficiently reliable failure probability estimations, which will largely increase the number of g -function calls. For rare event analysis, the proper selection of the three values c_1 , c_2 and c_3 is also a challenging problem because in most cases the distance of the intersection points from the origin is unknown, and improper selection of the three points will also result in a poor estimation of the failure probability. One can also increase the number of points on each line to improve the accuracy of estimating the intersection points, but this will also increase the number of required g -function calls. Besides, improper selection of the important direction will also result in poor performance as more lines are required for identifying the whole important failure region. In the next section, we inject the adaptive GPR model into LS to tackle the above disadvantages.

3 The proposed method

3.1 Brief introduction of the GPR model

Before the development of AGPR-LS, it is necessary to briefly review the GPR model. One can refer to Ref. [32] for more details. Given the performance function $g(\mathbf{z})$, the GPR model (denoted as \mathcal{GP}) assumes that:

$$\hat{g}(\mathbf{z}) \sim \mathcal{GP}(m(\mathbf{z}), c(\mathbf{z}, \mathbf{z}')) \quad (8)$$

, where $m(\mathbf{z})$ is the mean function which can be assumed to be zero, constant, linear, or any closed-form function, and $c(\mathbf{z}, \mathbf{z}')$ is the kernel function representing the covariance between two realizations \mathbf{z} and \mathbf{z}' . Many kinds of kernel functions have been developed for different situations, and one can refer to Ref. [32] for more information. The forms of the mean and kernel functions reflect part of our prior information on the GPR model. Assume we have a set of N_c training data (\mathbf{Z}, \mathbf{y}) , where \mathbf{Z} is a $(N_c \times n)$ matrix with each row being a sample of \mathbf{z} , and \mathbf{y} is a N_c -dimensional column-wise vector with the i -th value being the performance function evaluated at the i -th sample point of \mathbf{z} . Then, the maximum likelihood method can be utilized for estimating the values of the hyper-parameters included in the mean function $m(\mathbf{z})$ and the kernel function. Once these hyper-parameters have been computed, the posterior prediction $\hat{g}(\mathbf{z})$ of the GPR model at a new realization \mathbf{z} is also a Gaussian variable with expectation

and variance given by:

$$\hat{\mu}_g(\mathbf{z}) = m(\mathbf{z}) + c(\mathbf{z}, \mathbf{Z})^\top C^{-1}(\mathbf{y} - m(\mathbf{Z})) \quad (9)$$

, and

$$\hat{\sigma}_g^2(\mathbf{z}) = c(\mathbf{z}, \mathbf{z}) - c(\mathbf{z}, \mathbf{Z})^\top C^{-1}c(\mathbf{z}, \mathbf{Z}) \quad (10)$$

, where $c(\mathbf{z}, \mathbf{Z})$ is a column-wise vector of functions with the i -th component being the covariance between \mathbf{z} and the i -th row of \mathbf{Z} , and C is a $(N_c \times N_c)$ -dimensional matrix with the (i, j) -th entry being the covariance between the i -th and j -th rows of \mathbf{Z} . The variance $\hat{\sigma}_g^2(\mathbf{z})$ actually measures the variation of prediction.

Eq.(9) reveals that the GPR model prediction equals to the mean function (prior knowledge on $g(\mathbf{z})$) plus a linear combination of the kernel function between the new site and the training data, where the second term reflects the information learned from the training data. Eq. (10) indicates that the variance of GPR model prediction equals the prior variance minus a term which reflects the reduction of epistemic uncertainty on the value of $g(\mathbf{z})$ learned from the training data. The above interpretations indicate that, with more training data, the epistemic uncertainty on the prediction of any new sites will be reduced, and this property brings many more benefits for the algorithm to be developed. In the next subsection, we introduce a new learning function that serves as the engine of the proposed AGPR-LS algorithm.

3.2 Learning function

From the rationale of the GPR model, it is known that once the true performance function $g(\mathbf{z})$ is approximated by a GPR model $\hat{g}(\mathbf{z})$ with mean $\hat{\mu}_g(\mathbf{z})$ and variance $\hat{\sigma}_g^2(\mathbf{z})$, the prediction of the performance function at any new realization is a Gaussian variable. This property brings two benefits for LS. First, the distance $c^{(s)}$ w.r.t. the intersection point between the failure surface of $\hat{g}(\mathbf{z})$ and the s -th line can be easily computed by any numerical scheme due to the smoothness of $\hat{\mu}_g(\mathbf{z}^{\perp(s)} + z^{\parallel} \mathbf{e}_\alpha)$. Second, it can be used to judge whether the estimated value $c^{(s)}$ is accurate enough. For answering the second question, we develop a new definition of learning function, which is expressed as:

$$\kappa(\mathbf{z}) = \int_{-\epsilon + \hat{\mu}_g(\mathbf{z})}^{\epsilon + \hat{\mu}_g(\mathbf{z})} \phi(\hat{g}(\mathbf{z}) | \hat{\mu}_g(\mathbf{z}), \hat{\sigma}_g^2(\mathbf{z})) d\hat{g}(\mathbf{z}) \quad (11)$$

, where $\phi(\cdot | \hat{\mu}_g(\mathbf{z}), \hat{\sigma}_g^2(\mathbf{z}))$ refers to the probability density function of Gaussian distribution with mean $\hat{\mu}_g(\mathbf{z})$ and variance $\hat{\sigma}_g^2(\mathbf{z})$, and ϵ is the error tolerance to control the width of integral interval, whose value should be close to zero. Generally, the learning function can be interpreted as the probability of the true value of $g(\mathbf{z})$ being included in the small interval $[-\epsilon + \hat{\mu}_g(\mathbf{z}), \epsilon + \hat{\mu}_g(\mathbf{z})]$.

For reliability analysis, specifically for the intersection point $\mathbf{z}^{\perp(s)} + c^{(s)}\mathbf{e}_\alpha$ of a given line, where the value of $\hat{\mu}_g(\mathbf{z})$ theoretically equals to zero, the learning function actually measures the probability that the g -function value at the true intersection point being included in the pre-specified narrow bounds $[-\epsilon, \epsilon]$. The larger this probability is, the more accurately this intersection point is estimated. The learning function is schematically interpreted in Figure 2.

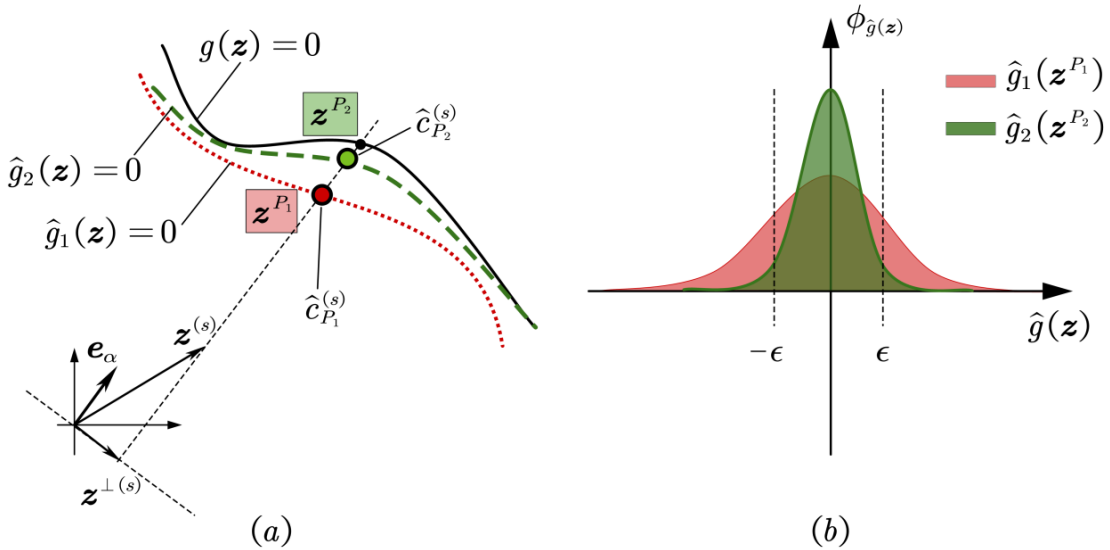


Figure 2 Schematic interpretation of the learning function $\kappa(\mathbf{z})$.

As can be seen in Figure 2(a), \mathbf{z}^{P_1} and \mathbf{z}^{P_2} are the intersection points of the same line $\mathbf{z}^{(s)} = \mathbf{z}^{\perp(s)} + z^{\parallel}\mathbf{e}_\alpha$ with the failure surfaces $\hat{g}_1(\mathbf{z}) = 0$ and $\hat{g}_2(\mathbf{z}) = 0$, and the two GPR models are both meta-models of the same limit state function. Figure 2(b) shows the corresponding probability density function of $\hat{g}(\mathbf{z})$ at the two points. Obviously, $\hat{g}_1(\mathbf{z}^{P_1})$ has a larger variation of prediction than $\hat{g}_2(\mathbf{z}^{P_2})$, thus its probability mass contained within the interval $[-\epsilon, \epsilon]$ is less than that of $\hat{g}_2(\mathbf{z}^{P_2})$; accordingly, the learning function value at \mathbf{z}^{P_1} is smaller than that evaluated at \mathbf{z}^{P_2} . Thus, a larger value of the learning function indicates a

better estimation of the intersection point. It is easy to observe that $0 \leq \kappa(\mathbf{z}) \leq 1$, where $\kappa(\mathbf{z}) \approx 0$ indicates that the corresponding intersection point is poorly estimated, and $\kappa(\mathbf{z}) \approx 1$ reveals that the intersection point is accurately computed. Commonly, $\kappa(\mathbf{z}) \geq \kappa^* = 0.985$ provides satisfactory estimation, here κ^* denotes the learning function threshold. In the next subsection, we develop the AGPR-LS algorithm with the proposed learning function $\kappa(\mathbf{z})$.

3.3 The AGPR-LS algorithm

The basic idea of the AGPR-LS algorithm is then adaptively learning the correct intersection points for each line of LS based on the GPR model, which is actively updated by including the most informative points identified by the learning function $\kappa(\mathbf{z})$. The flowchart of the algorithm is represented in Figure 3. The detailed procedure is also described as follows.

◆ Step 1: Initialization

The algorithm is started by setting the total number N of candidate lines, the number N_0 of initial lines for training the initial GPR model, the threshold κ^* and the error tolerance ϵ . Then, generate N samples $\mathbf{Z}_k = (\mathbf{z}^{(1)}, \mathbf{z}^{(2)}, \dots, \mathbf{z}^{(N)})$ so as to create N lines along the important direction \mathbf{e}_α by using, e.g., Latin-hypercube sampling. Then randomly select N_0 lines from those N lines, and estimate the intersection point for each of these N_0 lines by using TPSO polynomial interpolation that is also mentioned in section 2; the found intersection points are expressed by $\mathbf{z}^{(s)\perp} + c^{(s)}\mathbf{e}_\alpha$ ($s = 1, \dots, N_0$). This procedure introduces $3N_0$ training data points, which are added to the training data set \mathbf{S} . After that, evaluate the g -function of the N_0 intersection points, and also add them into the training data set. In practical applications, the important direction generally cannot be derived analytically, and numerical procedures such as FORM need to be used for calculating it numerically [2]. This numerical procedure also introduces $N_{\mathbf{e}_\alpha}$ extra g -function calls, and it is recommended to also add these data points into the training data set \mathbf{S} . Let N_c denote the training sample size of \mathbf{S} , so that the training sample size after initialization will become $N_c = N_{\mathbf{e}_\alpha} + 3N_0 + N_0$. The number of lines N can be set to be the same as in the classical LS algorithm. Commonly, higher nonlinearity and/or larger span failure regions require a larger number of candidate lines. N_0 can be set to be a

small value less than ten, e.g., 4.

◆ **Step 2: Train or update the GPR model**

Train or update the GPR model $\hat{g}(\mathbf{z})$ by using the training data set \mathbf{S} . In this step, one needs to specify the mean function $m(\mathbf{z})$ and the kernel function $c(\mathbf{z}, \mathbf{z}')$. Commonly, if the nonlinearity of the performance function is not high, zero or constant mean function is recommended. However, if the nonlinearity is high, linear or quadratic polynomial mean function is recommended. For the kernel function, the squared exponential kernel is utilized in this work. The function “fitrgp” in the Matlab Statistic and Machine Learning Toolbox is utilized in this work for training the GPR model.

◆ **Step 3: Learning from the GPR model**

The GPR model trained in **Step 2** provides a pair of quantities, i.e., $\mu_g(\mathbf{z})$ and $\sigma_g^2(\mathbf{z})$, for any realization \mathbf{z} . Compute the intersection point $\mathbf{z}^{(s)\perp} + c^{(s)}\mathbf{e}_\alpha$ for each line (including the N_0 initial lines) by solving the univariate equation $\mu_g(\mathbf{z}^{(s)\perp} + z^\# \mathbf{e}_\alpha) = 0$. During this procedure, it may happen that, for some lines, no zero point can be found, indicating a large GPR prediction error in this line. One can simply set the corresponding value of $c^{(s)}$ as the average values of c for other lines, but this point is definitely not an estimated intersection point. Then, for each line, compute the learning function value $\kappa^{(s)}$ for the intersection point $\mathbf{z}^{(s)\perp} + c^{(s)}\mathbf{e}_\alpha$ by modifying the learning function of Eq. (11) as:

$$\kappa^{(s)} = \int_{-\epsilon}^{\epsilon} \phi(y|0, \sigma_g^2(\mathbf{z}^{(s)\perp} + c^{(s)}\mathbf{e}_\alpha)) dy. \quad (12)$$

Find the minimum value $\kappa_{\min} = \min_{s=1}^{N_0} (\kappa^{(s)})$. If $\kappa_{\min} < \kappa^*$, find the intersection point with the minimum value of learning function, compute the corresponding g -function value, and add this point to the training data set \mathbf{S} , let $N_c = N_c + 1$, and go back to **Step 2**; else go to **Step 4**.

◆ **Step 4: Estimation and Iteration**

Estimate the failure probability p_f with the intersection point computed for each line in **Step 3** by Eqs. (5) and (6). If the COV estimated by Eq. (7) is higher than a pre-specified tolerance, say 0.05, then create N^a more lines. Let $N = N + N^a$, and go back to **Step 3**; otherwise, end the algorithm. N^a can be set to be 50 or more. ■

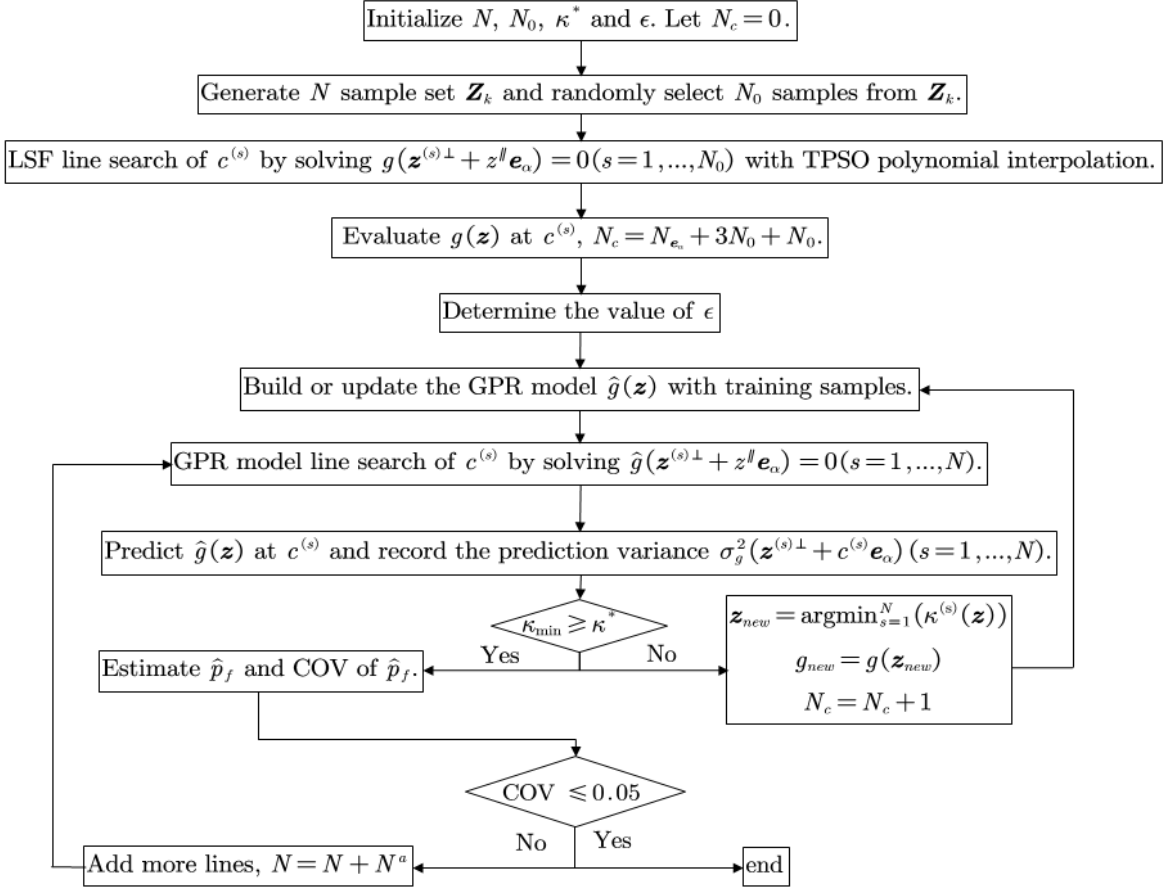


Figure 3 Flowchart of the AGPR-LS algorithm.

In **step 1**, the value of the error tolerance ϵ should be carefully treated. Since the GPR prediction at each calculated intersection point equals to zero, the next point being selected by the learning function in Eq. (12) is always the one with the largest value of prediction variance if it is an intersection point, or the one on a line whose intersection point is not available by solving $\mu_g(z^{(s)\perp} + z'' e_\alpha) = 0$. The value of ϵ does not affect the determination of training data to be added in each iteration. However, this value definitely affects the stopping criterion in **step 3**. A larger value of ϵ results in faster convergence but also poorer accuracy of each intersection point, while smaller value requires more training data, leading to higher computational cost. Therefore, a proper tradeoff should be made for ϵ . Based on our experience, it is suggested to set ϵ as p times the average absolute values of g -function at the intersection points of the initial N_0 lines estimated by TPSO interpolation, where $p = 10 \sim 100$. Another choice of ϵ is suggested as $(0.01 \sim 0.10)\sigma_y$, where σ_y is the standard deviation of the g -function. This value can

also be updated at each iteration based on the intersection points which are being accurately estimated by the trained GPR model.

It is found in the last step that, increasing the number of lines will not increase the required number of g -function calls too much. As for most newly added lines, the well-fitted GPR model can produce accurate estimations of the intersection points. In the case that for some newly added lines, the intersection points are not accurately estimated, the active learning function $\kappa(\mathbf{z})$ can commonly improve those estimations to required accuracy level with only a small number of training data (thus g -function calls) being added. Thus, compared with the classical LS algorithm, the AGPR-LS is more applicable to highly nonlinear performance function, and also the case where the important direction is not accurately specified. Besides, for rare event analysis, searching the intersection point based on the fitted GPR model can be much easier and more efficient due to the smoothness of the GPR predictor.

The AGPR-LS algorithm also has more appealing advantages over the advanced AK-MCS algorithms. The classical AK-MCS algorithm is known to be not effective for rare event analysis due to the large size of the required sample pool. Many improved algorithms such as the AK-MCMC have been developed [24][25]. As will be illustrated in the test examples, the AK-MCMC algorithm needs to approximate a set of intermediate failure surfaces adaptively, which will cost a considerable number of g -function calls. However, due to the high efficiency of the one-dimensional line search, the AGPR-LS method can be much more efficient for identifying the failure surface, especially when the failure probability is extremely small (less than 10^{-6}). Besides, all the AK-MCS and advanced AK-MCS algorithms require a large sample pool (with e.g., 10^5 samples) especially for extremely small failure probability, making the implementation inefficient. The AGPR-LS algorithm avoids this shortcoming since only a much small line pool (commonly with several hundreds of lines) is required.

However, the AGPR-LS algorithm also has its limits. The high efficiency of line searching is based on the specified important direction. In most applications, the failure region is mainly concentrated in one direction, and the proposed algorithm can be extremely efficient. However, if multiple important directions exist, the algorithm can be less effective for approaching the

whole failure region.

4 Case studies

4.1 A two-dimensional numerical example

A two-dimensional toy example is considered with limit state function:

$$y = g(\mathbf{x}) = 1 - \frac{(x_1 - 1)^2}{a^2} - \frac{(x_2 - 1)^3}{b^2} + d \sin(cx_1) \quad (13)$$

, where a and b are constants used for determining the magnitude of p_f , c and d are also constants used to justify the nonlinearity of the limit state function. x_1 and x_2 are two independent random input variables, both of which follow standard Gaussian distribution. The important direction for this example is assumed to be known precisely, and given in Table 1.

Next, we consider three cases for this example. The first case is utilized for demonstrating the robustness of the proposed AGPR-LS algorithm given different important directions, the second case is used for demonstrating its performance for extremely small failure probability, and the third case is designed for investigating its performance for highly nonlinear problems.

For implementing the classical LS in case 1 and case 2, the intersection point for each line is calculated by the three-point interpolation, thus the total number of function calls is $N_c = 3N_{line}$; while for case 3, the intersection point for each line is computed by the four-point interpolation due to the high nonlinearity, thus the total number of function calls is $N_c = 4N_{line}$. For all three cases, the classical LS algorithm is implemented by the COSSAN software [33].

For implementing the AGPR-LS algorithm, four initial training lines are created in the same way with the classical LS algorithm, and for each line, the three-point interpolation is utilized for calculating the intersection points. Thus, the total number of initial training samples is sixteen.

◆ Case 1: $a = 6$, $b = 7$ and $d = 0$

The reference result is computed by LS and IS, as given in Table 1. We implement the LS algorithm by setting the line size as 10, 100, and 1000 respectively, and the corresponding results are reported in Table 1. As can be seen, although the mean estimates of the three runs are all near to the reference solution, the COVs with 10 and 100 lines are both higher than 20%,

indicating that the accuracy is not acceptable. When the line size is increased to 1000, the COV drops to 2.7%, indicating the convergence of the LS algorithm.

For implementing the AGPR-LS algorithm, the important direction is set to $\mathbf{e}_\alpha = (0, 1)$ and $\mathbf{e}_\alpha = (-0.3420, 0.9397)$ to demonstrate the insensitivity of the algorithm to the accuracy of important direction. For both runs, the stopping criterion are set to be $\text{COV}(\hat{p}_f) \leq 5\%$.

The training process of AGPR-LS for case 1 with the important direction $\mathbf{e}_\alpha = (0, 1)$ is schematically shown in Figure 4. As can be seen, four lines are first generated randomly, and for each line, the three-point second-order interpolation is utilized for calculating the intersection point with the limit state function. The above procedure introduces sixteen input-output samples for training the initial GPR model. By setting the parameters as $\epsilon = 0.01$ and $\kappa^* = 0.985$, 596 more lines are generated, but only four more training samples are added sequentially based on the learning function $\kappa(\mathbf{x})$. Based on the 20 training samples, the intersection points for all the 600 lines are accurately estimated, and the failure probability is then calculated based on the LS estimators, and the results are shown in the second row of Table . The reference results generated by another adaptive learning method AK-MCMC developed in Ref. [24] are also listed for comparison. As can be seen, results generated by all the methods are in good agreement, and the COV of the estimate by AGPR-LS is quite small (approximately 4.5%), indicating that the failure probability estimation by AGPR-LS for this case is accurate, robust and efficient.

We then change the important direction to $\mathbf{e}_\alpha = (-0.3420, 0.9397)$ to test the sensitivity of the performance of AGPR-LS to the important direction. The training process is shown in Figure 5, and the results are given in Table 1. It is shown that, although the utilized important direction is distinct from the most informative one, the AGPR-LS algorithm still produces a correct and robust estimation, and the total number of g -function calls is still 20. It is also shown that the total number of required lines has increased to 1500, indicating when the important direction is not the most informative one, more lines are required. However, this does not result in a significant increment of the computational cost since the required number of required

training samples is still 20. This indicates that, for this case, the AGRP-LS method is not very sensitive to the important direction.

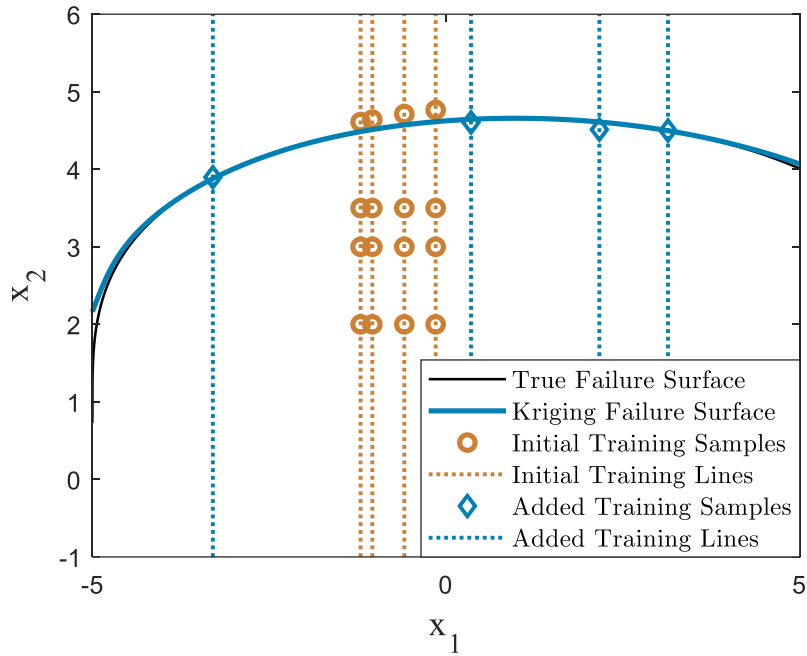


Figure 4 Results of AGPR-LS for case 1 of the toy example with important direction being
 $e_\alpha = (0, 1).$

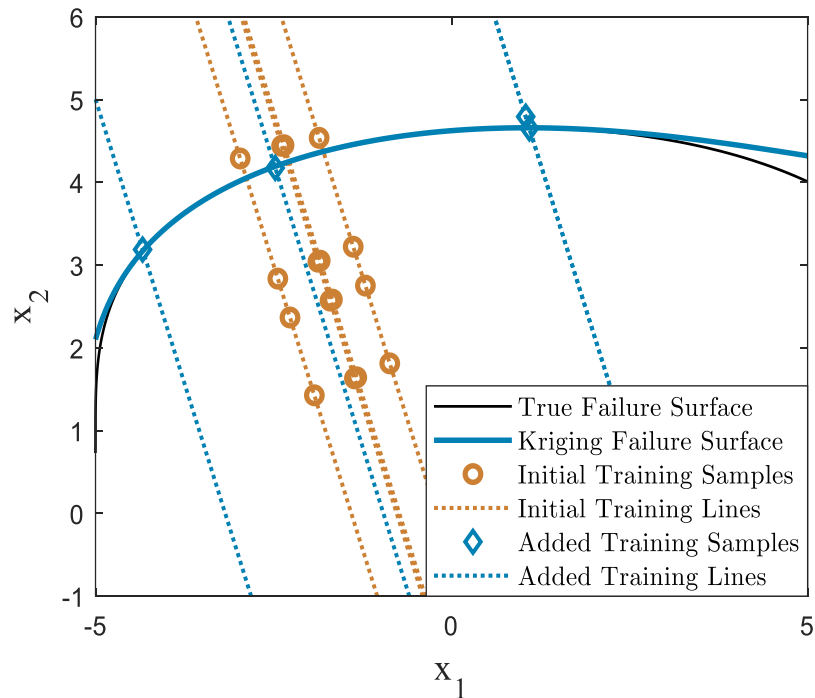


Figure 5 Results for case 1 of the toy example generated by AGPR-LS by setting the important direction as $e_\alpha = (-0.3420, 0.9397).$

◆ **Case 2:** $a = 9$, $b = 11$ and $d = 0$

With this setting, we aim at testing the performance of the AGPR-LS algorithm for analyzing the extremely rare failure events. In this case, the important direction is set to be $\mathbf{e}_\alpha = (0, 1)$. The classical LS algorithm is still implemented using COSSAN with 10, 100, and 1000 lines, respectively, and the results are reported in Table 1. As can be seen, with the line size less than 100, it is impossible to create a robust estimate with COV less than 10%.

We then implement the AGPR-LS algorithm by setting the stopping criterion as $\text{COV}(\hat{p}_f) \leq 5\%$, and we use four initial training lines (thus sixteen initial training samples) to start the AGPR-LS algorithm. The details of the training process are illustrated in Figure 6, and the estimation results are listed in Table 1, together with the estimations by AK-MCMC, LS, and IS for comparison.

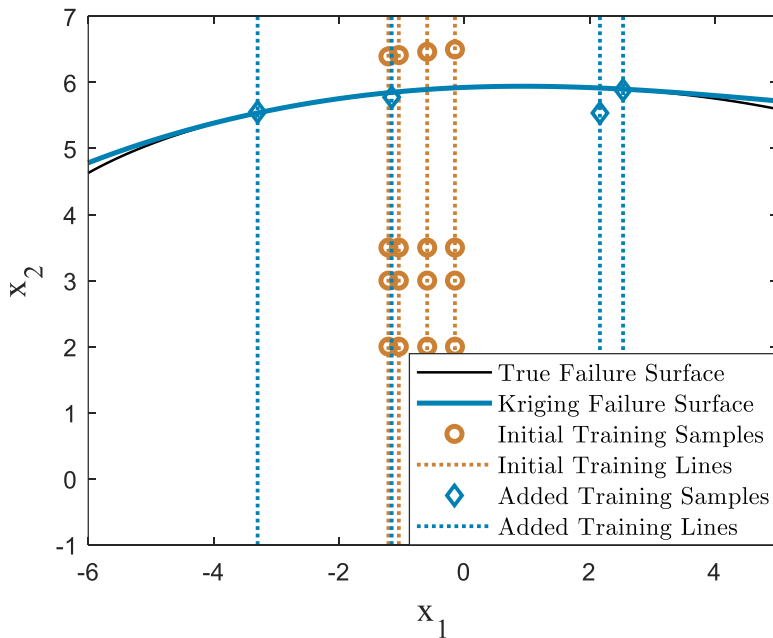


Figure 6 Training process of APGR-LS algorithm for case 2 of the toy example.

It is seen that, although the failure probability is extremely small (with the order of magnitude being 10^{-9}), the AGPR-LS algorithm can still give an accurate and robust estimation, with the same number of g -function calls as in case 1. This means that estimating a smaller failure probability does not necessarily increase computational cost, attributed to the high efficiency of line search. It is also found that the COV of the estimation, in this case, is even

smaller than that in case 1, although the line size (250) is less than that in case 1, indicating that the AGPR-LS method can be especially useful for extremely rare event analysis. Figure 6 shows that the intersection points between the initial four lines and limit state function computed by three-points second-order interpolations are not as accurate as those in case 1. However, during the adaptive training process, the intersection points for all lines (including the four initial training lines) are adaptively updated, and the final intersection points for all lines are much accurately calculated. This indicates that, in the classical LS method, the inaccuracy of estimating the intersection points will result in an extra numerical error, however, by injecting the active learning procedure into LS, this shortcoming can be largely alleviated.

◆ **Case 3:** $a = 9$, $b = 10$, $c = 4$ and $d = 0.5$.

With this setting, the failure probability is still very small, but the nonlinearity of the limit state function is much higher than that of the former two cases (see Figure 7 for the true limit state function). The classical LS algorithm is implemented using COSSAN with line sizes varying, and the results are listed in Table 1. As can be seen, for this highly nonlinear problem, even when the line size touches 1000, the COV is still higher than 5%, which is much higher than those in case 1 and case 2. This is unquestionably caused by the high nonlinearity of the g -function. This phenomenon indicates that, for highly nonlinear problems, the classical LS algorithm requires many more lines to achieve acceptable accuracy. As will be shown later, this can be largely alleviated by the AGPR-LS algorithm.

The stopping criterion of the AGPR-LS algorithm is still set to be $\text{COV}(\hat{p}_f) \leq 5\%$, and the important direction is set to be $\mathbf{e}_\alpha = (0, 1)$. The training process is then shown in Figure 7. For this highly nonlinear limit state function, 41 more samples are adaptively added to accurately estimate the intersection points for all the candidate lines, thus the total number of g -function calls is 57, which is still much smaller than that of AK-MCMC algorithm, which is 173, as shown in Table 1. This indicates that, for even highly nonlinear problems, the AGPR-LS algorithm is much more efficient than the AK-MCMC algorithm. This is because, for small failure probability, many g -function calls need to be performed for approximating a set of

intermediate failure surfaces, and this number can be large when the nonlinearity of the limit state function is high; however, the AGPR-LS algorithm can approach the true failure surface very efficiently along each line without the requirement of approximating any intermediate failure surface, no matter how far the failure surface is, thus can be extremely effective. It can be seen from Table 1 that, both the estimations of AGPR-LS and AK-MCMC algorithms are accurate when compared with the reference solutions computed by LS and IS algorithms, but the estimation of AGPR-LS is a little bit better than that of AK-MCMC. In terms of efficiency, the AGPR-LS algorithm consumes much fewer g -function calls than AK-MCMC.

Compared with case 1 and case 2, the required number of training samples has increased, but it is still small. This increment is caused by the necessity of capturing highly nonlinear behavior along the failure surface. From Figure 7, it is also seen that, on some lines, more than one training sample is added, this is also due to the high nonlinearity of the limit state function along these lines. However, as long as the limit state function is continuous along this line, this active learning mechanism driven by the learning function can always approach the real intersection points within the allowed error range.

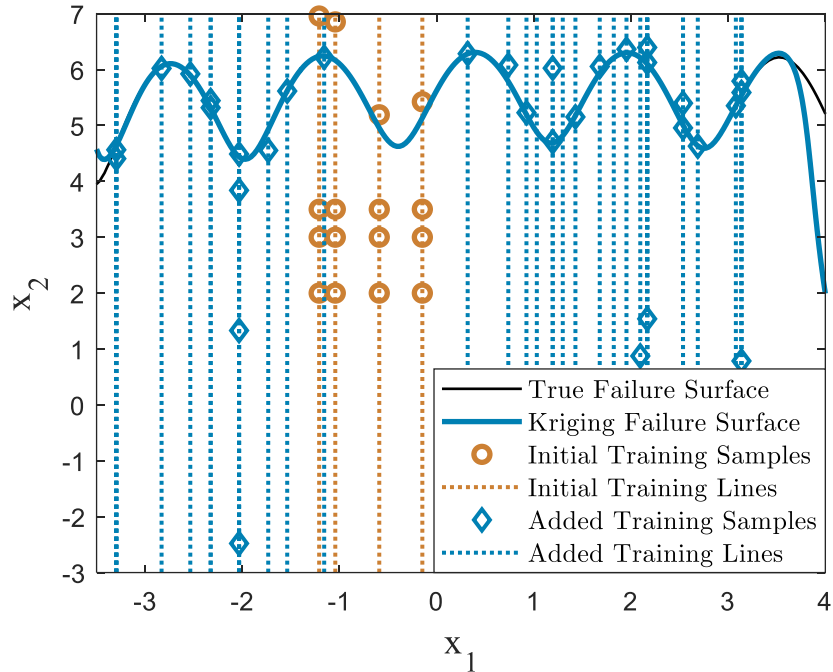


Figure 7 Learning details of AGPR-LS algorithm for case 3 of the toy example.

Table 1 Reliability analysis results of the toy example.

Methods	Parameter settings	N_{lines}	p_f	COV(%)	N_c
AGPR-LS	$\mathbf{e}_\alpha = (0, 1)$	600	2.596×10^{-6}	4.5	20
	$\epsilon = 0.01, \kappa^* = 0.985,$				
	$\mathbf{e}_\alpha = (-0.3420, 0.9397)$	1.5×10^3	2.740×10^{-6}	4.7	20
Case 1	$\epsilon = 0.01, \kappa^* = 0.985$				
	AK-MCMC	—	2.581×10^{-6}	7.3	47
	LS	10	3.606×10^{-6}	21.5	30
IS	$\mathbf{e}_\alpha = (0, 1)$	100	3.295×10^{-6}	20.9	300
		10^3	2.728×10^{-6}	2.7	3×10^3
	MPP = (0, 4)	—	2.646×10^{-6}	3.1	10^4
AGPR-LS	$\mathbf{e}_\alpha = (0, 1)$	250	1.891×10^{-9}	3.8	20
	$\epsilon = 0.01, \kappa^* = 0.985$				
	AK-MCMC	—	1.649×10^{-9}	7.7	150
Case 2		10	2.319×10^{-9}	19.1	30
	LS	100	2.305×10^{-9}	12.9	300
		10^3	2.033×10^{-9}	1.7	3×10^3
IS	MPP = (0, 5)	—	2.027×10^{-9}	3.6	10^4
	AGPR-LS	$\mathbf{e}_\alpha = (0, 1)$	1.9×10^3	3.520×10^{-7}	4.8
		$\epsilon = 0.01, \kappa^* = 0.985,$			
Case 3	AK-MCMC	—	3.141×10^{-7}	6.7	173
		10	5.331×10^{-7}	36.5	40
	LS	100	2.159×10^{-7}	21.2	400
IS		10^3	3.515×10^{-7}	6.8	4×10^3
	MPP = (0, 5)	—	3.560×10^{-7}	5.7	10^4

4.2 Dynamic response of a nonlinear oscillator

Consider a nonlinear undamped single degree of freedom system, shown in Figure 8, which is adapted from Ref.[14]. The limit state function is formulated as:

$$g(c_1, c_2, m, r, t_1, F_1) = 3r - \left| \frac{2F_1}{m\omega_0^2} \sin\left(\frac{\omega_0^2 t_1}{2}\right) \right| \quad (14)$$

, where $\omega_0 = \sqrt{(c_1 + c_2)/m}$. The six input variables are all assumed to follow Gaussian distribution with distribution parameters shown in Table 2.

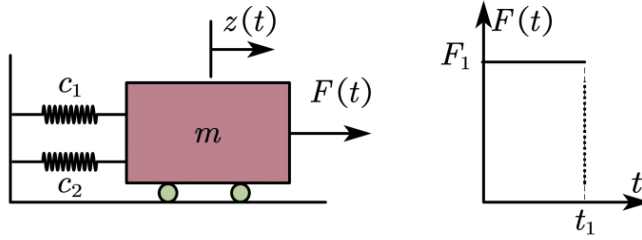


Figure 8 A nonlinear oscillator.

Table 2 Probability distributions of the six input variables of the nonlinear oscillator.

Variables	Distribution	Mean	COV
m	Gaussian	1	0.05
c_1	Gaussian	1	0.1
c_2	Gaussian	0.1	0.1
r	Gaussian	0.5	0.1
F_1	Gaussian	0.45	1/6
t_1	Gaussian	1	0.2

The results of the failure probability estimated by AGPR-LS, AK-MCMC, LS, and IS are listed in Table 3. The most probable point (MPP) is estimated by the FORM method to be (-0.4405, -1.2432, -0.1243, -4.0363, 2.6542, 2.3750), and the total number of function calls is seventeen. Then IS procedure is implemented by moving the sampling center from the mean point to the MPP. The important direction for AGRP-LS and LS is then derived from the MPP as (-0.0794, -0.2241, -0.0224, -0.7282, 0.4787, 0.4285).

The LS algorithm is implemented using COSSAN by setting the line size as 10, 100, and 500 respectively, and for each line, five points are used for estimating the intersection points. As can be seen, with ten lines, the accuracy is not acceptable as the COV is higher than 20%. The accuracy of results generated with 100 lines is acceptable for engineering computation, but the COV is still too high for academic research. With 500 lines, the COV is below 5%, and the estimate can be regarded as the reference solution.

For running the AGPR-LS algorithm, four initial training lines (thus sixteen initial training samples) are randomly generated. One notes that, in this example, the parameter κ^* is still set to be 0.985, while the parameter ϵ is set to be 0.005, which is different from the last example. This is because the level of magnitude of the response in this example is smaller than the last

example. For implementing the AK-MCMC algorithm in Ref. [24], the size N of the sample pool for each intermediate failure surface is set to be 10^5 , the initial training sample size N_0 is set to be 12, and the intermediate probability p_0 is set to be 0.01.

Table 3 shows that the results produced by the four methods are in good agreement. Compared with the AK-MCMC algorithm, the AGPR-LS demanded only 77 g -function calls, which is much less than that of the AK-MCMC algorithm. However, the AGRP-LS algorithm gives a better estimate since the COV of the estimation is much smaller than that of the AK-MCMC algorithm. This indicates that for this example with extremely small failure probability, the AGPR-LS method outperforms AK-MCMC. The AGPR-LS results are also competitive with those generated by the classical LS algorithm with 500 lines due to the same level of COV, but the computational cost is much lower.

For illustrating the learning process of AGPR-LS, we plot the minimum value of the learning function $\kappa(\mathbf{x})$ at each iteration step in Figure 9. As can be seen, with more training samples added, the minimum value of $\kappa(\mathbf{x})$ over all lines tends to increase, but this is not always the case at each step. With the minimum value adaptively approaching one, it is believed that the intersection point for each line is accurately calculated, resulting in an accurate estimation of failure probability as long as the number of lines is enough.

Table 3 Reliability analysis results of the nonlinear oscillator.

Methods	Parameter Settings	N_{lines}	p_f ($\times 10^{-8}$)	COV (%)	N_c
AGPR-LS	$\epsilon = 0.005$, $\kappa^* = 0.985$	300	1.530	4.1	$17+60=77$
AK-MCMC	$N = 10^5$, $N_0 = 12$, $p_0 = 0.01$	—	1.493	9.9	155
LS	—	10	2.370	27.8	$17+50=67$
	—	100	1.889	10.4	$17+500=517$
	—	500	1.775	4.6	$17+2.5 \times 10^3=2517$
IS	—	—	1.512	2.7	$17+10^4$

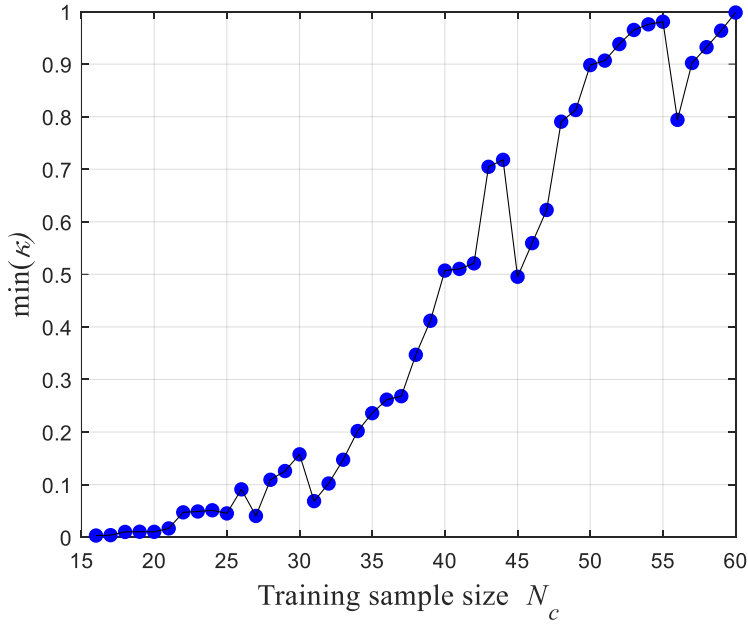


Figure 9 Plots of the minimum value of the learning function against the learning step for the nonlinear oscillator example.

4.3 Confined seepage model

A steady state of confined seepage below a dam discussed in Ref.[34] is considered, and the elevation of the dam is shown in Figure 10. The water flows from the upstream side (segment AB) towards the downstream side (segment CD) through the two permeable layers, silty gravel and silty sand, and an impermeable layer is below these two permeable layers. It is assumed that there is no water flow on any of the boundaries except for the segments AB and CD. In Figure 10, the water height h_D in the upstream side of the dam is modeled as a random variable with uniform distribution $U(7[m], 10[m])$, the hydraulic head h_W over the impermeable layer is $h_W = h_D + 20[m]$. The permeability of the two permeable layers are assumed to be anisotropic and modeled as random variables following lognormal distribution, the horizontal and vertical permeabilities are denoted by $k_{xx,i}$ and $k_{yy,i}$ ($i=1$ for sand layer, $i=2$ for gravel layer). The distribution parameters of the permeability of the two soil layers as well as the water height are provided in Table 4. The governing partial differential equation of the seepage problem is

$$k_{xx,i} \frac{\partial^2 h_W}{\partial x^2} + k_{yy,i} \frac{\partial^2 h_W}{\partial y^2} = 0, \quad i = 1, 2. \quad (15)$$

The boundary conditions are the hydraulic head over segments AB and CD. A finite element mesh with 3413 nodes and 1628 quadratic triangular elements is established to solve the governing equation. The seepage q at the downstream side can be calculated by

$$q = - \int_{CD} k_{yy,2} \frac{\partial h_w}{\partial y} dx. \quad (16)$$

Note that the unit of q is the volume over time over distance [$L/h/m$]. Commonly, we expect the seepage to be small enough for ensuring a safe state of the dam, so the failure event of interest is defined when seepage q exceeds a prescribed threshold 50 [$L/h/m$], and the limit state function is $g(\mathbf{x}) = 50 - q(\mathbf{x})$.

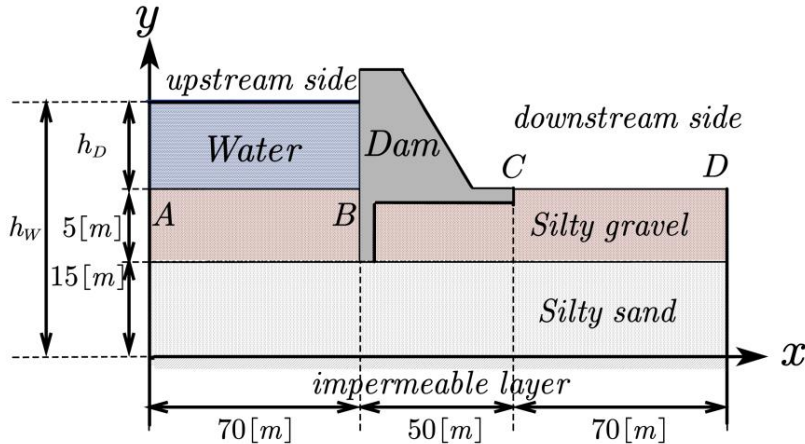


Figure 10 Elevation of the dam in confined seepage model.

Table 4 Distribution parameters of input variables for confined seepage model.

Variables	Description	Distribution type	Parameter1	Parameter2
$k_{xx,1} [10^{-7}\text{m/s}]$	Horizontal permeability of silty sand soil layer	lognormal	Mean=5	COV=1
$k_{yy,1} [10^{-7}\text{m/s}]$	Vertical permeability of silty sand soil layer	lognormal	Mean=2	COV=1
$k_{xx,2} [10^{-6}\text{m/s}]$	Horizontal permeability of silty gravel soil layer	lognormal	Mean=5	COV=1
$k_{yy,2} [10^{-6}\text{m/s}]$	Vertical permeability of silty gravel soil layer	lognormal	Mean=2	COV=1
$h_D [\text{m}]$	water height in upstream side of dam	uniform	$a_{h_D} = 7$	$b_{h_D} = 10$

We first calculate the MPP by FORM, and the result is (3.1257, 1.5715, 1.0808, 0.9211,

0.8865), thus the important direction can be specified as (0.8059, 0.4052, 0.2787, 0.2375, 0.2286) by normalizing the vector from the origin to MPP. The total number of function calls in FORM is 30. Then we implement the AGPR-LS algorithm with four lines and thus $N_0=16$ initial training points. The algorithm parameters are set to be $\epsilon=0.1$ and $\kappa^*=0.985$. The results are then reported in Table 5, together with the reference results computed by AK-MCMC, LS, and IS respectively, where IS is implemented by shifting the sampling center to the MPP. The LS is implemented by setting the line size to 10, 100, and 200, and it is shown that the COV of the estimate generated with 10 lines is over 20%, thus it is not acceptable. However, the results generated with 100 or more lines are robust and accurate, and can be served as reference solutions. As can be seen, the failure probability estimated by AGRP-LS is a little bit better than that calculated by AK-MCMC, when compared with the reference solutions computed by IS and LS. However, the AGRP-LS demands only 80 g -function calls, which is much less than that consumed by AK-MCMC. This indicates that, for this example, both the AGRP-LS and AK-MCMC algorithms work well, but the AGRP-LS algorithm is much more efficient than AK-MCMC.

Similarly, the minimum value of $\kappa(\mathbf{x})$ against the iteration step is schematically shown in Figure 11. A similar phenomenon as seen in Figure 9 is found here, that is, the minimum value of $\kappa(\mathbf{x})$ across all lines decreases rapidly with the increase of training samples identified by the learning function, and finally with only 50 training points, the AGPR-LS algorithm produces accurate estimations for the intersection points of all lines, and also accurate estimation of the failure probability.

Table 5 Reliability analysis results for the confined seepage model.

Methods	Parameter Settings	N_{lines}	$p_f (\times 10^{-5})$	COV (%)	N_c
AGPR-LS	$\epsilon=0.1, \kappa^*=0.985$	200	2.811	4.6	$30+50=80$
AK-MCMC	$N=1e5, N_0=12, p_0=0.01$	—	2.465	4.9	337
LS	—	10	1.696	25.6	$30+30=60$
	—	100	3.006	7.8	$30+300=330$
	—	200	2.933	4.2	$30+600=630$
IS	—	—	2.846	1.8	$30+5\times 10^4$

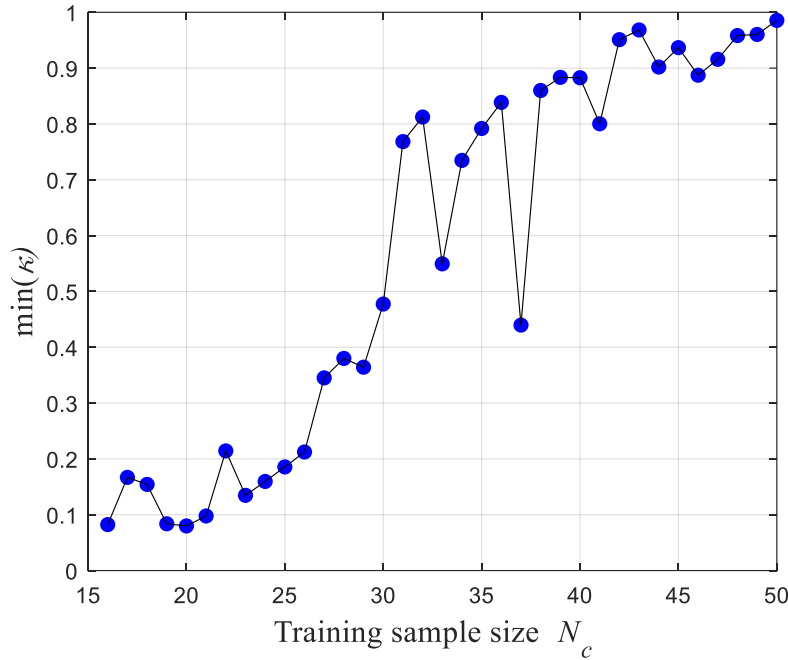


Figure 11 Plots of the minimum value of the learning function at each iteration step for the seepage model.

4.4 A two-dimensional wing flutter model

A two-dimensional wing flutter model adapted from Refs. [25] and [35] is introduced here.

As shown in Figure 12, the mass of the wing is denoted by m , the point G denotes the center-of-mass of the wing, E is the location of stiffness center. Let h and α denote the vertical and rotational displacements, respectively. K_h and K_α are the stiffness of the vertical spring and the torsional spring both of which are fixed at the stiffness center. The chord length of the wing is $2b$, the variable a refers to the dimensionless distance between the midpoint of the chord and the stiffness center, and the variable x_α refers to the dimensionless distance between the center-of-mass G and the stiffness center E . The phugoid mode frequency of the wing is $\omega_h = \sqrt{K_h/m}$, the pitching mode frequency is $\omega_\alpha = \sqrt{K_\alpha/m}$, the radius of the rotation of the wing towards G is expressed as r_α . The equation governing the vibration of the two-dimensional wing is derived as:

$$\begin{cases} \frac{d^2}{dt^2} \left(\frac{h}{b} \right) + x_\alpha \frac{d^2}{dt^2} \alpha + \omega_h^2 \frac{h}{b} = \frac{Q_h}{mb} \\ x_\alpha \frac{d^2}{dt^2} \left(\frac{h}{b} \right) + r_\alpha^2 \frac{d^2}{dt^2} \alpha + r_\alpha^2 \omega_\alpha^2 \alpha = \frac{Q_\alpha}{mb^2}. \end{cases} \quad (17)$$

Let $\mathbf{q} = (h/b, \alpha)^T$ express the general displacement, and $d\tau = \omega_\alpha dt$ denotes the dimensionless time, then the above governing equation can be rewritten as

$$\mathbf{M} \frac{d^2 \mathbf{q}}{d\tau^2} + \mathbf{K} \mathbf{q} = \mathbf{F} \quad (18)$$

, where

$$\mathbf{M} = \begin{bmatrix} 1 & x_\alpha \\ x_\alpha & r_\alpha^2 \end{bmatrix}, \quad \mathbf{K} = \begin{bmatrix} (\omega_h/\omega_\alpha) & 0 \\ 0 & r_\alpha^2 \end{bmatrix} \quad (19)$$

, and \mathbf{F} is the generalized aerodynamic force expressed as

$$\mathbf{F} = \frac{V^2}{\omega_\alpha^2 b^2} \frac{\pi \rho b^2}{m} \frac{1}{\pi} \left(\begin{bmatrix} C_L \\ 2C_{M_E} \end{bmatrix} \right) = \frac{1}{\pi} V_f^{*2} \left(\begin{bmatrix} C_L \\ 2C_{M_E} \end{bmatrix} \right) \quad (20)$$

, C_L and C_{M_E} are the aerodynamic force coefficient of the wing and aerodynamic moment coefficients towards the stiffness center E , respectively. Assume that the mass ratio is $\mu = m/\pi \rho b^2$, then $V_f^* = V/(\omega_\alpha b \sqrt{\mu})$ expresses the dimensionless flutter critical speed. Theo Dawson unsteady aerodynamic model is used to derive the aerodynamic force of the wing, and then the above flutter model is solved with V-g method, one can find more details about V-g method in subsection 3.7 of Ref.[35].

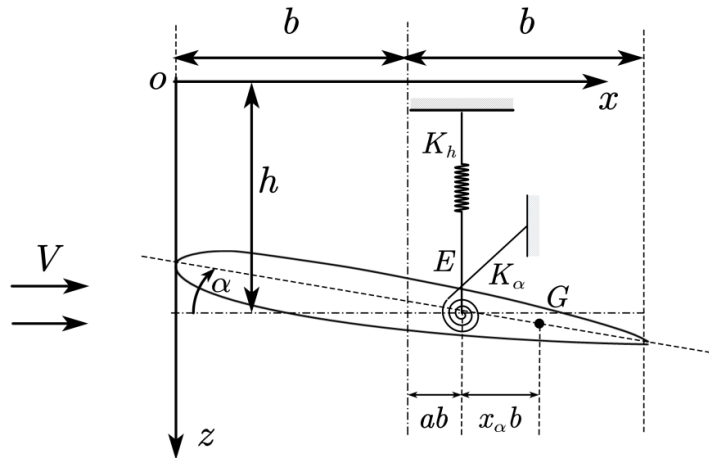


Figure 12 A two-dimensional wing flutter model.

The flutter will happen if the critical speed V_f^* is smaller than the threshold 0.4414, thus the performance function is defined as $g = V_f^* - 0.4414$. The six inputs variables, i.e. μ , r_α , ω_h , a , ω_α and x_α , are assumed to follow truncated Gaussian distribution with distribution parameters listed in Table 6 and truncated support $[m_i - 5\sigma_i, m_i + 5\sigma_i]$, where m_i and σ_i are

the mean and standard deviation of each input respectively.

Table 6 Distribution parameters of the input variables in the wing flutter model.

Variables	Description	Mean	COV
μ	Mass ratio	20	0.0425
r_a	Dimensionless radius of rotation	0.5	0.0425
ω_h	Phugoid mode frequency	30	0.0255
a	Dimensionless distance between midpoint of the chord and E	-0.4	0.0255
ω_a	Pitching mode frequency	50	0.0255
x_a	Dimensionless distance between E and G	0.2	0.0255

The MPP and important direction are first calculated by the FORM method, and the total number of function calls is 18. Then the AGPR-LS is implemented with six initial lines (thus 24 initial training samples) by setting $\epsilon = 0.0005$ and $\kappa^* = 0.985$, and the results are reported in Table 7, with the training process being schematically illustrated by the evolution of learning function values shown in Figure 13. The reference solutions computed by AK-MCMC, LS, and IS are also reported in Table 7 for comparison, where the LS algorithm is implemented by setting the line size as 10, 100, and 200 respectively, and for each line, five points are utilized for calculating the intersection point. As can be seen, both AGPR-LS and AK-MCMC algorithms produce satisfactory results, but still, the AGPR-LS algorithm is much more efficient than AK-MCMC, as revealed by the total number of g -function calls. It is also shown in Table 7 that, the AGPR-LS with totally 120 g -function calls produces the estimate with the same level of accuracy as the classical LS with 200 lines (thus $18+10^3$ g -function calls), indicating the superiority of the AGPR-LS algorithm to the classical LS algorithm.

Table 7 Reliability analysis results of the two-dimensional wing flutter model.

Methods	Parameter Settings	N_{lines}	$p_f (\times 10^{-4})$	COV (%)	N_c
AGPR-LS	$\epsilon = 0.0005, \kappa^* = 0.985$	200	9.332	2.7	$18+102=120$
AK-MCMC	$N = 3e4, N_0 = 12,$ $p_0 = 0.01$	—	9.409	6.0	346
LS	—	10	8.390	18.8	$18+50=68$
	—	100	10.552	7.1	$18+500=518$
	—	200	9.493	3.6	$18+10^3=1018$
IS	—	—	9.298	2.1	$18+10^4$

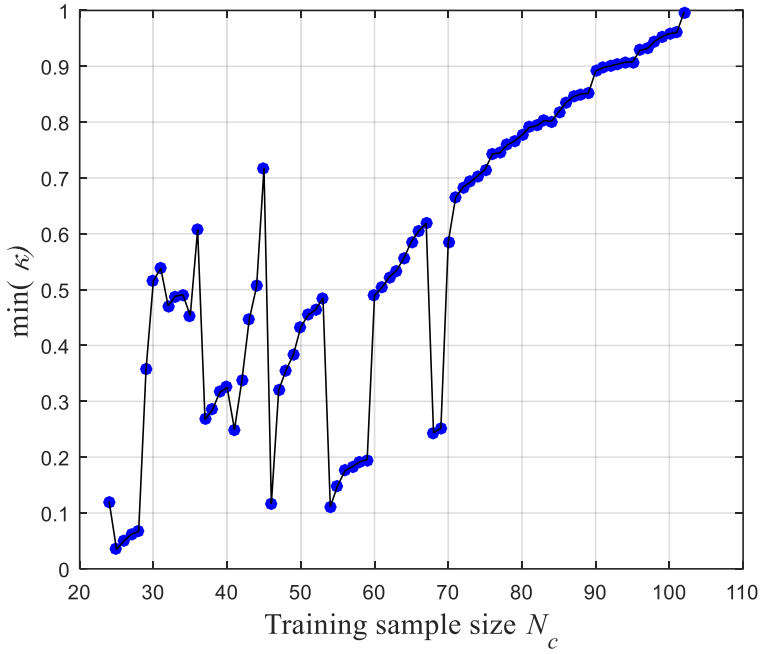


Figure 13 Plot of the minimum value of the learning function with respect to the training step for the wing flutter model.

4.5 Transmission tower

For demonstrating the performance of the AGPR-LS algorithm for high-dimensional problems, we consider an electricity transmission tower structure shown in Figure 14, which is adapted from Refs. [36] and [37]. The finite element model is established with Matlab. This structure consists of 80 bars, all of which behave within the linear elastic range. Four static loads are applied in the top nodes. All these four loads are assumed to be deterministic with magnitude $F=200$ [kN], and they are all applied in the direction $[\sin(\pi/3), \cos(\pi/3), 0]$. There are twenty corner bars whose cross-section areas (A_1^c, \dots, A_{20}^c) and Young's modulus (E_1^c, \dots, E_{20}^c) are assumed to be random input variables, and for the rest 60 bars, both the cross-section areas Young's modulus are assumed to be deterministic with magnitudes 4.35×10^{-3} [m^2] and 2.1×10^{11} [Pa] respectively. For the twenty corner bars, both A_i^c and E_i^c follow lognormal distribution with mean values being 7.45×10^{-3} [m^2] and 2.1×10^{11} [Pa] respectively. The COVs of all these 40 input random variables are assumed to be 0.1. The failure event is defined as the displacement of node A at the top of the tower exceeding 0.072 [m].

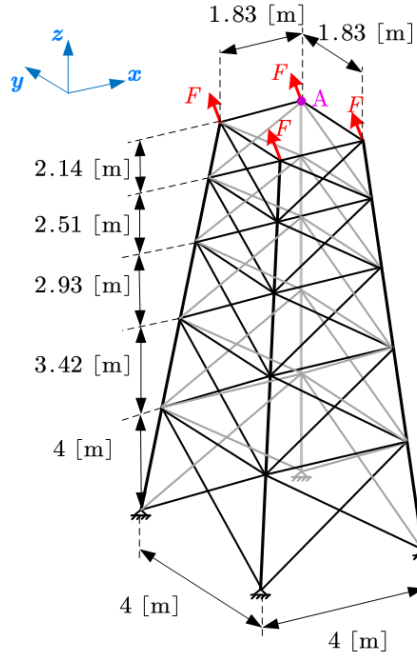


Figure 14 A transmission tower structure.

All the 40 lognormal random variables are first transformed into independent standard Gaussian variables by using the isoprobabilistic transformation, and then the MPP is calculated in the standard Gaussian space by using FORM, and 18 g -function calls are consumed. This MPP is then utilized for implementing the simulation. The LS and IS algorithms are implemented for providing reference solutions, as shown in Table 8. One notes that with the IS algorithm, only when the sample size being very large (e.g., 2×10^5), the COV of the estimate is less than 5%. The LS algorithm is implemented by setting the line size as 10, 100, and 200 respectively, and for each line, five points are utilized for calculating the intersection points with spline interpolation. It is shown that the accuracy of the result with 10 lines is not acceptable due to the large COV. When 200 lines are used, the COV of the estimate is less than 5%, and the result can be served as a reference solution.

The AGPR-LS algorithm is then implemented with three initial lines, and for each line, three points are used for calculating the intersection points, thus the initial training sample size is 12. The results are then reported in Table 8. As can be seen, the AGPR-LS algorithm consumes totally 231 g -function calls to produce the estimate of the same level of accuracy with the classical LS algorithm with 200 lines (18+1000 g -function calls), indicating that even for this

high-dimensional problem, the AGPR-LS algorithm outperforms the classical LS algorithm.

An interesting phenomenon appears in the implementation of the AGPR-LS algorithm for this high-dimensional problem. During the training process, especially in the first several dozens of iterations, it happens that for some lines, the intersection points defined by $\mu_g(\mathbf{z}^{(s)\perp} + z^\# \mathbf{e}_\alpha) = 0$ (see step 3 in subsection 3.3) do not exist. For this case, we set the corresponding $c^{(s)}$ values as the average value of c across other lines computed in the previous iteration to improve the robustness of the algorithm. Interestingly, this phenomenon rarely happens in low-dimensional problems. The reason behind it is that, with the increment of the input dimension, the distance between lines tend to be larger, indicating weaker correlation strength between lines. For the lines which are far from the training data, the GPR prediction errors can be large, making it sometimes intractable to solve the univariate equation $\mu_g(\mathbf{z}^{(s)\perp} + z^\# \mathbf{e}_\alpha) = 0$. This is also why we need more training samples, and thus g -function calls, for this high-dimensional problem than that for the several previous low-dimensional problems. However, as indicated, the AGPR-LS algorithm is still much more efficient than the classical LS algorithm if the target is to generate estimates with the same level of COV.

Table 8 Reliability results of the transmission tower.

Methods	Parameter Settings	N_{lines}	$p_f (\times 10^{-9})$	COV (%)	N_c
AGPR-LS	$\epsilon = 0.1, \kappa^* = 0.980$	200	5.297	4.5	$18+213=231$
		10	3.995	25.9	$18+50=68$
LS	—	100	5.576	8.0	$18+500=518$
		200	5.009	4.9	$18+10^3=1018$
IS	—	—	5.458	4.5	$18+2\times 10^5$

4.6 Final remarks

With the above five test examples, we have shown the high performance of the AGRP-LS algorithm. The results have proved that, with the introduction of the adaptive learning procedure, the AGPR-LS algorithm has the potential to outperform classical LS algorithm for problems with extremely rare failure events, nonlinear performance function, and high-dimensional inputs. The reason behind this improvement is that the AGPR-LS algorithm,

on the one hand, takes full advantage of the high efficiency of the one-dimensional line search of the classical LS algorithm and, on the other hand, makes the best use of the spatial correlation information among lines and training samples to improve the speed and accuracy of calculating the intersection point for each line.

One notes that there are also other improved LS schemes being developed, and one of the most related developments is the metamodel LS (MLS) developed in Ref. [29], which improves the classical LS by combining it with the GPR without adaptive learning. We make a simple comparison of AGPR-LS with the MLS by using the second test example (a parallel system) of Ref. [29] and their results (Table 6 of Ref. [29]). The performance function is highly nonlinear. It is reported in that paper that, the results with MLS and LS are 2.42×10^{-4} (with COV being 3.52%) and 2.45×10^{-4} (with COV being 4.00%) respectively, and the corresponding total numbers of g -function calls are 762 and 2905 respectively. We then implement AGPR-LS algorithm to achieve the same level of estimation accuracy, and the mean estimate and the corresponding COV are 2.42×10^{-4} and 3.58% respectively, while the total number of g -function calls is only 42, indicating that for this highly nonlinear problem, the AGPR-LS algorithm is much more efficient than both the MLS and LS algorithms. This high efficiency benefits from the adaptive learning scheme. The combination of the GPR model, the active learning scheme, and LS has largely improved the efficiency and robustness of the LS algorithm for different types of problems.

5 Conclusions and discussions

The LS algorithm is one of the most competitive stochastic simulation algorithms for small failure probability estimation. However, it is mostly applied to problems with moderately nonlinear performance functions, and the correct identification of the important direction is extremely important for the efficient implementation of the algorithm. The reason is that, for highly nonlinear performance function, many more lines are required for accurately estimating the failure probability. Besides, for highly non-linear performance functions, more g -function calls are required for accurately calculating the intersection point for each line. All the above

elements may lead to a considerable increment of g -function calls. However, compared with the other stochastic simulation algorithms such as SS, the LS can be especially efficient due to the high searching efficiency along lines, each of which is equivalent to solving a one-dimensional nonlinear equation.

The AGPR-LS algorithms developed in this paper has tackled the above disadvantages, but keeping the high efficiency of one-dimensional searching. The devised learning function $\kappa(\mathbf{z})$ is proven to be especially effective for improving the accuracy of calculating the intersection point for each line, and the induced AGPR-LS algorithm is shown to be extremely efficient for extremely small failure probability estimation, and also less sensitive to the specified important directions and the nonlinearity of performance function as more lines can be added without largely increasing the number of performance function evaluations. Compared with the other active learning algorithms such as AK-MCMC, due to the high efficiency of one-dimensional search, the AGPR-LS algorithm is more efficient especially for rare events since the line search allows approaching the failure surface very easily. Besides, the introduction of a small line pool in the AGPR-LS algorithm, instead of the large sample pool as used in the AK-MCS and advanced AK-MCS methods, makes it even more efficient for numerical implementation. However, for problems with multiple important directions and/or failure modes and/or failure domains, the proposed algorithm is still less effective, and needs to be improved in future work.

Acknowledgment

This work is supported by the National Natural Science Foundation of China (NSFC 51905430) and ANID (Agency for Research and Development, Chile) under its program FONDECYT, grant number 1180271. The first author is supported by the program of China Scholarships Council (CSC). The second and third authors are both supported by the Alexander von Humboldt Foundation of Germany. The second author is also supported by the Top International University Visiting Program for Outstanding Young Scholars of Northwestern Polytechnical University. We would also like to thank our colleague Dr. Matteo Broggi for his strong support on COSSAN.

References

- [1] Zio, E. (2009). Reliability engineering: Old problems and new challenges. *Reliability Engineering & System Safety*, 94(2), 125-141.
- [2] Hasofer, A. M. (1974). An Exact and Invariant First Order Reliability Format. *Journal of Engineering Mechanics. Proc. ASCE*, 100(1), 111-121.
- [3] Der Kiureghian, A., Lin, H. Z., & Hwang, S. J. (1987). Second-order reliability approximations. *Journal of Engineering mechanics*, 113(8), 1208-1225.
- [4] Li, J., Chen, J., Sun, W., & Peng, Y. (2012). Advances of the probability density evolution method for nonlinear stochastic systems. *Probabilistic Engineering Mechanics*, 28, 132-142.
- [5] Chen, G., & Yang, D. (2019). Direct probability integral method for stochastic response analysis of static and dynamic structural systems. *Computer Methods in Applied Mechanics and Engineering*, 357, 112612.
- [6] Au, S. K., & Beck, J. L. (1999). A new adaptive importance sampling scheme for reliability calculations. *Structural safety*, 21(2), 135-158.
- [7] Beaurepaire, P., Jensen, H. A., Schuëller, G. I., & Valdebenito, M. A. (2013). Reliability-based optimization using bridge importance sampling. *Probabilistic Engineering Mechanics*, 34, 48-57.
- [8] Au, S. K., & Beck, J. L. (2001). Estimation of small failure probabilities in high dimensions by subset simulation. *Probabilistic engineering mechanics*, 16(4), 263-277.
- [9] Papaioannou, I., Betz, W., Zwirglmaier, K., & Straub, D. (2015). MCMC algorithms for subset simulation. *Probabilistic Engineering Mechanics*, 41, 89-103.
- [10] Schuëller, G. I., Pradlwarter, H. J., & Koutsourelakis, P. S. (2004). A critical appraisal of reliability estimation procedures for high dimensions. *Probabilistic engineering mechanics*, 19(4), 463-474.
- [11] de Angelis, M., Patelli, E., & Beer, M. (2015). Advanced line sampling for efficient robust reliability analysis. *Structural safety*, 52, 170-182.
- [12] Melchers, R. E. (1994). Structural system reliability assessment using directional

- simulation. Structural Safety, 16(1-2), 23-37.
- [13] Wang, Z., Broccardo, M., & Song, J. (2019). Hamiltonian Monte Carlo methods for Subset Simulation in reliability analysis. Structural Safety, 76, 51-67.
- [14] Echard, B., Gayton, N., & Lemaire, M. (2011). AK-MCS: an active learning reliability method combining Kriging and Monte Carlo simulation. Structural Safety, 33(2), 145-154.
- [15] Bichon, B. J., Eldred, M. S., Swiler, L. P., Mahadevan, S., & McFarland, J. M. (2008). Efficient global reliability analysis for nonlinear implicit performance functions. AIAA journal, 46(10), 2459-2468.
- [16] Lv, Z., Lu, Z., & Wang, P. (2015). A new learning function for Kriging and its applications to solve reliability problems in engineering. Computers & Mathematics with Applications, 70(5), 1182-1197.
- [17] Sun, Z., Wang, J., Li, R., & Tong, C. (2017). LIF: A new Kriging based learning function and its application to structural reliability analysis. Reliability Engineering & System Safety, 157, 152-165.
- [18] Echard, B., Gayton, N., Lemaire, M., & Relun, N. (2013). A combined importance sampling and kriging reliability method for small failure probabilities with time-demanding numerical models. Reliability Engineering & System Safety, 111, 232-240.
- [19] Dubourg, V., Sudret, B., & Deheeger, F. (2013). Metamodel-based importance sampling for structural reliability analysis. Probabilistic Engineering Mechanics, 33, 47-57.
- [20] Cadini, F., Santos, F., & Zio, E. (2014). An improved adaptive kriging-based importance technique for sampling multiple failure regions of low probability. Reliability Engineering & System Safety, 131, 109-117.
- [21] Yun, W., Lu, Z., & Jiang, X. (2018). An efficient reliability analysis method combining adaptive Kriging and modified importance sampling for small failure probability. Structural and Multidisciplinary Optimization, 58(4), 1383-1393.
- [22] Huang, X., Chen, J., & Zhu, H. (2016). Assessing small failure probabilities by AK-SS: An active learning method combining Kriging and Subset Simulation. Structural Safety, 59, 86-95.

- [23] Zhang, J., Xiao, M., & Gao, L. (2019). An active learning reliability method combining Kriging constructed with exploration and exploitation of failure region and subset simulation. *Reliability Engineering & System Safety*, 188, 90-102.
- [24] Wei, P., Tang, C., & Yang, Y. (2019). Structural reliability and reliability sensitivity analysis of extremely rare failure events by combining sampling and surrogate model methods. *Proceedings of the Institution of Mechanical Engineers, Part O: Journal of risk and reliability*, 233(6), 943-957.
- [25] Wei, P., Song, J., Bi, S., Broggi, M., Beer, M., Lu, Z., & Yue, Z. (2019). Non-intrusive stochastic analysis with parameterized imprecise probability models: II. Reliability and rare events analysis. *Mechanical Systems and Signal Processing*, 126, 227-247.
- [26] Lelièvre, N., Beaurepaire, P., Matstrand, C., & Gayton, N. (2018). AK-MCSi: A Kriging-based method to deal with small failure probabilities and time-consuming models. *Structural Safety*, 73, 1-11.
- [27] Fauriat, W., & Gayton, N. (2014). AK-SYS: an adaptation of the AK-MCS method for system reliability. *Reliability Engineering & System Safety*, 123, 137-144.
- [28] Wei, P., Liu, F., & Tang, C. (2018). Reliability and reliability-based importance analysis of structural systems using multiple response Gaussian process model. *Reliability Engineering & System Safety*, 175, 183-195.
- [29] Depina, I., Le, T. M. H., Fenton, G., & Eiksund, G. (2016). Reliability analysis with metamodel line sampling. *Structural Safety*, 60, 1-15.
- [30] Zhang, X., Lu, Z., Yun, W., Feng, K., & Wang, Y. (2020). Line sampling-based local and global reliability sensitivity analysis. *Structural and Multidisciplinary Optimization*, 61(1), 267-281.
- [31] Lebrun, R., & Dutfoy, A. (2009). Do Rosenblatt and Nataf isoprobabilistic transformations really differ?. *Probabilistic Engineering Mechanics*, 24(4), 577-584.
- [32] Rasmussen, C. E. & Williams, C. K. I. (2006). Gaussian processes for machine learning. Cambridge: The MIT Press.
- [33] Patelli, E. (2016). COSSAN: A Multidisciplinary Software Suite for Uncertainty

- Quantification and Risk Management, in Handbook of Uncertainty Quantification Ghanem, R.; Higdon, D. & Owhadi, H. (Eds.) Springer International Publishing, 1-69.
- [34] Valdebenito, M. A., Jensen, H. A., Hernández, H. B., & Mehrez, L. (2018). Sensitivity estimation of failure probability applying line sampling. *Reliability Engineering & System Safety*, 171, 99-111.
- [35] Ye, Z. Y., WW, Z., & AM, S. (2010). Fundamentals of Fluid-Structure Coupling and Its Application. Harbin Institute of Technology Press, China.
- [36] Haukaas, T., & Der Kiureghian, A. (2006). Strategies for finding the design point in non-linear finite element reliability analysis. *Probabilistic Engineering Mechanics*, 21(2), 133-147.
- [37] Song, J., Valdebenito, M., Wei, P., Beer, M., & Lu, Z. (2020). Non-intrusive imprecise stochastic simulation by line sampling. *Structural Safety*, 84, 101936.

Conclusions and Prospects

1. Conclusions

The imprecise probability models and the non-probabilistic models have been widely recognized as the necessary developments for modeling uncertainties when epistemic uncertainty is presented due to scarcity, incompleteness, imprecision, vagueness, etc., of the available information. The imprecise probability models are utilized for modeling both the aleatory uncertainty and epistemic uncertainty of random variables, and the non-probabilistic models are widely used for modeling the epistemic uncertainty of deterministic-but-unknown variables. Compared with the prosperous developments of the plenty kinds of uncertainty characterization models, the developments of efficient propagation of these uncertainty models through the computer simulators are far from satisfying the needs of engineering applications. Although the general NISS methodology framework has been developed by me and my co-authors for tackling this kind of problems, it is still of great challenge when it comes to the case with both kinds of uncertainty characterization models being involved and the case with extremely small failure probability but computationally expensive computer simulators.

Within this thesis, further steps have been made to improve the NISS methods for the above challenges and to promote the real-world engineering applications of those methods. Three main contributions have been developed on different aspects of NISS. The first article concerns the generalization of the global NISS methods for computer simulators with all three kinds of uncertainty characterization models (precise probability model, distributional p -box model, and interval model) as inputs. The Bayesian formula and kernel density estimation have been developed for establishing NISS estimators for the interval input models as well as their interaction terms with the p -box models. As has been shown, all the advantages of the classical

NISS have been reserved in this new development. Only one stochastic simulation is required for implementing the generalized NISS method, and both kinds of numerical errors (statistical errors and truncation errors) are properly addressed. The Sobol indices of the epistemic parameters are also generated as by-products, which are shown for especially indicating the truncation errors and for instructing the further collection of information. The NASA Langley UQ challenge has been correctly solved by the generalized NISS method, and the results show that the proposed method works well for this high-dimensional (twenty-one input variables and thirty-one epistemic parameters) real-world problem. The limitation of this development is that, the component functions of the interval models over second-order cannot be properly estimated due to the limitation of kernel density estimation. Moreover, this development is based on the global NISS since the local NISS is not applicable for interval variables.

The second article then concerns the efficient stochastic simulation of the failure probability function for rare events. Two algorithms based on classical line sampling procedure, which is originally developed for precise probability models, have been developed for achieving the above targets, both of which can be regarded as post-processing of the classical line sampling implementation. Both strategies are devised based on the local NISS, but both can be extended to global NISS. Results of the test examples show that, although both strategies can be regarded as post-processing of one line sampling simulation, they show different performances for the estimation of the failure probability functions. It is also concluded in these results that, the important direction is substantially responsible for the efficiency of the two imprecise line sampling algorithms, which is the same as that in the classical line sampling. Therefore, for efficiently implementing both algorithms, the important direction should be accurately estimated in advance. Based on the rationale of the line sampling algorithm, both of these two algorithms are applicable for the problems with moderately nonlinear performance functions, and for highly nonlinear problems, more lines are required, which results in low efficiency.

The results of the second article also show that, although the two imprecise line sampling algorithms have been efficient for those test examples, however, when applied to complex structures where one deterministic simulation may take more than one hour, both algorithms are

still less efficient since at least several hundreds of g -function calls are required. To fix this challenge, the AGPR-LS algorithm has been developed in the third article. The engine of this algorithm is the newly developed learning function, with which the least number of training data can be identified iteratively to substantially improve the accuracy of estimating the intersection points for each line in line sampling implementation. Results show that, with this improvement, the line sampling algorithm becomes less sensitive to the important direction specified in advance, and gets more applicable to highly nonlinear problems, since, introducing more lines will not substantially increase the number of required g -function calls. Results of test examples also show that the method can be quite efficient for extremely rare events with failure probability even less than 10^{-6} , and this is attributed to the high efficiency of one-dimensional search of the classical line sampling algorithm. However, in the classical line sampling algorithm, more g -function calls are required for each one-dimensional search so as to accurately estimate the interaction points, whereas, in the AGPR-LS algorithm, this issue is relieved to large extent due to the high effectiveness of the developed learning function.

In summary, the three developments in this thesis have made contributions from different aspects, for improving the suitability and efficiency of NISS for dealing with the problems uncertainty propagation and structural reliability analysis when both aleatory and epistemic uncertainties are involved. All the developments aim at estimating the HDMR component functions of, e.g., model response expectation function and failure probability function, and the generated results can be of great importance for learning the behavior of these functions visibly, and also can be of great significance for instructing the future information collection for reducing the epistemic uncertainty. The main drawback of NISS has also been highlighted. All the NISS class methods perform well when the epistemic uncertainty presented in the input distribution parameters is small, however, for the situations with large epistemic uncertainty, the NISS estimators may have large variation due to the large variation of the density weight functions introduced in the NISS estimators.

Although this thesis takes the distributional p -box model and the interval model as examples to describe the developments. However, it is unquestionably that the developments are

also applicable to other kinds of distributional imprecise probability models such as distributional second-order probability model and distributional fuzzy probability models, as well as other kinds of non-probabilistic models such as convex model and fuzzy set model. For distribution-free models where the distribution type is also unknown, the current developments are not applicable.

2. Open problems and Prospects

Concerning the treatment of aleatory and epistemic uncertainties for real-world engineering applications, several challenges on both uncertainty characterization and propagation are still left to be fixed.

As has been widely mentioned in this thesis, the imprecise probability models are widely used for separately characterizing the aleatory and epistemic uncertainties in a unified model framework, and the distributional *p*-box model is utilized in this thesis. Although these models no longer attributes deterministic values for the distribution parameters, the assumption on distribution types is still required in these models, which may introduce another kinds of epistemic uncertainty, which indicates the difference between the real probability distribution and the assumed distributional *p*-box, and is named as model-form uncertainty. In applications with rare data, the distribution type generally cannot be inferred with high confidence, and thus may result in incorrect assumptions on the distribution types. This brings to challenges. The first is to develop a statistical inference method for testing the fitness of the distributional imprecise probability models to the real data. The second is to develop statistical methods for inferring distribution-free imprecise probability models with no model-form uncertainty, but still with tight probability bounds so that the models are still informative.

Considering the uncertainty propagation, this thesis has made big steps for propagating the distributional models, and also for estimating extremely small failure probability. However, one of the major challenges of the NISS class methods is that, for large epistemic uncertainty, the variations of NISS estimators can be very large due to the large variations of the density weight functions introduced in the NISS estimators. In some real-world engineering applications, the

available information can be extremely scarce and of poor quality, resulting in large epistemic uncertainty, and large spans of the epistemic space. In applications, the resultant failure probability bounds may even cover several orders of magnitudes, and the NISS methods can be less effective for dealing with this type of problem. In my future work, this challenge will be of great interest.

The necessity of developing distribution-free imprecise probability models also brings the necessity for efficiently propagating these models through the computer simulators so as to generate a reliable estimation of the probability bounds of model responses. The NISS methods can be further extended for dealing with this type of problem, but for large epistemic uncertainty cases, the NISS will also lose its advantages, and new methods need to be developed.

Besides, the NISS methods introduced in this thesis can also be applied to deal with the other typical tasks in uncertainty quantification such as sensitivity analysis and model updating, but requires specific developments.

All the test examples and applications in this thesis are mainly on structural engineering problems. However, the NISS methods are unquestionably also applicable to system reliability assessment when the life data on system components is rare and/or censored, thus may have potential contributions to the safety assessment of key infrastructures such as urban water-supply systems and power supply systems.

Bibliography

- Alvarez, D. A., Uribe, F., & Hurtado, J. E. (2018). Estimation of the lower and upper bounds on the probability of failure using subset simulation and random set theory. *Mechanical Systems and Signal Processing*, 100, 782-801.
- Au, S. K., & Beck, J. L. (1999). A new adaptive importance sampling scheme for reliability calculations. *Structural safety*, 21(2), 135-158.
- Au, S. K., & Beck, J. L. (2001). Estimation of small failure probabilities in high dimensions by subset simulation. *Probabilistic engineering mechanics*, 16(4), 263-277.
- Balesdent, M., Morio, J., & Marzat, J. (2013). Kriging-based adaptive importance sampling algorithms for rare event estimation. *Structural Safety*, 44, 1-10.
- Beer, M., Ferson, S., & Kreinovich, V. (2013). Imprecise probabilities in engineering analyses. *Mechanical systems and signal processing*, 37(1-2), 4-29.
- Bjerager, P. (1988). Probability integration by directional simulation. *Journal of Engineering Mechanics*, 114(8), 1285-1302.
- Box, G. E. P., Hunter, J. S., Hunter, W. G. (2005). *Statistics for Experimenters: Design, Innovation, and Discovery*. John Wiley and Sons, Hoboken, New Jersey, USA.
- Chen, G., & Yang, D. (2019). Direct probability integral method for stochastic response analysis of static and dynamic structural systems. *Computer Methods in Applied Mechanics and Engineering*, 357, 112612.
- Crespo, L. G., Kenny, S. P., & Giesy, D. P. (2013). Reliability analysis of polynomial systems subject to p-box uncertainties. *Mechanical Systems and Signal Processing*, 37(1-2), 121-136.
- de Angelis, M., Patelli, E., & Beer, M. (2015). Advanced line sampling for efficient robust reliability analysis. *Structural safety*, 52, 170-182.

- Der Kiureghian, A., & Ditlevsen, O. (2009). Aleatory or epistemic? Does it matter?. *Structural safety*, 31(2), 105-112.
- Dubourg, V., Sudret, B., & Deheeger, F. (2013). Metamodel-based importance sampling for structural reliability analysis. *Probabilistic Engineering Mechanics*, 33, 47-57.
- Echard, B., Gayton, N., & Lemaire, M. (2011). AK-MCS: an active learning reliability method combining Kriging and Monte Carlo simulation. *Structural Safety*, 33(2), 145-154.
- Faes, M., & Moens, D. (2019). Recent trends in the modeling and quantification of non-probabilistic uncertainty. *Archives of Computational Methods in Engineering*, 1-39.
- Ferson, S., Kreinovich, V., Grinzbburg, L., Myers, D., & Sentz, K. (2015). Constructing probability boxes and Dempster-Shafer structures (No. SAND-2015-4166J). Sandia National Lab. (SNL-NM), Albuquerque, NM (United States).
- Helton, J. C., Johnson, J. D., & Oberkampf, W. L. (2004). An exploration of alternative approaches to the representation of uncertainty in model predictions. *Reliability Engineering & System Safety*, 85(1-3), 39-71.
- Helton, J. C., Johnson, J. D., Oberkampf, W. L., & Sallaberry, C. J. (2010). Representation of analysis results involving aleatory and epistemic uncertainty. *International Journal of General Systems*, 39(6), 605-646.
- Jiang, C., Bi, R. G., Lu, G. Y., & Han, X. (2013). Structural reliability analysis using non-probabilistic convex model. *Computer Methods in Applied Mechanics and Engineering*, 254, 83-98.
- Jiang, C., Ni, B. Y., Liu, N. Y., Han, X., & Liu, J. (2016). Interval process model and non-random vibration analysis. *Journal of Sound and Vibration*, 373, 104-131.
- Kennedy, M. C., & O'Hagan, A. (2001). Bayesian calibration of computer models. *Journal of the Royal Statistical Society: Series B (Statistical Methodology)*, 63(3), 425-464.
- Li, J., & Chen, J. B. (2004). Probability density evolution method for dynamic response analysis of structures with uncertain parameters. *Computational Mechanics*, 34(5), 400-409.
- Patelli, E., Alvarez, D. A., Broggi, M., & Angelis, M. D. (2015). Uncertainty management in multidisciplinary design of critical safety systems. *Journal of Aerospace Information*

- Systems, 12(1), 140-169.
- Pedroni, N., & Zio, E. (2015). Hybrid uncertainty and sensitivity analysis of the model of a twin-jet aircraft. *Journal of Aerospace Information Systems*, 12(1), 73-96.
- Pradlwarter, H. J., Schueller, G. I., Koutsourelakis, P. S., & Charmpis, D. C. (2007). Application of line sampling simulation method to reliability benchmark problems. *Structural Safety*, 29(3), 208-221.
- Sankararaman, S., & Mahadevan, S. (2011). Likelihood-based representation of epistemic uncertainty due to sparse point data and/or interval data. *Reliability Engineering & System Safety*, 96(7), 814-824.
- Schöbi, R., & Sudret, B. (2017). Structural reliability analysis for p-boxes using multi-level meta-models. *Probabilistic Engineering Mechanics*, 48, 27-38.
- Sentz, K., & Ferson, S. (2002). Combination of evidence in Dempster-Shafer theory (Vol. 4015). Albuquerque: Sandia National Laboratories.
- Stein, M., Beer, M., & Kreinovich, V. (2013). Bayesian approach for inconsistent information. *Information sciences*, 245, 96-111
- Verhaeghe, W., Desmet, W., Vandepitte, D., & Moens, D. (2013). Interval fields to represent uncertainty on the output side of a static FE analysis. *Computer Methods in Applied Mechanics and Engineering*, 260, 50-62.
- Wei, P., Lu, Z., & Song, J. (2014). Extended Monte Carlo simulation for parametric global sensitivity analysis and optimization. *AIAA Journal*, 52(4), 867-878.
- Wei, P., Lu, Z., & Song, J. (2015). Variable importance analysis: a comprehensive review. *Reliability Engineering & System Safety*, 142, 399-432
- Wei, P., Song, J., Bi, S., Broggi, M., Beer, M., Lu, Z., & Yue, Z. (2019a). Non-intrusive stochastic analysis with parameterized imprecise probability models: I. Performance estimation. *Mechanical Systems and Signal Processing*, 124, 349-368.
- Wei, P., Song, J., Bi, S., Broggi, M., Beer, M., Lu, Z., & Yue, Z. (2019b). Non-intrusive stochastic analysis with parameterized imprecise probability models: II. Reliability and rare events analysis. *Mechanical Systems and Signal Processing*, 126, 227-247.

- Wei, P., Tang, C., & Yang, Y. (2019c). Structural reliability and reliability sensitivity analysis of extremely rare failure events by combining sampling and surrogate model methods. *Proceedings of the Institution of Mechanical Engineers, Part O: Journal of Risk and Reliability*, 233(6), 943-957.
- Yang, X., Liu, Y., Gao, Y., Zhang, Y., & Gao, Z. (2015). An active learning kriging model for hybrid reliability analysis with both random and interval variables. *Structural and Multidisciplinary Optimization*, 51(5), 1003-1016.
- Zhang, H., Dai, H., Beer, M., & Wang, W. (2013). Structural reliability analysis on the basis of small samples: an interval quasi-Monte Carlo method. *Mechanical Systems and Signal Processing*, 37(1-2), 137-151.
- Zhang, J., & Shields, M. D. (2018). On the quantification and efficient propagation of imprecise probabilities resulting from small datasets. *Mechanical Systems and Signal Processing*, 98, 465-483.
- Zhao, Y. G., & Ono, T. (1999). A general procedure for first/second-order reliability method (FORM/SORM). *Structural safety*, 21(2), 95-112.

Curriculum Vitae

◆ PROFILE

Surname:	Song	Given name:	Jingwen
Nationality:	Chinese	Gender:	Female
Data of Birth:	26/07/1991	Place of birth:	Hubei, China

◆ EDUCATION

Ph.D. student, Institute for risk and reliability, Faculty of Civil Engineering and Geodetic Science, Leibniz Universität Hannover, Germany. Since 09/2018

M.S., Aeronautical Engineering, School of Aeronautics, Northwestern Polytechnical University, Xi'an, China. 09/2013-04/2016

Title of dissertation:
Global and regional sensitivity analysis for uncertainties in structural system.

B.S., Flight Vehicle Design and Engineering, School of Aeronautics, Northwestern Polytechnical University, Xi'an, China. 09/2009-07/2013

◆ List of Publications

Journal paper

Song, J., Wei, P., Valdebenito, M., Bi, S., Broggi, M., Beer, M., & Lei, Z. (2019). Generalization of non-intrusive imprecise stochastic simulation for mixed uncertain variables. *Mechanical Systems and Signal Processing*, 134, 106316.

- Song, J.**, Valdebenito, M., Wei, P., Beer, M., & Lu, Z. (2020). Non-intrusive imprecise stochastic simulation by line sampling. *Structural Safety*, 84, 101936.
- Song, J.**, Wei, P., Valdebenito, M., Beer, M. (2020). Active Learning Line Sampling for Rare Event Analysis. *Mechanical Systems and Signal Processing*, 147, 107113.
- Song, J.**, Wei, P., Valdebenito, M., Beer, M. (2020) Adaptive reliability analysis for rare events evaluation with global imprecise line sampling. *Computer Methods in Applied Mechanics and Engineering*, in press.

Conference paper

- Song, J.**, Lu, Z., Beer, M. (2019). Components importance ranking considering the effect of epistemic uncertainty. *29th European Safety and Reliability Conference* (ESREL 2019), Germany, Hannover, Sept. 22-26.

◆ Conference presentations

Song J. (2019). Efficient imprecise line sampling for estimating failure probability function and parameter sensitivity analysis. *16th International Conference on Civil, Structural & Environmental Engineering Computing* (CIVIL-COMP 2019), Italy, Riva del Garda, Sept. 16-19.

Song J. (2019). Regional sensitivity analysis for multivariate outputs based on generalized variance. *9th International Conference on Sensitivity Analysis of Model Output* (SAMO 2019), Spain, Barcelona, Oct. 28-30.